Slope Stability Analysis Along Selected Steep Sections of Adama Ridges Using Limit Equilibrium Method (LEM) and Finite Element Method (FEM).

By

Mr. Tola Garo

Dr. Yadeta Chimdessa

Dr. Pradeep Kamaraj

A Final Research Report Submitted to Adama Science and Technology University

Adama, Ethiopia
October 2023

ABSTRACT

Adama town is one of the rapidly growing towns in the country, and its population is growing at a staggering rate as well. The town is bounded by the two steeply sloped ridges that strike in the NNE-SSW direction. The urbanization and population growth of the town is leading to the construction of infrastructures near these steeply sloped ridges. However, these ridges (particularly Dibibisa ridge) are frequently affected by slope instability problems posing a danger to human lives and nearby infrastructures. Thus, this study is aimed at identifying and analyzing/or modeling slope stability along the ridges of Adama town using the Kinematic, Limit Equilibrium Method (LEM), and Finite Element Method (FEM). The input parameters for these techniques were determined through field surveys and laboratory testing of samples. Accordingly, three critical structural controlled (i.e. RS1 and RS2) and four non-structural controlled slope sections (i.e. SS1, SS2, SS3, and SS3) were identified based on field manifestations. The stability analysis of structural controlled slope sections was first done via kinematic technique and the results showed that RS1 and RS2 are susceptible to planar and wedge modes of failures. LEM modeling in terms of Factor of Safety (FOS) using Rocplane 2.0 software has shown that the planar failures of both RS1 and RS2 are unstable under dynamic and saturated conditions. Similar modeling for wedge failure via Swedge 2.0 software has also shown that the two wedges of RS1 are unstable under saturated conditions while the wedge of RS2 is stable under all conditions. Similarly, stability modeling of non-structural controlled slope sections using both LEM and FEM has shown that SS1, SS2, and SS3 are unstable under saturated conditions while SS4 is stable under all conditions. Moreover, the FOS obtained from LEM-based Slide 6.0 software and SRF obtained from FEM-based Phase 2.0 software are in very close agreement for slope sections SS1, SS2, and SS4 while the results show variation for slope section SS3. All the modeling results showed that the stability of the critical slopes of the study area is primarily controlled by saturation and slope geometry factors. Based on modeling results, this study has designed rock bolts and shotcrete to stabilize unstable rock blocks of structurally controlled slope sections. Moreover, for non-structural controlled slope sections, slope flattening, benching, and coupled slope flattening and benching were designed to stabilize unstable geological formations.

Keywords: Slope Stability, Kinematic Method, Limit Equilibrium Method, Finite Element Method

ACKNOWLEDGMENTS

Above all, we offer our deepest gratitude to GOD for being with us from the very beginning to the end and for countless blessings. Our deepest appreciation also goes to the Engineering Corporation of Oromia for their generous laboratory service. Moreover, we genuinely acknowledge Adama Science and Technology University (ASTU) for funding this research work.

Contents

LIST OF FIGURES

LIST OF TABLES

LIST OF ACRONYMS

ASTM	American Society for Testing Materials Standard
FEM	Finite Element Method
FOS	Factor of Safety
ISRM	International Society of Rock Mechanics
JCS	Joint Wall Compressive Strength
JRC	Joint Roughness Coefficient
Jv	Volumetric Joint Count
LEM	Limit Equilibrium Method
RMR	Rock Mass Rating
RQD	Rock Quality Designation
SMR	Slope Mass Rating
SRF	Stress Reduction Factor
UCS	Uniaxial Compressive Strength

CHAPTER 1

1. INTRODUCTION

1.1 **Background and Justification**

In recent years, different towns in the country are growing and expanding at a staggering rate owing to economic and population growth. The territorial expansions of some of these towns are toward hillsides and slopes that are vulnerable to landslides and slope instabilities. Therefore, civil engineering structures such as roads, highways, and buildings that are constructed in such areas are susceptible to landslide and slope instabilities. Many geotechnical engineers and engineering geologists have conducted several studies on slope stability analyses. Nevertheless, slope instability problems repeatedly occur due to human and natural disturbances to the delicate nature of the soil and rock slope (Abramson et al., 2002). Thus, slope design and stability analyses should be given deliberate attention by the design engineers above all during the slope cut and construction of civil engineering structures in the hillslopes and/or steeply sloped areas.

In Ethiopia, landslides and slope instabilities are common geological hazards. They are mostly concentrated in the north, south, and western part of the Ethiopian plateau, and rift margins (Ayalew, 1999). As a result, they have been causing loss of lives, failures in engineering structures, damage to agricultural lands, and the natural environment in different parts of the country (Temesgen et al., 2001; Abebe et al., 2010; Woldearegay, 2013). For example, over 300 human lives were claimed, above 200 dwelling houses, more than 200 Km of asphalt road, and over 500 ha of land have been damaged in the past decade (Woldearegay, 2013).

The stability of the slope is concerned with the relationship between driving and resisting forces (Hocking, 1976; Hoek & Bray, 1981 Bell, 2007; Raghuvanshi, 2017). Some factors contribute to driving forces whereas others add to the resisting forces. Therefore, these governing factors are very important for the stability analysis of the rock and soil slopes in general. These governing factors are divided into internal and external factors. The main internal governing factors are; geometry of the slope, potential failure plane characteristics, surface drainage, and groundwater condition (Anbalagan et al., 1992; Ayalew et al., 2004), whereas the external factors are rainfall, seismicity, and manmade activities (Dahal et al., 2006; Wang and Niu, 2009; Raghuvanshi et al., 2014; Girma et al., 2015). Rock slope instability occurs mostly in the form of circular, planar, wedge, and/or

toppling modes of failure while soil slope failure follows circular mode (Wyllie and Mah, 2004). Concerning hard and slightly fractured and weathered rocks, the failures mostly occur along the discontinuity planes in the form of a planar, wedge, or toppling mode of failures (Hocking, 1976; Hoek and Bray, 1981; Wyllie and Mah, 2004) while failures follow circular paths in the slope sections constituted by soils, and intensively fractured and weathered rocks (Wyllie and Norrish, 1996; Abramson et al., 2002).

Rock slope stability analyses for slope sections with slightly fractured and weathered rocks can be undertaken through a two-step process (Park and West, 2001). The first step is to evaluate kinematic analyses to determine the mode of rock slope failure (Markland, 1972; Hocking, 1976; ZainAlabideen and Helal, 2016) followed by determining the factor of safety most commonly through Limit Equilibrium (LEM) and finite Element Methods (FEM) (Raghuvanshi, 2017). The stability analysis of soil, and intensively fractured and weathered slope sections, however, only involves the latter as a mode of failure is predetermined to be circular (Wyllie and Norrish, 1996). The kinematic method deals with the failure mode of the rock slope without reference to the forces that cause them to move (Goodman, 1989; Hudson & Harrison, 1997; Park & West, 2001). Limit Equilibrium Method (LEM) determines the stability of the slope by evaluating the Factor of Safety (FOS) which is the ratio of resisting force to driving force along the failure plane (Duncan, 2000; Chowdhury et al., 2009). On the other hand, the Finite Element Method (FEM) determines the stability of the slope by computing the Stress Reduction Factor (SRF) based on the relationship between the stress and strain components of the slope (Eberhardt et al., 2004).

1.2 Statement of the Problem

Adama town is one of the rapidly growing towns in the country, and its population is growing at a staggering rate as well. The town is bounded by two ridges that are striking nearly in the NNE-SSW direction. The urbanization and population growth of the town are leading to the construction of infrastructures such as roads and residential buildings near these relatively steeply sloped ridges. With the expansion of the construction industry, parts of these bounding ridges of the town are also currently being used for quarry sites for the extraction of construction materials. However, parts of these relatively steeply sloped ridges of the town are affected by slope instability problems posing danger to human lives and infrastructures constructed in nearby areas (Figures 1.1A, B, and C). Furthermore, the study area is located in a seismically active region of the Main Ethiopian

Rift (MER) (Figure 1.2) which further exaggerates this instability problem. Therefore, it is extremely important to identify, locate and analyze slope instability problems along these relatively steeply sloped ridges to ensure safe territorial expansion and extraction of construction materials in these parts of the town. Hence, in this research work, an attempt was made to determine the geotechnical properties of rocks and soils along critical slope sections and analyze their stability using LEM and FEMs.

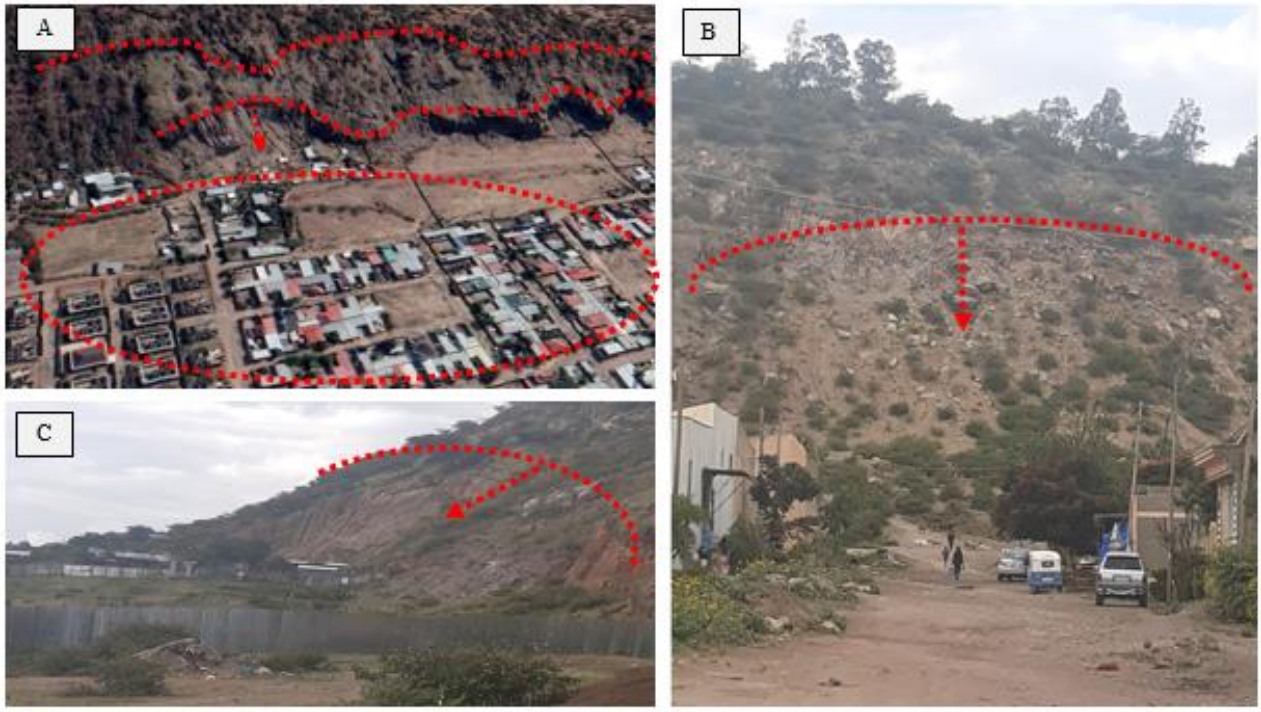

Figure 1. 1 A) Google Earth Image of part of the study area showing slope instability problem toward residential buildings, and B and C) field photograph illustrating a similar problem.

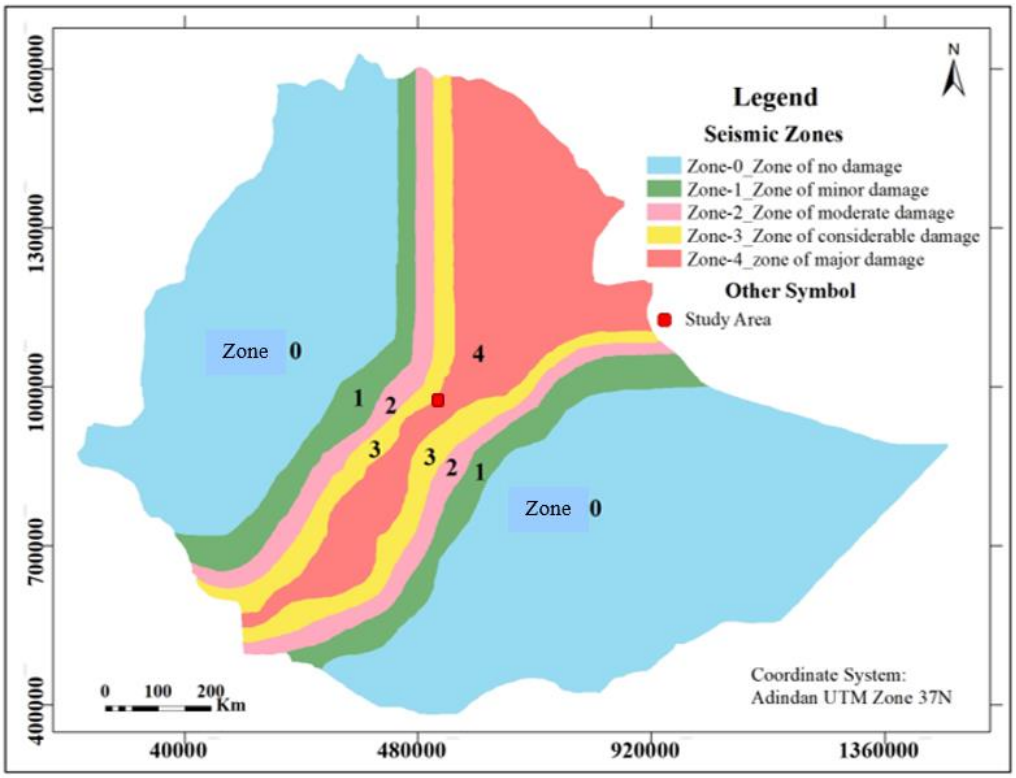

Figure 1. 2 Seismic hazard map of Ethiopia for 100 years return period (EBCS, 1995)

1.3 Location

The study area for the research work is located in the Eastern Showa zone of the Oromia regional state, Central Ethiopia (Figure 1.3). It is incorporated in the Northern Main Ethiopian Rift (NMER) with the Wonji Fault Belt (WFB). It is situated at around 100 Km from the capital, Addis Ababa, in the Southeastern direction. It is bounded by geographic coordinates of 521703 to 535303 UTM E and 938454 to 948691 UTM N in the UTM Zone of 37. Topographically, it is characterized by flat to rugged topography. The physiographic setting of the area is mainly the result of volcano-tectonic and sediment deposition associated with some erosional activities. The locations of some quarry sites are also incorporated in this map (Figure 1.3).

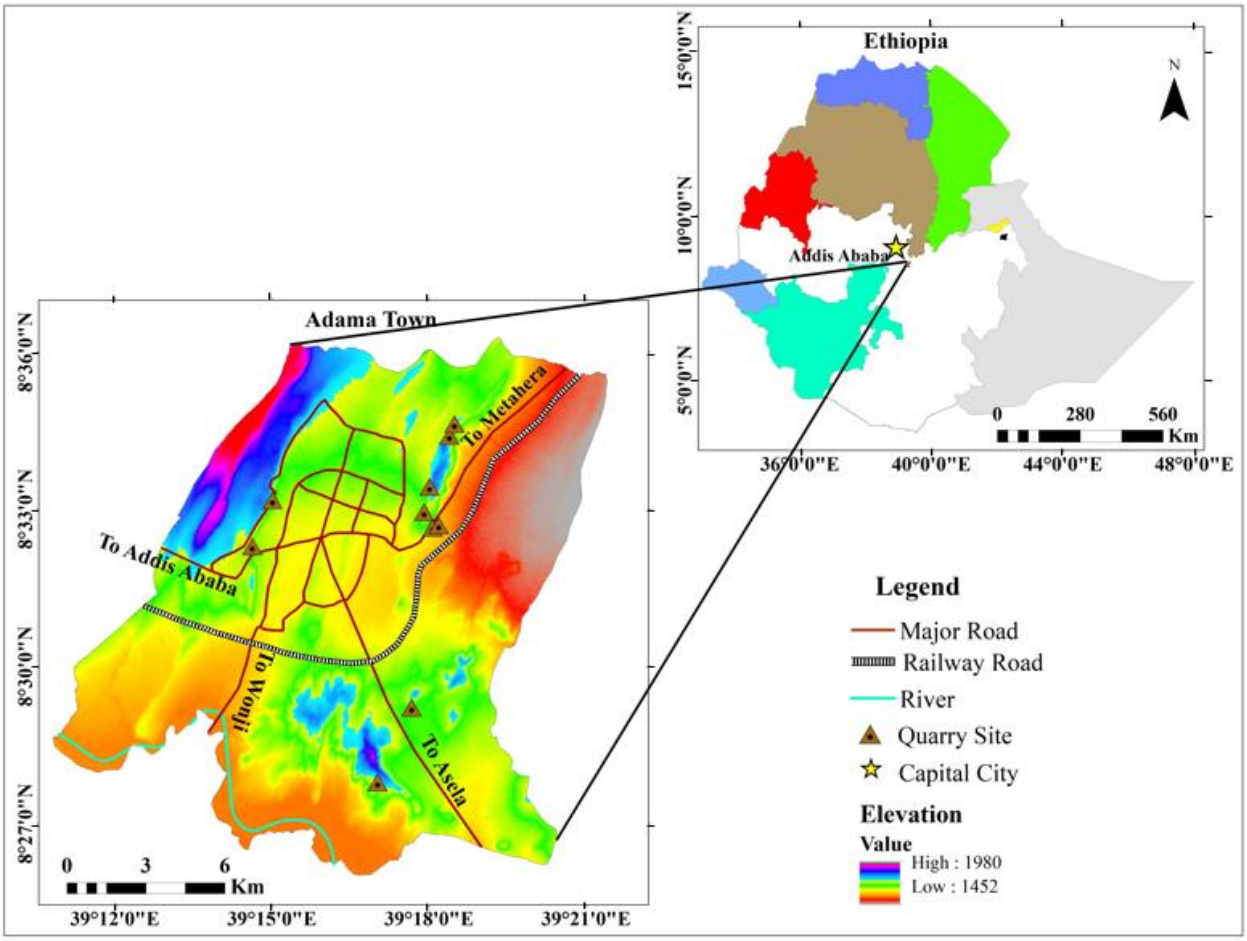

Figure 1. 3 Location map of the study area.

1.4 Objectives

1.4.1 Major objective

The major objective of this research is to identify and analyze slope instability problems along the selected steep sections of ridges surrounding Adama town.

1.4.2 Specific objective

- ✓ To identify and locate the potential slope instability problems along steep sections of the town.
- ✓ To determine the geological and geotechnical properties of soils and rock of the critical slope sections.
- ✓ To determine the factor of safety and failure probability of the critical slope sections.
- ✓ To identify the dominant causative factors responsible for slope instability via sensitivity analysis.
- ✓ To suggest effective remedial measures for the identified problems.

1.5 Significance & Beneficiaries

Slope instability is becoming one of the major causative factors for the failure of various types of civil engineering structures in the different parts of the country including the study area. Therefore, analyzing the stability of the critical slope section with respect to engineering structures, and forwarding appropriate remedial measures are extremely important for the design and construction of these structures in the study area. Hence, this study analyzed some critical slope sections along two ridges of Adama town and forwarded corresponding corrective measures. Therefore, the findings of this study can be used to give more insight to the designers, administrators, and planners to make decisions on the safety of local people, and different infrastructures due to slope instability.

CHAPTER 2

2. LITERATURE REVIEW

2.1 Introduction

Slope instabilities are one of the most common and difficult problems in mining and the construction of civil engineering infrastructures like roads, tunnels, and dams all over the world (Hoek and Bray 1981; Pantelidis 2009; Bekele and Meten 2022). The consequence of slope failure leads to the loss of billions of dollars in infrastructure and property damage in the world each year (Pantelidis, 2009). In an Ethiopian context, slope failure along the rugged topography of the northern, southern, and western plateau and rift margins has been identified as one of the most frequent geological hazards (Ayalew 1999). According to Woldearegay (2014), about 60 % of the total population of Ethiopia lives in highlands areas that are susceptible to slope failure. Therefore, understanding the mechanism of slope failure and conducting a rigorous investigation and analysis is critical to reduce the loss caused by slope failure. In the following sections, governing factors of slope failure, mechanism of failure and analysis will be method will be discussed in detail.

2.2 Governing Factors of Slope Failure

The governing factors of slope failure are categorized into internal (intrinsic) and external (triggering) factors (Raghuvanshi 2017). The intrinsic factor includes geological factors (i.e. lithology or soil type, structural discontinuity characteristics, shear strength of the slope material), the geometry of the slope (i.e. slope inclination, aspect, elevation, and curvature), and land use/land cover (Wang and Niu, 2009; Rahuvanshi et al., 2014; Hamza & Raghuvanshi, 2017; Lamessa and Meten, 2021). The external factors which generally trigger slope failures are rainfall, seismicity, the influence of surface and subsurface water, and manmade activities such as; construction activities and cultivation practices in mountainous regions (Collison et al., 2000; Keefer, 2000; Bommer and Rodrıguez, 2002; Dai, et al., 2002; Dahal et al., 2006; Wang and Niu, 2009; Raghuvanshi et al., 2014).

2.2.1 Internal Factors

2.2.1.1 Geometry of the Slope

The geometry of the slope is characterized in terms of the inclination of the slope and upper slope face, slope height, tension crack or upper release joint, and the lateral release surfaces (Hoek and Bray, 1981). The steeper slope will be more susceptible to instability as slope failure is proportional to the gravitational force (Hamza and Raghuvanshi, 2017;

Raghuvanshi et al., 2014). The slope failure also increases with an increase in the inclination of the upper slope angle as an additional weight due to a higher angle adds to the weight component. Moreover, an increase in the height (h) of the slope will increase the shear stresses (Raghuvanshi et al., 2014; Anbalagan, 1992; Hack, 2002) thereby decreasing slope stability. When the tension is more developed, the rock tends to detach from the slope thereby increasing the probability of failure (Sharma et al., 1995; Hoek and Bray, 1981).

2.2.1.2 Shear Strength Parameters

The shear strength parameters (i.e. Cohesion and friction angle) of materials that compose the slope are one of the principal internal factors that determine resisting force acting perpendicular to the failure surface of the slope (Raghuvanshi, 2017). In both rock and soil slopes, the friction angle should be less than the inclination of the slope for slope failure to take place (Hoek and Bray, 1981; Cravero et al., 2010). Further, back analysis is considered the most reliable method to estimate the cohesion (c) and friction angle of rocks while laboratory techniques are widely used for soil slopes (Sharma et al., 1999; Singh and Goel, 2002).

2.2.1.3 Potential Failure Plane Characteristics

One of the principal factors that control the stability of a structurally controlled slope section is the characteristics of the failure plane (Lamessa and Meten, 2021). Of the major resisting force of the slope, the shear strength parameters of the failure plane are the principal ones (Raghuvanshi, 2017). In turn, the shear strength along the potential failure plane depends on the engineering geological characteristics of the discontinuity surface. These include the orientation of the failure plane, continuity of the failure surface, the roughness of the surface, aperture, etc. (Johnson and Degraff, 1991). Assessment of these characteristics is important in defining the shear strength of the potential failure plane. The law of friction proposed by Barton and Bandis (1990) can estimate the angle of friction and cohesion along the potential failure plane.

2.2.1.3 Surface Drainage and Groundwater Conditions

Surface drainage and groundwater conditions of the site are the common cause of slope failure. For example, water flow in the upper slope to discontinuities of rocks and voids of soils can develop pore water force on the slope (Hoek and Bray, 1981). Moreover, shallow groundwater conditions can also create an uplift water force on the slope thereby reducing the slope stability (Hossain, 2011; Ahmadi and Eslami, 2011; Sharma et al., 1995).

Moreover, the water along the potential failure surface will reduce the shear strength and lubricate the surface which may facilitate the sliding process (Raghuvanshi et al., 2015; Hack, 2002).

2.2.2 External Factors

2.2.2.1 Rainfall

Rainfall is the major triggering factor of slope failure (Ayalew et al., 2004) and this is evident as numerous slope failures have occurred during rainy reasons at the global scale (Ermias et al., 2017; Raghuvanshi et al., 2014). As per Raghuvanshi (2017), if rainfall water gets its way to the slope it will generate the following thereby reducing the slope failure.

- It decreases the shear strength of the slope materials and hence, decreases the resistance force of the slope as well.
- It increases the rate of weathering of rocks.
- It adds weight and hence, contributes to the driving force of the slope.
- It lubricates the sliding surface.

2.2.2.2 Seismicity

Earthquake is another major triggering factor of slope failure (Wyllie and Mah, 2004). The effect of earthquakes on slope instability is higher in the area characterized by high seismic activity as stable slopes under static conditions destabilize under dynamic conditions in such areas (Hoek and Bray, 1981). Hence, it suggested considering earthquakes during stability analysis to ensure the safety of the slope (Raghuvanshi, 2017). Ground shaking due to earthquakes can cause the opening of joints and movement along joints thereby leading to a decrease in the shear strength of slope-forming materials (Raghuvanshi et al., 2014). As per Pantelidis (2009), the minimum magnitude of earthquake required to cause slope failure is 4 to 5 MM.

2.2.2.3 Human Activity

In addition to rainfall and earthquake, manmade activities can also trigger slope failure (Ermias et al., 2017; Wang and Niu, 2009). Cutting the slope steeply, removing geological materials at the toe of the slope, and uncontrolled rock excavation via blasting technique can trigger slope failure (Wang and Niu, 2009; Shukla et al., 2009; Raghuvanshi et al., 2014; Tang et al., 2016).

2.3 Types of Slope Failure

There are four common modes of slope failure: planar, wedge, toppling/fall, and circular (Hoek & Bray, 1981; Singh & Goel, 1999).

2.3.1 Planar Failure

When rock blocks lie on an inclined failure like a junction that lets daylight into free space (Figure 2.1), planar rock slope failure occurs (Sharma et al., 1999). This mode of failure usually occurs along structural weaknesses such as faults and Joints (Hoek & Bray, 1981).

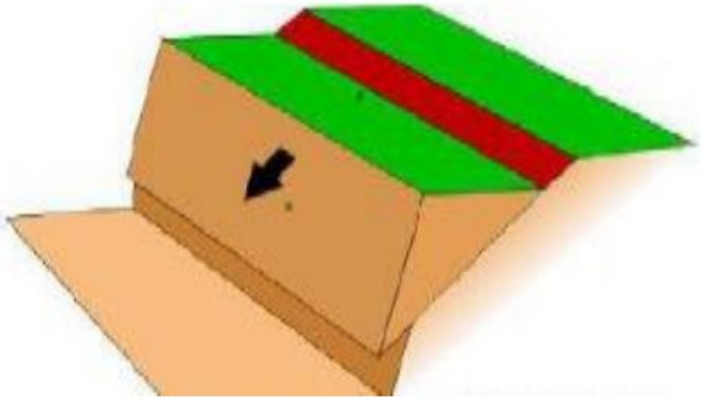

Figure 2. 1 Simplified illustrations of planar failure (Hoek and Marinos, 2007).

2.3.2 Wedge Failure

Wedge failure occurs when two discontinuities strike obliquely across the slope face and their line of intersection daylights in the slope face (Figure 2.2) (Hoek & Bray; Wyllie and Mah, 2004). The wedge mode of rock slope failures occurs over a wider range of geologic geometric conditions than the planar mode of failure (Goodman and Kieffer, 2000; Wyllie and Mah, 2004).

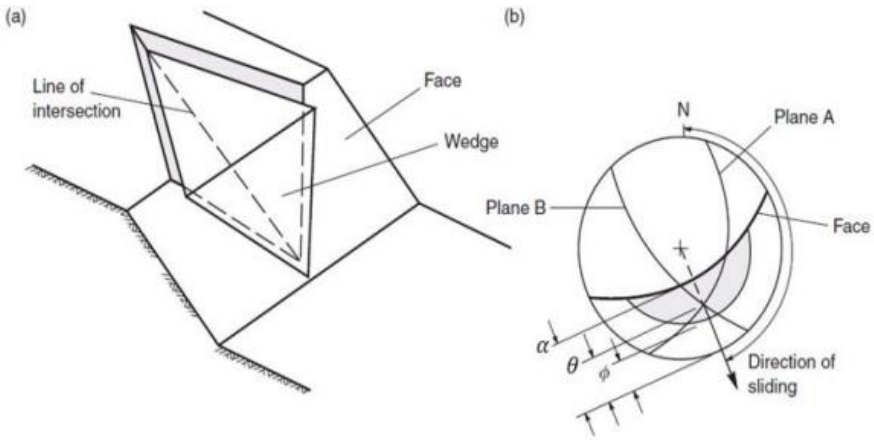

Figure 2. 2 (a) pictorial view of wedge failure; (b) stereo plot showing the orientation of the line of intersection (Wang & Ji, 2013).

2.3.3 Toppling Failure

A toppling is the overturning of a rock block at a pivot point located below its center of gravity (Wyllie and Mah, 2004). The toppling mode of rock slope occurs due to the overturning of rock layers or discontinuities that are dipping steeply into the slope face (Goodman and Kieffer, 2000) as shown in Figure 2.3. It involves the rotation of columns or blocks of rocks about a fixed base (Wyllie and Mah, 2004).

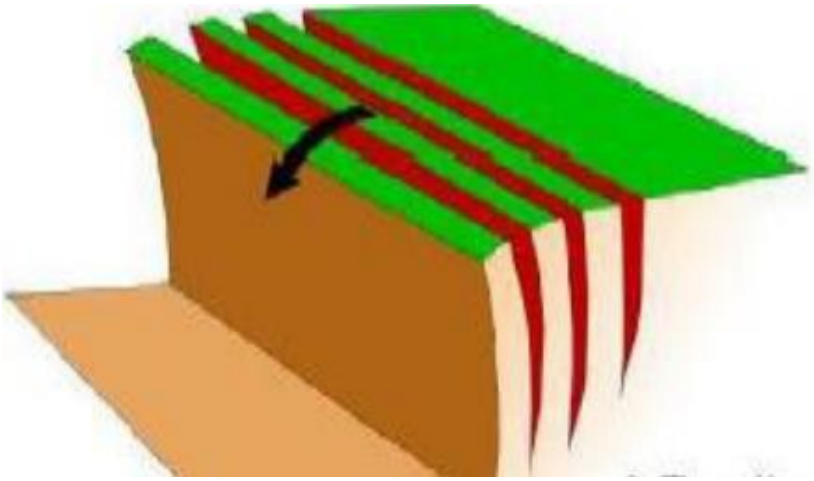

Figure 2. 3 Simplified illustrations of toppling failure (Hoek and Marinos, 2007).

2.3.4 Circular Failure

Circular failure occurs in slopes with homogeneous materials, primarily soil slopes, and in heavily fragmented rock on occasion (Abramson et al., 2002). This mode of failure commonly occurs in soil slopes and occasionally in the rock-slopes constituted by intensively weathered and fractured rocks (Chowdhury, 2010).

2.4 Slope Stability Analysis Methods

Empirical methods, Kinematic analysis, Limit Equilibrium Method (LEM), and Numerical Methods are the most widely used techniques in slope stability modeling (Abramson, et al., 2002; Raghuvanshi, 2017**;** Salunkhe et al., 2017).

2.4.1 Rock Mass Rating (RMR)

Bieniawski (1973) first developed this technique for the application of tunnels, dams, and excavation. Later, Bieniawski (1979) extended the application of this technique to slope modeling. This technique determines the quality of rock mass from input parameters such as Uniaxial compressive strength of rock material (UCS) (R1), Rock Quality Designation (RQD) (R2), discontinuity spacing (R3), joint condition (R4, groundwater condition (R5),

and joint orientation (R6) (Singh & Goel, 1999). Of these parameters, discontinuity spacing (R3), joint condition (R4, groundwater condition (R5), and joint orientation (R6) can be directly estimated in the field using instruments such as tape meter, Brunton compass, and others. The Uniaxial compressive strength of rock material (UCS) (R1) can also be determined either in the field from Schmidt hammer rebound value or in the laboratory from a point-load strength test. Moreover, RQD (R2) can be determined from the percentage of intact rock pieces greater than 10cm in the total core length (Eq. 2.1) (Deere and Deere, 1988). However, this equation is only applicable if the core sample is available and hence, it cannot be used for estimating rock mass quality of surface rocks. Palmstrom (2005) developed the volumetric joint method for the estimation of RQD of surface exposure (Eq. 2.2).

$$\text{RQD} = \frac{\sum \text{Length of Core Pieces} > 10\text{cm}}{\text{The total length of the Core}} \times 100\% \quad (2.1)$$

$$\text{RQD} = 110 - 2.5\ \text{Jv} \quad (2.2)$$

Where Jv is Volumetric Joint count is given by the following equation.

$$\text{Jv} = \left(\frac{1}{S_1}\right) + \left(\frac{1}{S_2}\right) + \left(\frac{1}{S_3}\right) \ldots + \left(\frac{1}{S_n}\right) + \left(\frac{N_r}{5\sqrt{A}}\right) \quad (2.3)$$

Where S1, S2, and S3 are the average spacings for the joint sets, Nr is the number of random joints in the actual location and A is the area in m².

The RMR can be calculated using the following equation

$$\text{RMR}_{\text{Basic}} = \text{R1} + \text{R2} + \text{R3} + \text{R4} + \text{R5} \quad (2.4)$$

Finally, the total RMR can be calculated using the following equation by analyzing the effect of orientation of discontinuity and slope into consideration.

$$\text{RMR}_{\text{Total}} = \text{RMR} + \text{R6} \quad (2.5)$$

2.4.2 Slope Mass Rating (SMR)

For evaluating the stability of rock slopes, Romana (1985) proposed a classification system called the "Slope Mass Rating" (SMR) system. SMR is obtained from Bieniawski's rock mass rating (RMR) by subtracting adjustment factors of the joint–slope relationship and adding a factor depending on the method of excavation.

$$\text{SMR} = \text{RMR}_{\text{Basic}} + (\text{F1} * \text{F2} * \text{F3}) + \text{F4} \quad (2.6)$$

Where

- RMR_{Basic} is a basic rock mass rating as per Beniawski (1989).
- F1- depends upon parallelism between joints and slopes face strikes. ($\alpha_j - \alpha_s$) where α_j is a joint strike and α_s is a slope strike.
- F2- refers to joint dip angle (β_j) or plunge of a line of intersection of two wedge-forming planes (β_j).
- F3- depends upon the relationship between the joint dip or plunge of a line of intersection of two wedge-forming planes and slope inclination. (β_j - (β_s) or ($\beta_i - \beta_s$) where β_s is the inclination of slope.
- F4- is considering about method of excavation. It includes the natural slope or the cut slope excavated by pre-splitting, smooth blasting, normal blasting, poor blasting, and mechanical excavation.

2.4.2 Kinematic Analysis

The kinematic analysis is a technique that is widely utilized to differentiate the mode of rock slope failures that takes place due to unfavorable orientation of discontinuities such as joints, faults, bedding planes, foliation, and shear zones (Hoek and Bray, 1981; Wyllie and Norrish, 1996; Wyllie and Mah, 2004). This technique uses the orientation of discontinuities and slope face (i.e. dip and dip direction) to determine the mode of rock slope failure through stereographic projections that allow the 3D data to be represented and analyzed in 2D (Wyllie and Norrish, 1996). In-depth treatments of the principles of this technique for different modes of failures for plotting, analyzing, and interpreting data were given by Markland (1972), Goodman (1989), Hoek and Bray (1981), and Rockscience (2001). Accordingly, this analysis can be done either manually using Streonet or with Dips 6.0 software (Dips 2.0 Rockscience, 2004) from input parameters such as friction cone/angle of joints, dip and dip directions of slope and discontinuities. The former involves the identification of failure mechanisms through the great circle on streonet and is very tedious when large orientation data are involved (Richards and Atherton, 1987).

The planar type of failure is down-dip sliding on a single discrete discontinuity surface whose orientation with respect to the face of the slope plays a crucial in its analyses (Hoek and Bray, 1981 Lisle, 2015; Wyllie and Norrish, 1996). According to Hoek and Bray (1981), Goodman (1989), Wyllie and Norrish (1996), and Wyllie and Mah (2004), the following structural conditions should be fulfilled during using Streonet or Dips 6.0

software analysis for kinematic admissibility of a planar mode of failure.

- The dip direction of the discontinuity must be within 20^0 from the slope face.
- The dip of discontinuity must be less than the dip of slope and it must daylight on the slope face.
- The dip of the planar discontinuity must be greater than the angle of friction of the surface.
- The lateral extent of the potential failure mass must be defined.
- The upper part of the sliding surface must intersect the upper slope, or end with a tension crack.

Wedge failure occurs when rock masses slide along two intersecting discontinuities both of which dip out of the cut slope at an oblique angle to the cut face forming a wedge-shaped block (Hoek and Bray, 1981; Wyllie and Norrish, 1996). As per Hoek and Bray (1981) and Wyllie and Mah (2004), the following structural conditions should be fulfilled during analysis using Streonet or Dips 6.0 software analysis for kinematic admissibility of wedge mode of failure.

The dip of the slope must exceed the dip of the line of intersection of the two discontinuities.

- The line of intersection must daylight on the slope face.
- The dip of the line of intersection must be in such a way that the strength of two planes is reached.
- The upper end of the line of intersection should intersect either the upper slope or end in a tension crack.

Similarly, according to Hoek and Bray (1981), the following structural conditions should be fulfilled during analysis using streonet or Dips 6.0 software analysis for kinematic admissibility of wedge mode of failure.

- The presence of jointed rock mass closely spaced and steeply dipping discontinuity sets that dip away from the slope surface.
- The strikes of the sliding plane and the slope face lie parallel (± 10^o) to each other.

2.4.3 Limit Equilibrium method (LEM)

The LEM is the most popular and frequently used method in the slope stability modeling of both rock and soil slopes (Mebrahtu et al., 2022). This technique determines stability analysis in terms of FOS by dividing available resisting force by the driving force of the slope along the failure surface (Wyllie and Norrish, 1996; Pardeshi et al., 2013). For the rock slopes, the first step is to determine the mode of rock failure via the kinematic method (Section 2.4.1) and then followed by FOS determination via LEM for identified mode of failure (Park and West, 2001).

2.4.3.1 LEM Stability Analysis of Rock Slope (Planar Failure)

The FOS of a planar mode of failure is calculated by resolving forces acting on the failure surface into perpendicular and parallel components (Hoek and Bray, 1981; Wyllie and Norrish, 1996). These forces include the weight of the sliding mass (W), shear strength along the failure surface (i.e. cohesion (c) and friction (ϕ), uplift force due to the water pressure on the sliding mass (U), force due to water pressure in the tension crack (V), seismic accelerations (α) and orientation of joints and slope (Figure 2.4) (*Hoek and Bray, 1981;* Wyllie and Norrish, 1996). The conditions for calculation of FOS usually rely on saturation and seismic conditions and geometric configuration of the slope such as the absence or presence of the tension crack and its location within the slope (Hoek and Bray, 1981; Wyllie and Norrish, 1996). Hence, the stability analysis for this mode of failure can be determined in the conditions where seismic acceleration is present or not and where a tension crack is absent or present within the slope, and where this tension crack is considered dry or saturated with water. Accordingly, a FOS for planar mode of failure under static saturated condition can be determined using Eq. 2.7, which was forwarded by Hoek and Bray (1981) and Hoek (2000).

$$\text{FOS} = \frac{Resisting\ Force}{Driving\ Force} = \frac{cA+\sum \sigma tan\phi}{\tau} \quad 2.7$$

$$\text{FOS} = \frac{cA+\sum \sigma tan\phi}{\tau} = \frac{cA+(W+cos\psi p-U-Vsin\psi p)tan\phi}{Wsin\psi b+Vcos\psi b} \quad 2.8$$

where c is cohesion and friction along the failure plane, is failure plane dip, A is the base area of the wedge, U is water forces acting on the failure plane, V is the force vector applied to the tension crack, and W is the weight of rock wedges that rest on failure plane.

As per Hoek (2000), Eq. 2.8 can also be modified into Eq. 2.9 to determine FOS of planar failure under static dry condition.

$$FOS = \frac{cA}{Wsin\psi b} + \cot\psi p \times \tan\phi \quad 2.9$$

Moreover, Eq. 2.8 can also be modified into Eq.2.10 to determine the FOS of this mode of failure under the influence of seismicity (α) and saturation (Hoek and Bray, 1981; Willy and Mah, 2004)

$$FOS = \frac{cA+(W(cos\psi p-\alpha sin\psi p)-U-Vsin\psi p)tan\phi}{W(sin\psi b+\alpha cos\psi p)+Vcos\psi p} \quad 2.10$$

In the above equations, A is the base area of the wedge; U is the water force acting on the failure plane; V is the force vector applied to the tension crack and the weight of the wedge (W) can be determined using Eq. 2.11, Eq. 2.12, Eq. 2.13, and Eq. 2.15/2.16, respectively.

$$A = (H - z)\,\mathrm{cosec}\psi p \quad 2.11$$

$$U = \tfrac{1}{2}(\gamma w)(Zw)(A) = U = \tfrac{1}{2}(\gamma w)(Zw)(H - z)\mathrm{cosec}\psi p \quad 2.12$$

$$V = \tfrac{1}{2}(\gamma w)(Zw)^2(\mathrm{cosec}\psi p) \quad 2.13$$

$$z = H\left(1-\sqrt{cot\psi f \; x \; tan\psi p}\right) \quad 2.14$$

$$W = \tfrac{1}{2}(\gamma)(H)^2((1-z/H)^2\cot\psi p - \cot\psi f)) \quad 2.15$$

$$W = \tfrac{1}{2}(\gamma)(H)^2((1-z/H)^2\cot\psi p(\cot\psi p\tan\psi f-1)) \quad 2.16$$

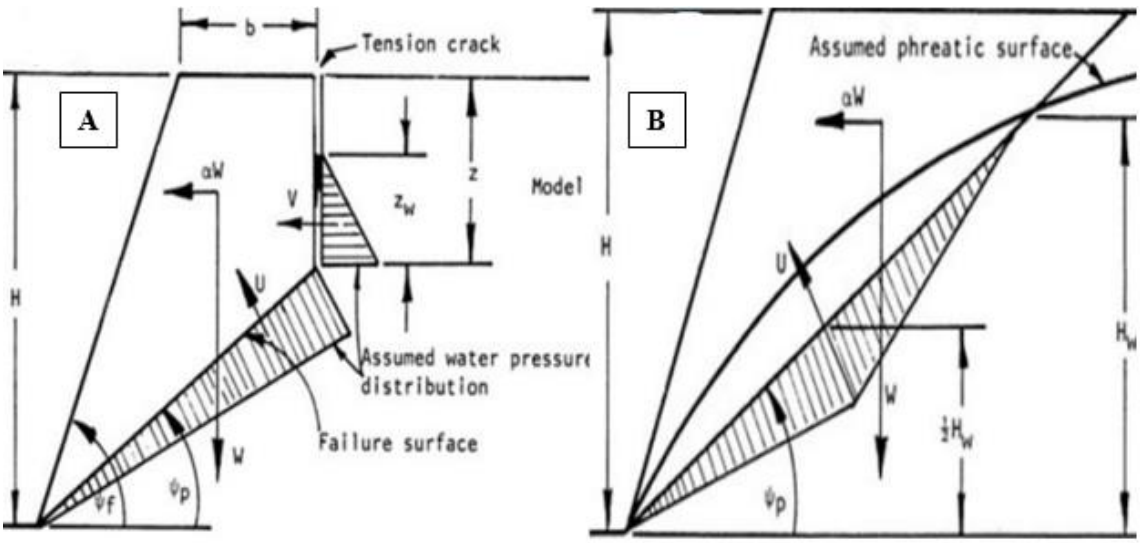

Figure 2. 4 Geometry of planar rock slope failure with tension crack in the upper slope face (A) and no tension crack on slope face (B) (Hoek and Bray, 1981)

2.4.3.2 LEM Stability Analysis of Rock Slope (Wedge Failure)

The stability analysis of the wedge mode of failure requires the determination of geometry and orientation of wedge elements such as two discontinuities, the slope face, the upper

slope face, and if present the plane representing tension crack (Hoek and Bray, 1981; Wyllie and Norrish, 1996). Sliding of the wedge mostly takes place along the line of intersection of the two wedge-forming joints (e.g. Wedge A and Wedge B) (Figure 2.5A) or both of the joints (Hoek and Bray, 1981; Park and West, 2001). The FOS of the wedge mode of failure along the line of intersection (i.e. line 5 in Figure 2.5A) can be calculated using Eq. 2.17, which was forwarded by Hoek et al. (1973), and Hoek and Bray (1981).

$$\text{FOS} = \frac{3}{\gamma.H}\ (cAX + cBY) + \left(A - \frac{\gamma w}{z\gamma}X\right) tan\phi A + (B - \frac{\gamma w}{z\gamma}Y) an\phi B \qquad 2.17$$

Where cA and cB are the cohesive strength of planes A and B, respectively; Aϕ and Bϕ are friction angles along planes A and B respectively, γ unit of rock, γw unit weight of water, and H, total height of the wedge. Dimensionless factors X, Y, A, and B depend upon the geometry of the slope and they are determined by the following equations:

$$\text{X} = \frac{sin\theta 24}{sin\theta 45\ x\ cos 2.na} \qquad 2.18$$

$$\text{Y} = \frac{sin\theta 13}{sin\theta 35\ x\ cos 1.nb} \qquad 2.19$$

$$\text{A} = \frac{cos\psi a - cos\psi b\ x\ cos\theta na.nb}{sin\psi 5\ x\ sin 2na.nb} \qquad 2.20$$

$$\text{B} = \frac{cos\psi b - cos\psi a\ x\ cos\theta na.nb}{sin\psi 5\ x\ sin 2na.nb} \qquad 2.21$$

Where Ψa and Ψb are dips of planes A, B respectively, and Ψ5 is dips of the line of intersection, and θ24, θ13, θ35, and θ45 can be estimated from Figure 2.6 as suggested by Hoek and Bray (1981).

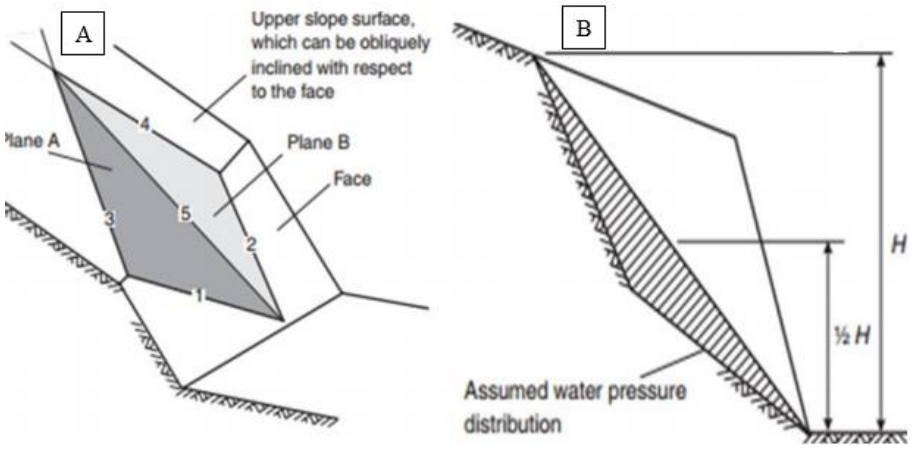

Figure 2. 5 A) Graphic view of wedge showing the number of intersections of lines and planes; B) view normal to the line of intersection (5) showing wedge height and water pressure distribution (Wyllie and Mah, 2004)

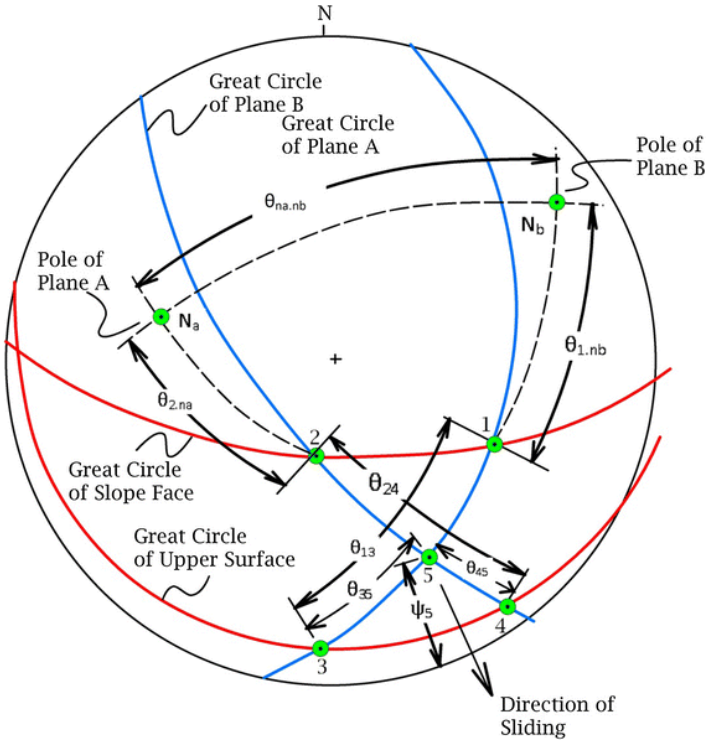

Figure 2. 6 Stereoplot of data required for wedge stability analyses (Modified after Hoek & Bray, 1981).

2.4.3.3 LEM Stability Analysis of Soil and Heavily Fractured and Weathered Rocks

Unlike planar and wedge modes of failure where failure takes along joints, there are no predefined failure surfaces for slopes with soil and/or heavily fractured and weathered rocks (Wyllie and Mah, 2004). In such a scenario, the failure surface is free to find the line with the least resistance to a failure and it usually takes a circular or near circular shape (Hoek and Bray, 1981; Hoek, 2000, Wyllie and Mah, 2004). In such slopes, this technique determined the FOS of the slope by differentiating the mass of the slope into different slices from which normal and shear inter-slice force and equilibrium can be determined (Abramson et al., 2002; Krahn, 2004). Some of the methods of slices that determine FOS through the LEM include the ordinary method (Fellenius, 1936), Janbu Simplified (Janbu, 1954), Bishop Method (Bishop, 1956), Morgenstern-Price method (Morgenstern-Price, 1965) and Spencer method (Spencer, 1967). In the following sections, Bishop, Janbu, and Morgenstern-Price Methods will be briefly discussed.

2.4.3.3.1 Bishop Method

Bishop Method is developed by Bishop (1956) and is used for analyzing the circular mode of slope failure. It considers moment equilibrium and inter-slice normal force acting on

the slope (Fredlund et al., 1981; Aryal, 2008). However, this method fails to consider force equilibrium in the y-direction (Aryal, 2008). Nevertheless, this technique is among the most utilized method in slope engineering (Lamessa and Meten, 2021).

To determine the FOS of the failure surface lines, Bishop Method assumes that the slope materials behave as per the Mohr-Coulomb failure criterion:

$$\tau = c + \sigma n + \tan \phi \qquad 2.22$$

Where τ is the shear strength of the soil, σn is the normal effective stress, c is the cohesion and ϕ is the friction angle of the slope materials.

This method then relies on a slice (Figure 2.7) to determine the FOS of the slope under consideration. First, the shear force (T) acting on the base of each slice will be calculated using Eq. 2.23 as per Bishop (1956).

$$T = \frac{c*L+N`\tan(\phi)}{FOS} \qquad 2.23$$

Where L is the arc length of the slice's base which is approximated to a line segment, c is the cohesion, and ϕ is the friction angle of the soil.

Afterwards, the equilibrium force in the vertical direction can be calculated using Eq. 2.24

$$\Sigma F_{vertical} = 0 <> (N`+U) * \cos(\alpha) + \frac{1}{FOS} * [(cl + N`\tan(\phi)) * \sin(\alpha)] - W = 0 \qquad 2.24$$

Where α is the angle of inclination

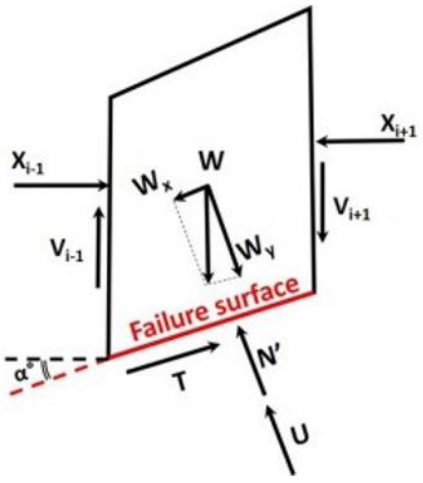

Figure 2. 7 Force acting on a single slice (W - the weight of the soil above the failure surface; Xi-1, Xi+1, Vi-1, VI+1 - interslice reactions from the adjacent slices; N'- normal effective; T - shear component and U - the boundary water force.

Subsequently, the moment equilibrium around the center of rotation can be calculated using Eq. 2.25, and the details are shown in Figure 2.8.

$$\Sigma T * R = \Sigma W * R \sin(\alpha) \qquad 2.25$$

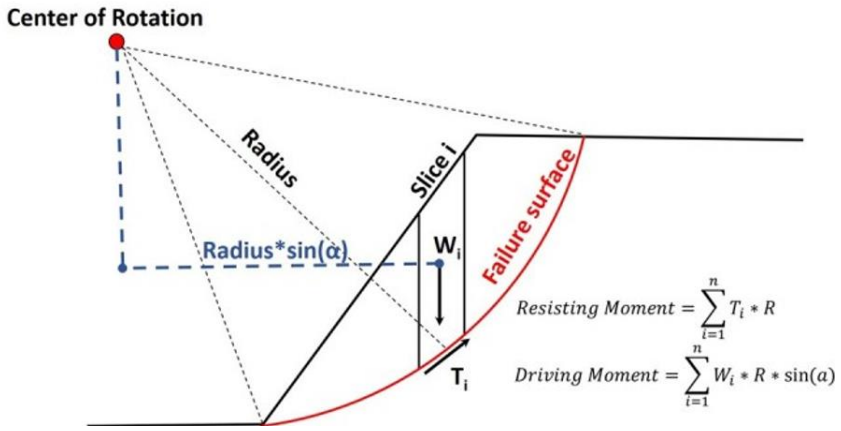

Figure 2. 8 Moments about the center of rotation generated by each slice.

FOS can be then easily calculated by dividing the resisting moment by the driving moment. The FOS for the entire failure surface can be computed by using equation 2.26.

$$FOS = \frac{\Sigma T\max * R}{\Sigma W * R * Sin(\alpha)} = \frac{\Sigma\,(c * Li + N`i \tan(\phi))}{\Sigma W * \sin(\alpha)} \qquad 2.26$$

Where R is the radius of the rotational surface.

Considering Eq. 2.24 and substituting the length of the slice's base as a function of its width and inclination (L = B* sin (α)), the FOS can also be calculated by the following equation.

$$FOS = \sum \left\{ \frac{[(\, c * b + \left(W - \frac{U}{\sec(a)}\right) * \tan(\phi)] * \sec\,(a)}{1 + [\frac{\tan(a)\tan(\phi)}{FOS}]} \right\} \frac{1}{\Sigma W * \sin(\alpha)} \qquad 2.27$$

Moreover, by considering the ru coefficient for the water force, FOS can also be calculated using the following equation.

$$FOS = \sum \left\{ \frac{[(c * B + W\,(1 - ru) * tan(\phi))]\, sec\,(\alpha)}{1 + [\frac{tan(a)\, tan(\phi)]}{FOS}} \right\} \frac{1}{\Sigma W * \sin(\alpha)} \qquad 2.28$$

Where r_u = U/σ, U= pore water pressure, and σ= normal stress at the point of interest.

2.4.3.3.2 Janbu Method

Janbu (1954) develops this method and it considers force equilibrium (Lamessa and Meten, 2021). However, the method fails to satisfy moment equilibrium and it considers zero normal and shear inter-slice force (Wyllie and Mah, 2004).

Accordingly, Janbu Simplified method uses the Mohr-Coulomb failure criterion to derive the shear strength of the slope material for a single slice as stated in Eq. 2.29.

$$T_{ULT} = c_i * L_i + N_i \tan(\varphi i) \qquad 2.29$$

Where ***c*** and ***φ*** refer to the cohesion and the friction angle of the ground, respectively, ***L*** is the length of the slice's base, and ***N'*** is the effective normal force acting at the base of the slice.

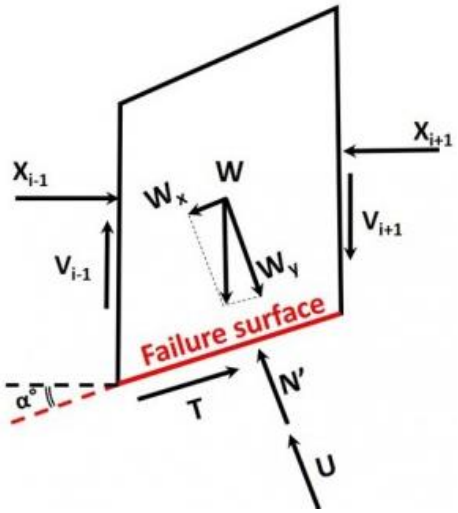

Figure 2. 9 Forces acting on a single slice: i) the weight of the soil above the failure surface W, ii) the interslice reactions from the adjacent slices Xi-1, Xi+1, Vi-1, Vi+1, iii) the reaction of the stable ground which consists of a normal effective N' and a shear component **T**, respectively, and iv) the boundary water force **U**.

Afterwards, this technique determines the horizontal force equilibrium for each slice from the horizontal components of the shear resistance stated in Figure 2.9.

$$\sum F^{i}_{Horixontal} = 0 \quad <\cdots> \quad Ticos\,(ai) = (Ni + Ui)\sin(ai) \qquad 2.30$$

Subsequently, the correspondent vertical force equilibrium for each slice can also be determined using Eq. 2.31

$$\sum F^{i}_{vertical} = 0 \quad <\cdots> \quad Wi + (V_{i+1}) = Tisin(ai) + (Ni + Ui)\cos(ai) \qquad 2.31$$

Combining Eq. 2.30 and Eq. 2.31, we get:

$$\text{Wi} + V_{i-1} - V_{i+1} = \frac{Ti}{\sin(ai)} \quad 2.32$$

Finally, the overall horizontal equilibrium yields:

$$\sum_{i=1}^{N} Ti \cos(ai) = \sum_{i=1}^{N} (Ni + Ui) \sin(ai) \quad 2.33$$

Given the determination of Ti using Eq. 2.34, the FOS can be determined using Eq. 2.35.

$$\text{Ti} = \frac{Ti\ (ultimate)}{FOS} \quad \text{Hence,} \quad \text{Ti} = \frac{ci*L+Ni\tan(\varphi)}{FOS} \quad 2.34$$

$$\text{FOS} = \frac{\left(\sum_{i=1}^{N} Ci\right)*Bi+\sum_{i=1}^{N}(Wi+(V_{i-1}-V_{i+1})*\cos(ai)*\tan(\varphi)-\sum_{i=1}^{N} Uicos(ai)*\tan(\varphi i)}{\sum_{i=1}^{N}(Wi+(V_{i-1}-V_{i+1})*\cos(\theta i)*\sin(\theta i)} \quad 2.35$$

Where *B* is the width of each slice, $B_i = L_i * \cos(\alpha_i)$.

2.4.3.3.1 Morgenstern-Price Method

Unlike Bishop and Janbu's Methods, Morgenstern-Price considers both force and moment equilibrium (Wyllie and Norrish, 1996; Wyllie and Mah, 2004). As per Morgenstern and Price (1965), the following assumptions were made to calculate FOS using LEM considering the schematic sketch shown in Figure 2.10

- Dividing planes between blocks is always vertical
- The line of action of the weight of block W_i passes through the center of the i^{th} segment of slip surface represented by point M
- The normal force N_i is acting in the center of the i^{th} segment of slip surface, at point M
- The inclination of forces E_i acting between blocks is different on each block (δ_i) at slip surface endpoints is $\delta = 0$

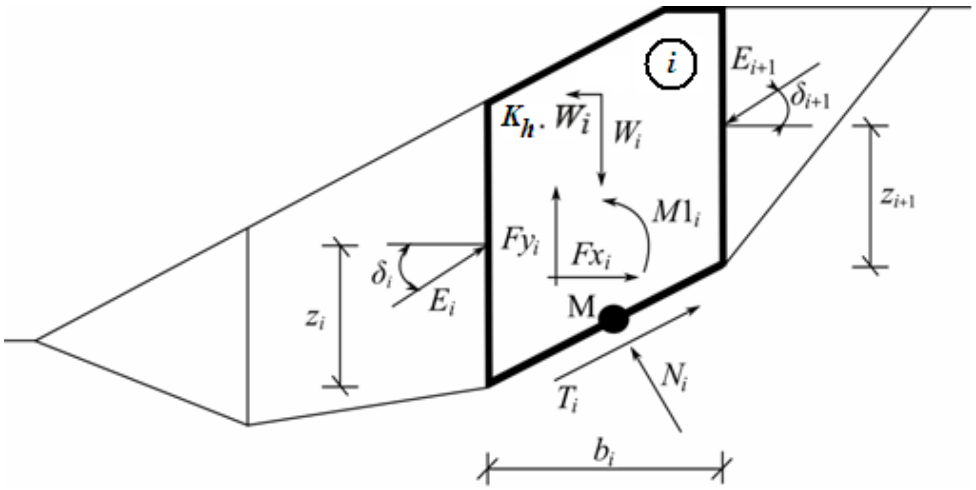

Figure 2. 10 Static scheme - Morgenstern-Price method. (Wi) is block weight including material surcharge and coefficient of vertical earthquake Kv, (Kh) is the factor of horizontal acceleration during the earthquake, (Ni) Normal force on the slip surface, (Ti) shear force on the slip surface, (E_i, E_{i+1}) forces exerted by neighboring blocks, (Fx_i, Fy_i) other horizontal forces, (Mli) moment forces, and (Ui) Pore pressure.

In this method, the FOS can be calculated by using the following equations.

$$\text{FOS} = \frac{\text{Shear strength available}}{\text{Shear strength mobilized}} \qquad 2.36$$

$$\text{FOS} = \tan\phi_i \tan(\sigma_{i+1} - \alpha_i) \qquad 2.37$$

Where, ϕ_i = angle of internal friction segment, α_i = inclination of the slip surface segment.

2.4.4 Numerical Methods (Finite Element Method (FEM))

Conventional LEMs are one of the most widely utilized techniques in slope stability modeling (Abd El-Latif, 2012; Mebrahtu et al., 2022). Rock slopes and perhaps some soil slopes exhibit heterogeneity in the geological formation, and variation in slope geometry, water distribution, and response to seismic conditions (Alzo'ubi, 2016; Raghuvanshi, 2017). However, the stability of modeling of such a complex slope cannot be determined using conventional LEM (Karaman et al., 2013; Eberhardt, 2003). According to Tang et al. (2016), the stability modeling of such complex slopes can be best simulated using Numerical methods. Numerical methods include continuum, discontinuum, and hybrid methods (Stead et al., 2006; Tang et al., 2016).

Of continuum numerical methods, the displacement-based Finite Element Method (FEM) became increasingly popular in analyzing slope stability problems (Bouzid, 2022). The FEM provides the following advantage over LEM (Swan et al, 1999; Griffiths, 1999):

- No assumptions are needed regarding the shape of the failure or location.
- It can be applied for slopes with complex slope geometry in either 2D or 3D.
- Mohr-Coulomb failure criterion and numerous other failure criteria can be employed.
- The equilibrium stresses, strains, and the associated shear strengths in the soil mass can be computed very accurately.
- This technique can also consider seepage-induced failures, brittle soil behaviors, random field soil properties, and engineering interventions such as geo-textiles, soil nailing, drains, and retaining walls
- This method can also give information about the deformations at working stress levels and can monitor progressive failure including overall shear failure.

FEM usually takes three different forms (Bouzid, 2022). These include Gravity Increase Method (GIN), Finite Element Limit Analysis (FELA), and Strength Reduction Factor (SRF). The GIM involves increasing the gravitational acceleration of the slope while keeping the properties of geological materials unchanged until the slope reaches a failure state during a finite element process (Swan and Seo, 1999; Li et al., 2009; Sternik, 2013; Bouzid, 2022). This technique is less popular (Bouzid, 2022) and sometimes overestimates the stability of the slope (i.e. FOS), especially for low slopes (Sternik, 2013). The FELA uses an optimization technique to compute the upper or lower bound plastic load (or limit load) for FOS calculation (Sloan, 2013; Krabbenhoft et al., 2007; Tschuchnigg et al., 2015a). However, FELA is restricted to problems where only the associated plasticity flow rule is allowed (Bouzid, 2022). The SRM involves progressively reducing the shear strength of slope-forming materials to compute the stability of the slope (Stead, et. al., 2006; Abd El-Latif, 2012). In this study, SRF was used for stability modeling and hence, it will be briefly discussed in the following sections.

2.4.3.1 Stress Reduction Factor (SRF)

In the SRF, the slope is considered to fail because its material shear strength on the sliding surface is insufficient to resist the actual shear stresses (Rocscience, 2004). Following the shear failure (Liu et al., 2015; Bouzid, 2022), the FOS/or SRF against slope failure is simply calculated as:

$$\text{SRF} = \frac{\tau}{\tau_f} \tag{2.38}$$

Where τ is the shear strength of the slope material, which is calculated through the Mohr-Coulomb criterion as:

$$\tau = C + \sigma_n + tan\phi \quad 2.39$$

The τ_f is the shear stress on the sliding surface can also be calculated using the following Eq. 2.40.

$$\tau_f = C_f + \sigma_n \tan \phi_f \quad 2.40$$

Afterwards, the SRF can be calculated from either one of the following factored shear strength parameters C_f and ϕ_f is given using Eq. 2.41 and Eq. 2.42, respectively.

$$C_f = \frac{C}{SRF} \quad 2.41$$

$$\phi_f = tan^{-1}\left(\frac{tan\phi}{SRF}\right) \quad 2.42$$

2.5 Remedial Measures for Slope Failure

In Geological Engineering, the problem of slope failure has been a subject of research and investigation for the past 70 to 80 years (Bouzid, 2022). Hence, numerous remedial measures have been proposed in accordance with available modeling techniques and real field experience. In this regard, the methods of slope stabilization are categorized into reinforcement, slope protection, and removal (Table 2.1) (Hoek and Bray, 1981; Wyllie and Mah, 2004; Abramson et al., 2002; Wyllie and Mah, 2004; Cheng and Lau, 2014).

The reinforcement techniques are used to stabilize loosened rock blocks without rock or soil removal (Lamessa and Meten, 2021). The most widely used reinforcement techniques are shear keys, rock anchors, shotcrete, and drainage (Hoek and Bray, 1981; Cheng and Lau, 2014). Shear keys are structures that are used to improve the strength of slope material and it involves the insertion of 25 to 32 mm diameter and 500 - 750 mm length keys into stable rock (Wyllie and Mah, 2004). Similarly, rock anchors are also used to prevent the sliding of rock blocks along joints by modifying the shear and normal forces acting on the sliding planes (Hoek & Bray, 1981). Shotcrete is fine aggregate with 50 to 100 mm thickness and is usually used to prevent falling and/or raveling of rocks of soils and highly fractured rocks (Hoek & Bray, 1981). Moreover, drainage involves the removal of water that accumulates in the joints and void of soils (Abramson et al., 2002).

Removal techniques involve slope flattening, trimming, and scaling (Wyllie & Mah, 2004). Slope flattening is the process of removing overburdened soil or rock material that occurs on the upper part of the slope and making its angle flatter than the underlying rock component (Hoek and Bray, 1981). Slope flattening techniques include decreasing slope angle, multi-sloping, benching, and combined slope angle reduction and benching.

Table 2. 1 Slope stabilization methods (Hoek & Bray, 1981; Wyllie & Mah, 2004; Cheng & Lau, 2014)

Methods	Stabilization Measures
Slope Protection	Ditches, mesh, catch fences, warning fences
Removal Techniques	Slope flattening, trimming, scaling
Reinforcement	Rock bolts, rock anchors, dowels, shotcrete, drainage, etc.

2.6 Slope Stability Studies in Ethiopia

In Ethiopia, slope failure is one of the recurring geological hazards that cause damage to infrastructure and human lives (Woldearegay, 2013; Bushira et al., 2018; Lamessa and Meten, 2021; Bekele and Meten, 2022; Mebrahtu et al., 2022; Tesfaye et al., 2023). Hence, several researchers have conducted all over the country to analyze the stability of the slope.

Mebrahtu et al. (2022) conducted stability modeling for the Debre Sina area using LEM and FEM. This study has identified large-scale slope failure controlled by faults and saturation and seismic condition. Moreover, this study showed LEM overestimates the stability of heterogeneous slope in which large-scale failure surface is involved. In general, this study has recommended the use of integrated LEM and FEM for modeling slopes with complex slope geometry and heterogeneous materials.

Bushira et al. (20180 also analyzed the stability of Cut soil slope stability analysis along the National Highway at Wozeka–Gidole Road using LEM and FEM. This study showed that the results of LEM and FEM are in very close agreement for slope with simple geometry. In addition, this study demonstrated that LEM techniques such as Bishop, Janbu, Morgenstern-Price, GLE, and Spencer methods yield in most cases identical FOS for the circular mode of failure. However, the ordinary method may underestimate the FOS by 5 to 6%. Moreover, this study also showed that the application of a single slope stabilization technique is ineffective in most slopes.

Lamessa and Meten (2021) also conducted a stability analysis of the rock slope along the road section of Gutane Migiru town to the Fincha sugar factory using kinematics and LEM. This study has identified planar and wedge modes of rock slope failures along the selected road section. This study has branded rainfall as the major causative factor for slope failure along this road. Moreover, Tesfaye et al. (2023) also analyzed the stability of rock slopes along Woliso to Wonchi Lake road using kinematics and LEM. This study also identified planar and wedge failure, and designed rock bolts and shotcrete to stabilize unstable rock blocks.

In addition, Jemal (2005), Samuel (2011), Kasahun (2014), and Bekele and Meten (2022) conducted slope stability analysis mainly via LEM. All of these studies have shown that slope failure takes place under saturated and dynamic conditions. Hence, rainfall was designated as a major causative factor for slope failure by these studies.

CHAPTER THREE

3. METHODS AND MATERIALS

3.1 Introduction

In this study, slope stability analysis has been conducted using Kinematic analysis, Limit Equilibrium, and Finite Element Methods. Data for the analysis were gathered through a detailed literature review, field surveying and testing, and laboratory testing of soils and rocks. In the following sections, data acquisition, processing, and stability analysis techniques will be discussed.

3.2 Desk Study

At this stage, the study area was first studied based on available geological, geotechnical, and topographical data. A preliminary analysis of the material property of the study area was done based on information obtained from available geological and engineering geological maps. The topographic nature of the study area was also studied based on information obtained from satellite imagery (i.e. Google Earth) and the Digital Elevation Model (DEM) to infer potential critical slope sections of the study area. Based on such information, detailed fieldwork was planned and executed to generate primary data.

3.3 Field Surveying

A detailed field surveying was conducted along the study area to identify critical slope sections and generate primary data for slope stability analysis or modeling. The critical slope sections were identified based on field indicators such as the condition of the slope toe, presence of failed rocks (Figure 3.1A), tilting of the slope face, development of tension crack, presence of release surface (Figure 3.1B), the orientation of discontinuity that favors slope failures and, others. Upon identification of critical slope sections, the geological units that constitute corresponding slope sections were determined. Afterward, the identified critical slope sections were classified into either structural controlled or non-structural controlled based on geological conditions. Accordingly, the slopes were classified as a structural controlled section if potential failure is assumed to take place along discontinuities. This type of failure mostly occurs on the slope of strong rocks with a slight degree of fracturing and weathering. On the contrary, the slopes were classified as non-structural controlled if soils and/or highly fractured and weathered rocks constitute them.

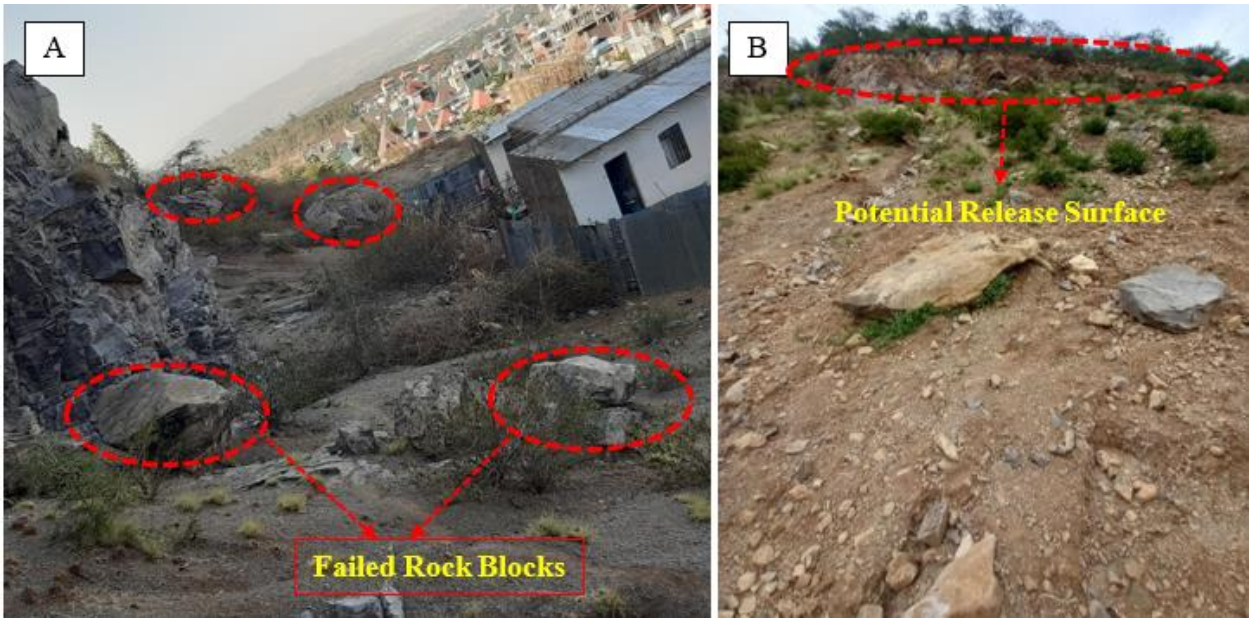

Figure 3. 1 Critical slope indicator A) Failed rock blocks and B) Release surface

3.3.1 Discontinuity Surveying

Upon classification of the slope section, a discontinuity survey was carried out to determine discontinuity parameters such as orientation, spacing, persistence, aperture, infill material, wall weathering, roughness, and groundwater condition following ISRM (1978) standards. Moreover, for structurally controlled slope sections, parameters such as dip amount and direction of the slope and upper face, bench width (if any), and occurrence of tension crack and its dip amount (if any) were also determined during this survey. Similarly, for non-structural controlled slope sections, the full geometry of the slope was also determined.

3.3.2 In-situ Strength Test

Intact rock strength (UCS) is one of the key factors in determining shear strength parameters, which in turn are used as input parameters for slope stability modeling. In this study, the UCS of the rocks is determined using the Schmidt hammer rebound test. ISRM (1978) and ASTM C 805 (2018) have forwarded guidelines for selecting the Schmidt hammer type and conducting the test. Accordingly, the former guideline recommended the use of L-type while the latter did not specify the hammer type. In this regard, Aydin (2009) suggested that N-type hammers are less sensitive to surface irregularities and are preferred for field surveys whereas L-type hammers are more sensitive to lower ranges and give better results for weak, weathered and porous rocks. Considering the surface irregularities of rocks of the study area, an N-type Schmidt hammer was used in this study following

the ASTM C 805 (2018) standard to acquire rebound values of the rock of the study area. Accordingly, the following procedures were followed as per ASTM C 805 (2018) for the acquisition of rebound values:

- The hammer was perpendicularly held against the test surface and progressively pushed to the rock (Figure 3.2) until the hammer gives an impact sound. When the hammer gives an impact sound, it was locked and the rebound value was recorded.
- Ten readings were taken at each test section with no two impact tests closer together than 25mm.
- When the hammer impact crushes or breaks the test surface, the reading was discarded and then, repeated at other locations.
- Finally, a representative rebound value was obtained by discarding the rebound values that differ from the average of 10 readings by more than 7 units and then by determining the average values of the remaining readings. Besides, the entire reading was discarded and the rebound values were determined at other nearby locations in case more than two readings differ from the average of 10 readings by more than 7 units.

The rebound values that were not acquired at an angle normal to the test surface are influenced by gravitational forces and need to be normalized with reference to the horizontal direction (ASTM, 2001; Aydin and Basu, 2005). In this study, since all rebound values were taken at an angle normal to the surface no corrections were applied to the representative value. Finally, the UCS of rocks of the study area was determined from the rebound value using Eq. 3.1. which was given by Barton and Choubey (1977).

$$\text{Log (10) UCS} = 0.00088\gamma R + 1.01 \qquad 3.1$$

Where UCS is uniaxial compressive strength in Mpa, γ is the dry unit weight of the rock in KN/m^3, and R is the representative rebound value.

Figure 3. 2 In-situ strength test of rock determination of rebound values.

3.3.3 Sampling

Representative rock and soil samples were collected from the critical slope sections for laboratory testing to determine input parameters for stability modeling. Accordingly, about five samples were taken from the critical slope section at different depth intervals (Table 3.1). At slope section SS1, in particular, two soil samples were taken considering variation in soil texture via visual observation. Based on field manifestation, the pumice of the critical slope was considered as a soil, and the sample was taken accordingly. Moreover, more than 20 rock samples were also taken from critical slope sections for the determination of unit weight.

Table 3. 1 Location of test pits and their corresponding sampling depths

No.	Slope Section	Sample I.D.	Easting	Northing	Sampling Depth (m)
1	SS1	SS1-A	532998	945418	1.8 – 2.2
2		SS1-B	532998	945418	2.4 – 2.6
3	SS2	SS2-A	533241	946570	1.4 – 1.8
4		PS1	533262	946581	1.2 – 1.5
5	SS3	SS2-A	533048	945862	1.4 – 1.7

3.4 Laboratory Test

Unit weight and shear strength parameters are among the most important parameters in slope stability analysis. Accordingly, to obtain these parameters, laboratory tests such as unit weight and direct shear tests were conducted for soils whilst unit weight tests were conducted for rocks.

3.4.1 Laboratory Test of Rocks

Unit weight test was conducted for rock samples using the buoyancy technique suggested by ISRM (1978). The test was conducted by weighing the rock specimens at their natural moisture content (M1) and then by determining their dry weight (M_d) after oven-drying the rock at 105^0C for 24 hours. Oven-dried rock specimens were then submersed into a cylinder filled with a known volume of water (V1) and the corresponding volume due to immersion of the rock specimen was noted as (V2). Afterward, the corresponding dry density (ρ_d) and dry unit weight (γ_d) of rock were determined using (Eq. 3.2 and 3.3) respectively.

$$\rho_d = \frac{M_d}{V_2 - V_1} \quad 3.2$$

$$\gamma_d = \rho_d * g \quad 3.3$$

The saturated unit weight (γ_{sat}) of the rocks was also determined by using a similar mechanism. However, during this determination, the rock sample was fully saturated by submerging them into the water for 24 hours to obtain saturated weight (M_{sat}). Afterwards, saturated unit weight (γ_{sat}) was determined using Eq. 3.2 by replacing M_d with M_{sat}.

3.4.2 Laboratory Test of Soils

The shear strength parameters and unit weight of soil are the predominant input parameters for the slope. Hence, in this study, unit weight and shear strength parameters of the soils were determined in the laboratory following ASTM D 3080 (1998) and ASTM D 7263 (2009) standards, respectively. For determining shear strength parameters, the direct shear test method was used. In this test, a known dimension of soil specimen was compacted and remolded at their natural moisture contents. The specimen was then subjected to a shear force loading system in the shear box to measure horizontal and vertical displacement. Afterward, the specimens were sheared at initial consolidation pressure of 100 kPa by applying horizontal shear load at a rate slow enough to allow pore water pressure to

dissipate until the specimens fall. The horizontal and vertical shear displacements at failure were then recorded. Afterward, part of the failed specimen was sampled for water content determination, and the test was repeated on the different specimens of the same soil at 200 and 300 kPa. Finally, from the test results, shear stress (τ) and normal stress (σ) were computed. Then, the values of shear stress (τ) and normal stress (σ) were then plotted on normal paper from which shear strength parameters (i.e. cohesion (c) and friction angle (ϕ)) were determined using Mohr-Coulomb Failure criteria.

3.5 Data Processing, Analyzation, and Interpretation

3.5.1 Determination of Shear Strength Parameters and Elastic Modulus of Rocks

The cohesion (C) and friction angle (ϕ) of discontinuities leading to planar, wedge, or toppling failures are crucial parameters for analyzing the stability of the slope using LEM (Wyllie and Norrish, 1996; Wyllie and Mah, 2004). Similarly, cohesion (C), friction angle (ϕ), and elastic modulus (E) are among the major input parameters for analyzing the stability of non-structural controlled slope sections (Wyllie and Norrish, 1996). Accordingly, in this study, the abovementioned parameters were separately determined for discontinuities (for structurally controlled slope sections) and for rock mass in the case of non-structural controlled slope sections using Rockdata software.

3.5.1.1 Determination of Shear Strength Parameters for Structural Controlled Slopes

The cohesion (C) and friction angle (ϕ) of discontinuities of non-structural controlled slope sections were determined using Barton and Bandi's (1990) non-linear failure criteria in the Rocdata software. This criterion uses parameters such as Joint Wall Compressive Strength (JCS), joint roughness, residual friction angle, slope height, and unit weight of rocks to determine cohesion and friction angle. The following procedures were followed in the Rocdata software to determine these parameters.

- JCS was determined by comparing UCS and the degree of weathering of wall rock. The JCS is equivalent to 50 % of UCS if the wall rock adjacent to the discontinuity is characterized by a moderate degree of weathering (Barton, 1976; ISRM, 1978; Sharma et al., 1999). Hence, in this study, JCS was determined using Eq. 3.4 and is given in Table 5.2.

$$\text{JCS} = 50\ \%\ \text{of UCS wall rock adjacent to discontinuity} \quad (3.4)$$

- Joint roughness was determined by comparing Barton and Choubey's (1977) standard roughness profile built in the Rocdata software to the existing roughness profile of discontinuities in the field.
- The residual friction angle (ϕr) was determined using Eq. 3.5 that was forwarded by Barton and Choubey (1977). In this calculation, a basic friction angle (ϕb) of 32.5 was used based on the study by Ulusay & Karakul (2015), and dry and wet Schmidt hammer rebound values were determined in the field using an N-type hammer.

$$\phi r = (\phi b - 20^0) + 20(r/R) \qquad 3.5$$

- The unit weight of the rock was determined using the buoyancy technique as stated in section 3.4.1 and is given in Table 5.4. The slope height was determined in the field using a tape meter.
- Finally, the shear strength parameter (i.e. C and ϕ) of the discontinuities were determined using Barton and Bandi's (1990) non-linear failure criteria. Figure 3.3 below shows a sample of shear strength parameters of discontinuity as determined using Barton and Bandi's (1990) non-linear failure criteria and detailed results are given in Appendix 1.

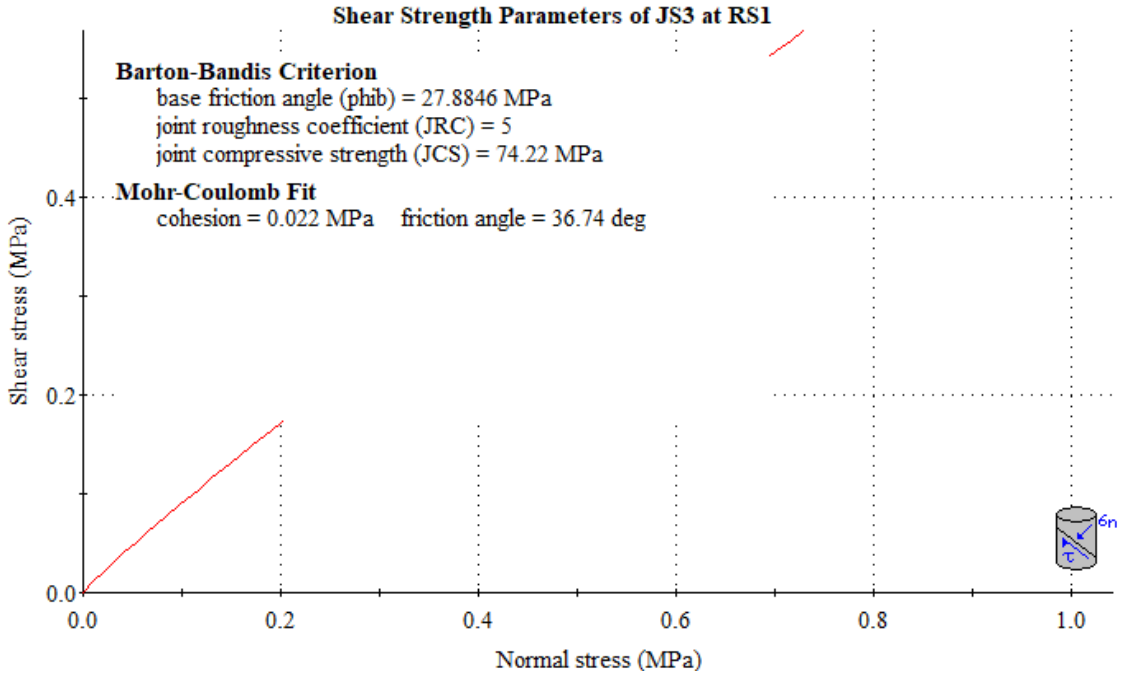

Figure 3. 3 A sample of shear strength parameters of discontinuity as determined using Barton and Bandi's (1990) non-linear failure criteria.

3.5.1.2 Determination of Shear Strength Parameters for Non-structural Controlled Slopes

The cohesion (C), friction angel (ϕ), and elastic modulus (E) of rocks of non-structural slope sections were also determined using Rockdata software (Rocdata 3.0 Rocscience, 2004) following generalized Hoek-Brown Failure criteria (Hoek et al., 2002). This criterion use parameter such as the Geological Strength Index (GSI), UCS of intact rocks, intact rock material constant (mi), disturbance factor (D), slope height, and unit weight of rocks to determine the abovementioned parameters. The following steps were followed in this criterion to determine these parameters.

- The Geological Strength Index (GSI) is determined in the field via a comparison of the standard GSI description (Appendix 3) provide in the Rockdata software (Rocdata 3.0 Rocscience, 2004) to the existing field condition.
- The UCS of intact rock was determined as stated in section 3.3.2 and the value is shown in Table 5.2 was used for this purpose.
- The material constant of intact rock (Mi) was adopted from Hoek (2007).
- The disturbance factor was estimated based on guidelines suggested by Wyllie and Mah (2004) as stated in the Rocdata software (Rocdata 3.0 Rocscience, 2004). Accordingly, the disturbance factor of 0.7 was used considering controlled blasting can create modest rock damage in the critical slope sections of the study area.
- The unit weight of rock was determined in the laboratory whilst slope height was determined in the field using a tape meter.
- Finally, the cohesion, friction angle, and modulus of deformation were determined using generalized Hoek-Brown Failure criteria. Figure 3.4 below shows a sample of shear strength parameters and modulus of elasticity as determined using Hoek-Brown Failure criteria. The detailed results are given in Appendix 2.

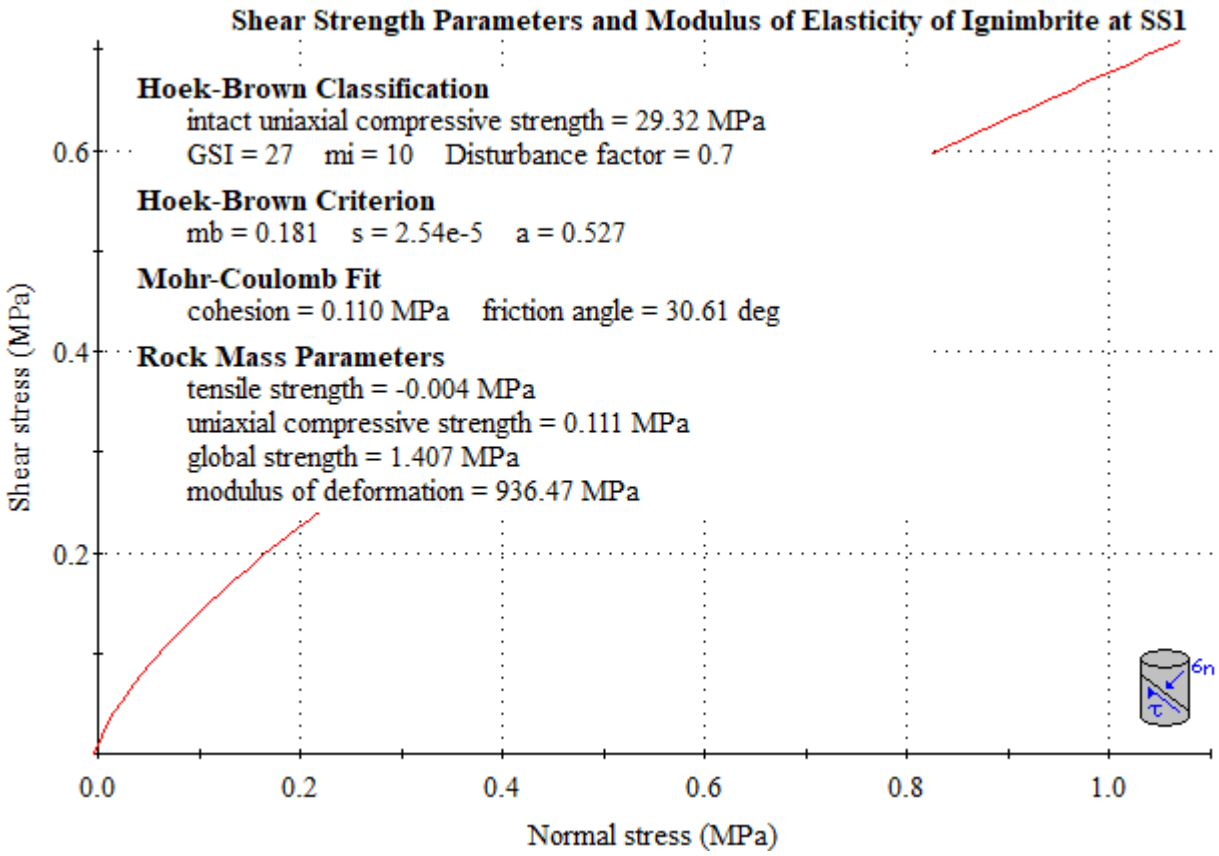

Figure 3. 4 A sample of shear strength parameters and modulus of deformation of the rock mass as determined using Hoek-Brown Failure criteria.

3.5.2 Elastic Modulus and Poisson Ratio of Soils and Rocks

The modulus of elasticity/deformation of rocks was determined as stated in section 3.5.1.2. On the other hand, the Poisson ratio (v) of rocks was determined using Eq. 3.6 forwarded by Vásárhelyi (2009) from input parameters such as GSI and intact rock material constant.

$$v = -0.002GSI - 0.003mi + 0.457 \quad 3.6$$

For soils, the modulus of elasticity was determined from corrected standard penetration (SPT) N using Eq. 3.7 or 3.8 as suggested by Begemann (1974). The corrected standard penetration (SPT) N was determined using Eq. 3.9 from friction angle (ϕ) of soils as forwarded by Japan Road Association (1990).

$$E = 1200(N + 6)\frac{KN}{m^2} \quad for\ N < 15 \quad 3.7$$

$$E = 4000 + 1200(N - 6)\frac{KN}{m^2} \quad for\ N > 15 \quad 3.8$$

$$\phi = (15N)^{0.5} + 15 \text{ for } \phi < 45^0 \quad 3.9$$

Similarly, the Poisson ratio of soils was estimated using Eq. 3.10 forwarded by Kulhawy & Mayne (1990).

$$v_d = 0.1 + 0.3(\frac{\phi-25}{20}) \qquad \text{For} \quad \phi < 45^{\circ} \qquad \text{Eq. 3.10}$$

3.5.4 Slope Stability Analysis

After the collection of all necessary data, stability modeling/or analysis was conducted using Kinematic, LEM, and FEMs depending on the type of slope section under consideration.

3.5.4.1 Stability Analysis/Modeling of Structural Controlled Slope Sections

3.5.4.1.1 Kinematic Modeling

For structurally controlled slope sections, the kinematic method was first used to identify the mode of rock slope failure/s with the aid of Dips 6.0 software. This software utilizes friction of angle of discontinuities (predefined failure plane), dip amount and dip direction of discontinuities, and slope as input parameters to identify the mode of failure. In this software, the input parameters are prepared and analysis was executed in the following way.

- The friction angle of discontinuity for the analysis will be determined using Barton and Bandi's (1990) non-linear failure criteria as stated in section 3.5.1.1.
- The dip amount and dip direction of discontinuities and the slope were determined during detailed field surveying.
- These input parameters were inserted into the software and the modeling was conducted by changing the analysis type to planar, wedge, and toppling.
- These possible modes of failures (i.e. planar, wedge, and toppling) were differentiated by identifying poles and/or joints that fall in the critical zone of the planar, wedge, and toppling failure, respectively.

3.5.4.1.2 LEM Modeling

In this study, only two modes of rock slope failures namely planar and wedge modes of failures were identified using the kinematic method. The further stability of these modes of failures was then determined using LEM in terms of FOS. Accordingly, the FOS for the planar mode of failure was then determined using LEM-based Rocplane 2.0 software (Rocplane 2.0 Rocscience, 2004) based on the study by Hoek & Bray (1981) and Sharma et al. (1995). Similarly, the FOS for wedge mode of failure was also determined using

LEM based approach developed by Hoek & Bray (1981) using Swedge 4.0 software (Swedge 4.0 Rocscience, 2004). Both software uses the orientation of discontinuities, slope geometry, unit weight of rocks, and shear strength parameters of discontinuities as input parameters (Table 5.8 for planar and Table 5.10 for wedge modes of failure) to determine the FOS. In this study, the orientation of discontinuities and geometry of the slopes were determined in the field during surveying. The unit of rocks was determined using buoyancy techniques suggested by ISRM (1978). The shear strength parameters of the discontinuities were determined using Rocdata software (Rocdata 3.0 Rocscience, 2004) as stated in Section 3.5.1.1. Finally, FOS was determined for both modes of failures under static dry, static saturated, dynamic dry, and dynamic saturated conditions. For dynamic conditions, a horizontal seismic acceleration of 0.1g was adopted from the study by EBCS (1995). Similarly, mid-height peak pore-water pressure with 100 % filling was used during saturated conditions.

3.5.4.2 Stability Analysis/Modeling of Non-structural Controlled Slope Sections

The stability modeling of non-structural controlled slope sections (i.e. slope constituted by soils and/or highly weathered rocks) was conducted using LEM and FEMs. LEM modeling was conducted using Slide 6.0 software (Slide 6.0 Rocscience, 2004) as per the Mohr-Coulomb strength criterion. This software uses input parameters (Table 5.14) such as slope geometry, unit weight, and shear strength parameters to determine the stability of the slope in terms of FOS. In this study, the geometry of the slopes was determined in the field using a tape meter and GPS while the unit weight of rock and soils were determined in the laboratory. The shear strength parameters were determined using a direct shear test for soil while they were determined using Rocdata software (Rocdata 3.0 Rocscience, 2004) for rock as stated in Section 3.5.1.2. Upon determination of these input parameters, the following procedures were followed in the Slide 6.0 software:

- The geometry of the slope was drawn using the ‘External Boundary’ tool. Afterward, the material boundary was drawn inside slope geometry using the ‘Material Boundary’ tool.
- Material properties such as unit weight and shear strength parameters were inserted into the software.
- GLE/Morgenstern-Price methods was used to determine FOS as it utilize both force and moment equilibrium to determine the FOS as suggested by Abramson et al. (2002).

- Upon selection of the analysis technique (i.e. GLE), Auto Grid Search Method was used for determining the minimum slip surface corresponding to FOS.
- Finally, the modeling was conducted under static dry, dynamic dry, static saturated, and dynamic saturated conditions.

LEM, however, does not consider stress acting on the slope during the stability modeling (Jing, 2003; Abd El-Latif, 2012; Bar et al. 2019). Nonetheless, stress can significantly contribute to the instability of some slopes. Moreover, in the LEM, the shape of the slip surface is predetermined as circular or near circular while in reality, it could be otherwise (Jing, 2003). In the FEM, however, the stress condition of the slope can be considered and potential failure can take any shape based on existing field conditions (Stianson et al., 2015). Hence, in this study, FEM was also used to determine the stability of the slope with the aid of Phase V 2.0 software (Phase V 2.0 Rockscience, 2004). This software uses the same input parameters as LEM-based Slide 6.0 software except for two additional parameters namely Poisson ratio and Young's modulus. In this study, these two parameters were determined using the procedures stated in Section 3.5.2. Finally, likewise LEM, the modeling was conducted under static dry, dynamic dry, static saturated, and dynamic saturated conditions to determine SRF. Later, SRF obtained from this was compared with FOS obtained from LEM for interpretation of the results.

In general, the general methodology followed in this research work is given in Figure 3.5.

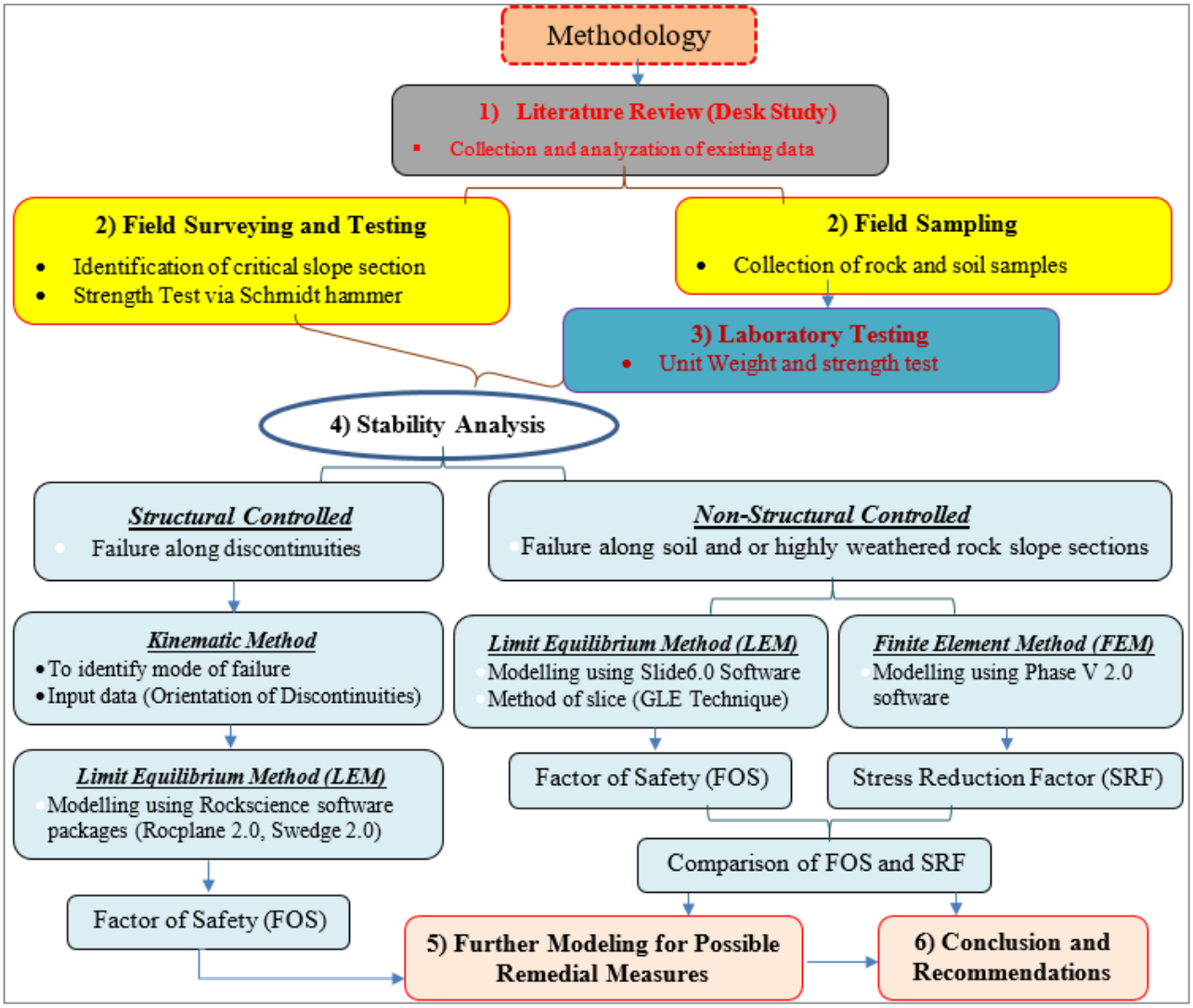

Figure 3. 5 Flow Chart showing research methodology.

CHAPTER FOUR

GEOLOGY OF THE STUDY AREA

4.1 Regional Geology

Regionally, the study area is located in the Northern Main Ethiopian Rift (NMER) within the Nazret-Dera area. The Nazret-Dera area represents the bridge zone between two right-stepping north-northeast trending sets of normal faults belonging to the Wonji Fault Belt (Boccaletti et al., 1999). The geology of this Nazret-Dera area has been well-studied by Damte et al. (1992) and Boccaletti et al. (1999). Accordingly, Nazret, Boku-Tede, Bofa, Dera-Sodere, and Wonji units are the most dominant lithostratigraphic units within the study area and its vicinities (Figure 4.1).

The Nazret unit consists of a sequence of ignimbrite sheets interbedded with palaeosols layers (Meyer et al., 1975) indicating frequent break up in the volcanic activity in the area (Boccaletti et al., 1999). The ignimbrite rocks of the Nazret series are frequently strongly welded at the base and un-welded at the top. The Boku-Tede unit overlies the Nazret unit and is associated with the collapse of a huge caldera called the Boku Caldera (Morton et al., 1979). This unit mainly comprises alkaline and per-alkaline rhyolite lava domes, flows, and pyroclastic falls, which cover the rift floor-complex ignimbrite deposits (Damte et al., 1992; Boccaletti et al., 1999). Radiometric age of this unit range from 0.83 Ma to 0.51 Ma (Morton et al., 1979). The Bofa unit overlies the Boku-Tede unit and mainly comprises mafic lava flows of dominantly fissural origin (Boccaletti et al., 1999). This unit mainly consists of transitional basalt with subordinate alkaline basalts having porphyritic texture. The radiometric ages determined from rocks of this unit range from 0.61 to 0.44 Ma (Morton et al., 1979).

Among the lithostratigraphic units of the Nazret-Dera area, the Dera-Sodere unit is the most widespread unit containing an ignimbrite sheet covering about 400 km^2 of the area (Damte et al., 1992; Boccaletti et al., 1999). It overlies the Bofa unit and is characterized by thin layers of un-welded to poorly welded ash containing small, scattered rounded pumice clasts and lithic fragments. It is mainly exposed in the southwest of Adama town. The Wonji unit is one of the youngest lithostratigraphic units in the area and consists of spatter and cinder cones associated with alkali basaltic lava flows which were erupted through several emission centers (Damte et al., 1992). These cones are mainly distributed in the SE and SW of Adama town.

4.2 Regional Structures

The regional structural geology of the study is primarily controlled by the NNE-SSW to N-S trending, right-stepping en-echelon fault system (i.e. the Wonji Fault Belt: WFB) (Boccaletti et al., 1999). According to Meyer et al. (1975), the WFB faulting started developing at the beginning of the Early Pleistocene (1.6 Ma ago), causing the important unconformity occurring between the 'Wonji Series' (Pleistocene-Holocene) and the underlying 'Nazreth Series', whose more recent products are about 1.8 Ma (Bigazzi et al., 1993).

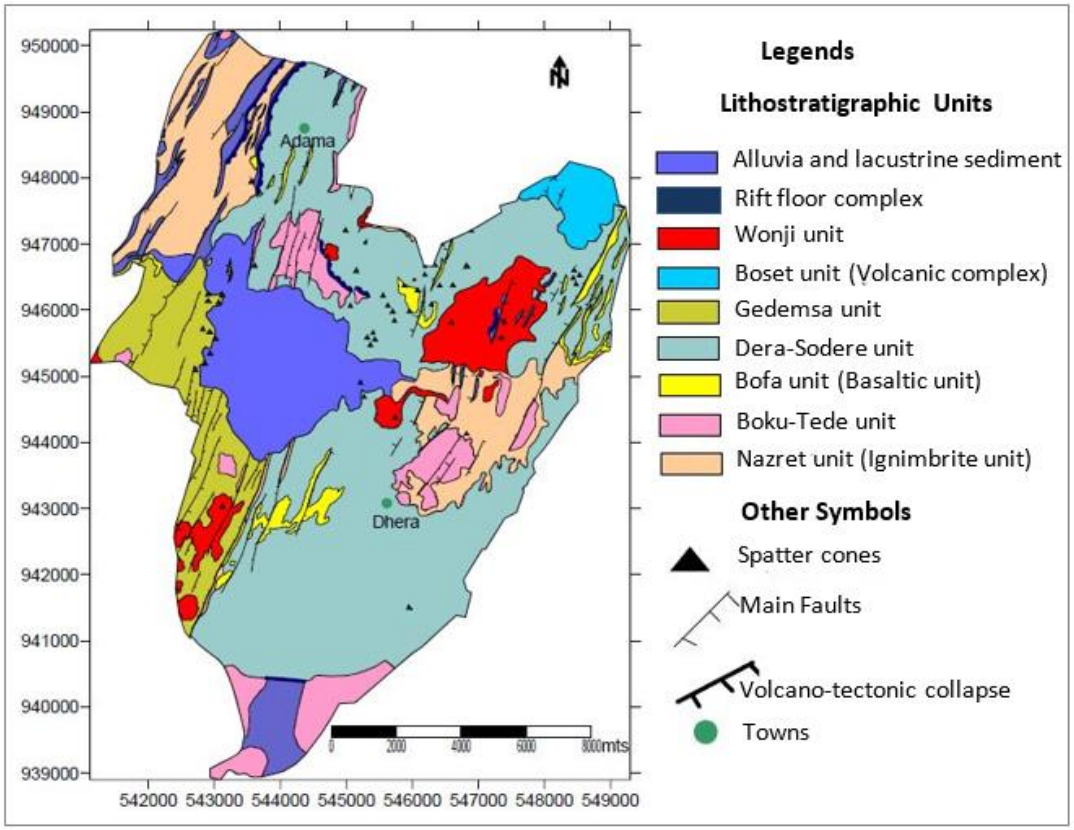

Figure 4. 1 Regional geological of the study area (Nazret-Dera area) (Modified after Damte et al., 1992).

4.3 Local Geology and Structures

Based on a study by Damte et al. (1992), the entire study area is mapped as a Dera-Sodera unit (Figure 4.1). The Dera-Sodera unit dominantly consists of an ignimbrite sheet with some rhyolite and basaltic flows, and pyroclastic deposits (Damte et al., 1992; Boccaletti et al., 1999). Moreover, Chemeda (2020) mapped quaternary sediment, ash with pumice, scoria, ignimbrite, rhyolite, and basalts (Figure 4.7). In this study, quaternary sediment,

pumice, and ignimbrite rocks are mapped in the critical slope sections. Hence, in the following section these geological units and structures of the critical slope sections.

4.3.1 Ignimbrite

This rock is the most widely exposed in all critical slope sections of the study area. In the study area, it is characterized by its grey color and aphanitic to eutaxitic texture (texture produced by the presence of fiamme). Moreover, it is also characterized by a moderate to high degree of weathering and fracturing (Figure 4.2) and is exposed forming a steep ridge oriented in the NNE-SSW direction. The structurally controlled critical slope sections of the study area are associated with moderately weathered ignimbrite while non-structural controlled critical sections are dominantly associated with highly weathered ignimbrite.

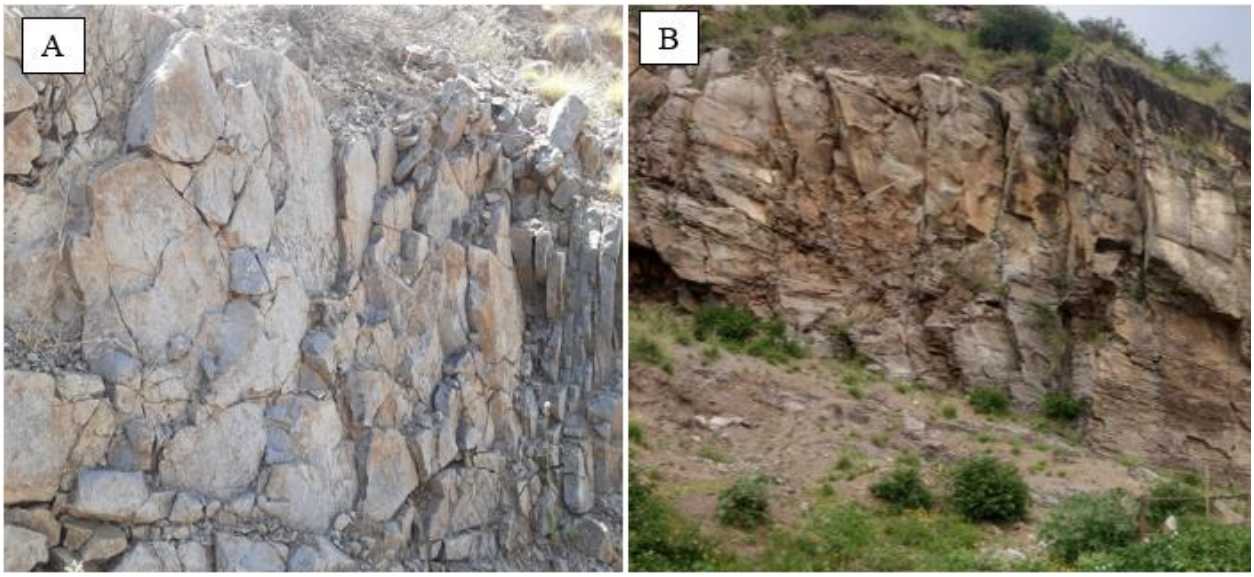

Figure 4. 2 A) Highly weathered and fracture ignimbrite and B) moderately weathered and fractured ignimbrite

4.3.2 Pumice

This geological unit is exposed in a small portion of the study, particularly along critical slope section SS2. It has a light grey color and vesicular texture (Figure 4.3). In the study area, this unit has been converted into the soil due to intensive weathering. Field investigation revealed that this unit is sandwiched between ignimbrite units in the study area.

Figure 4. 3 Pumice along critical slope section SS2.

4.3.3 Soil Deposit

Based on field conditions, there are three types of soil deposits in the study area. These include residual, eluvium, and colluvium soil deposits. The residual soils found in the present study area are originated from parent materials such as pumice and ignimbrite rocks (Figure 4.4A). Colluvium deposits are weathered materials that are transported by gravity and occasionally by water and that are deposited at the toe of the slope. In the study area, this deposit is outcropped at the toe of the Dibibisa ridge and it comprises grain of variable grain size ranging from clay to gravel (Figure 4.4B). Eluvium deposits are soils that formed from in-situ weathering of parent rock and which are not moved far away from their place of origin. Accordingly, in the study area, this deposit is outcropped on a steep slope on ignimbrite rock.

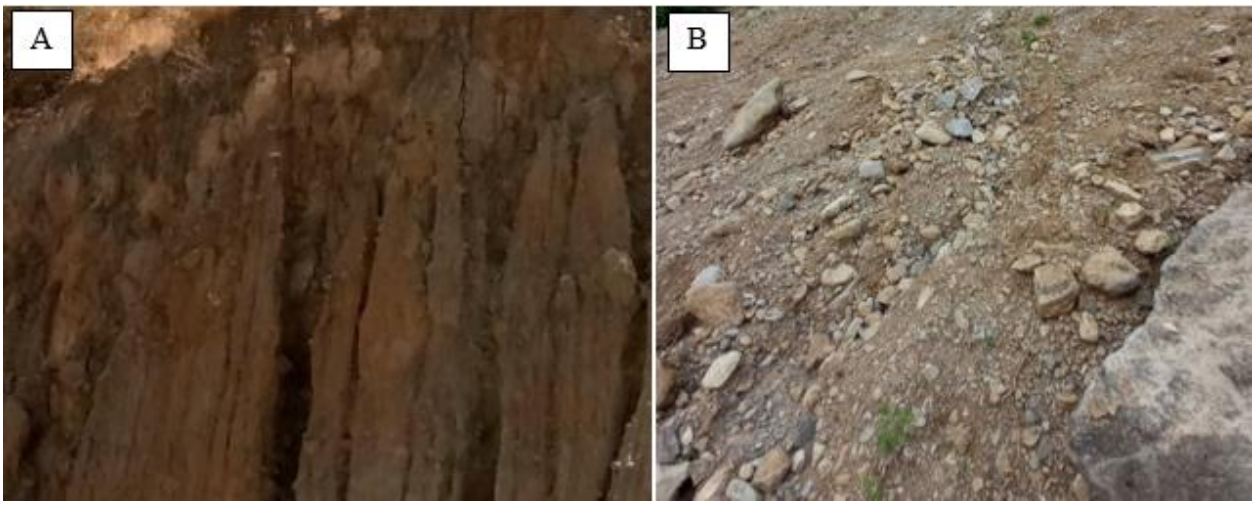

Figure 4. 4 A) Residual soil and B) colluvium soil deposits of the study area.

4.4 Geological Structures

Secondary geological structures are a common cause of slope failure (Raghuvanshi et al., 2017). Accordingly, in the study area, secondary geological structures such as joints and faults were identified.

4.4.1 Joints

The failure of structurally controlled critical slope sections is primarily controlled by the presence of persistent joints. In the study area, joints are characterized by open-to-tight openings, open-to-partially-filled infill properties, close-to-wide spacing, and high persistence continuity conditions. The orientation of joints of the study area was analyzed using Dips 6.0 (Dip6.0 Rocscience, 2004) and results showed the joints are oriented in NNE-SSW direction (Figure 4.5).

4.4.2 Faults

Information obtained from satellite imagery and 30m resolution SRTM DEM were used to infer and delineate major faults within and around the vicinity of the study area. Accordingly, the study results showed that there exists a major fault along the Dibibisa ridge and it dips in the western direction with a strike in the NNE-SSW direction. Moreover, there are also small faults in the study area that also strikes in the NNE-SSW direction (Figure 4.6).

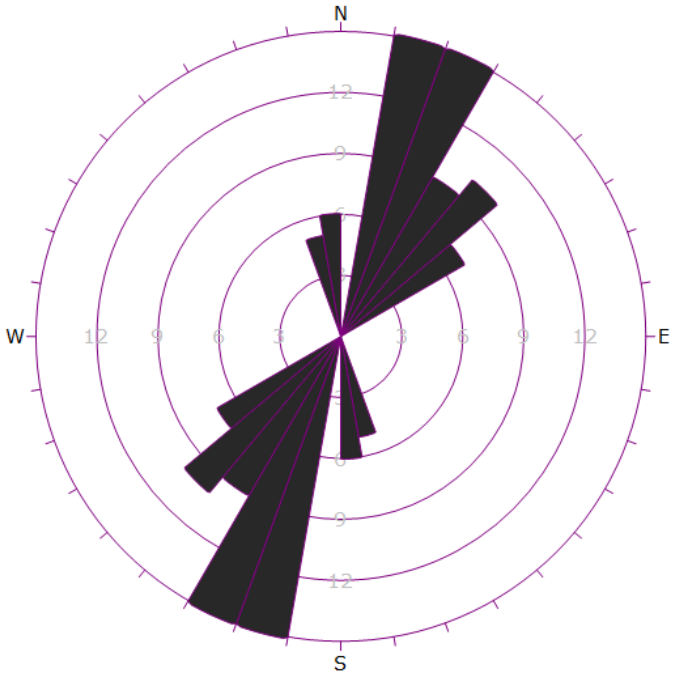

Figure 4. 5 Rosset diagram of discontinuity strikes plotted by dip.6.00 software

Figure 4. 6 Minor faults in the study area.

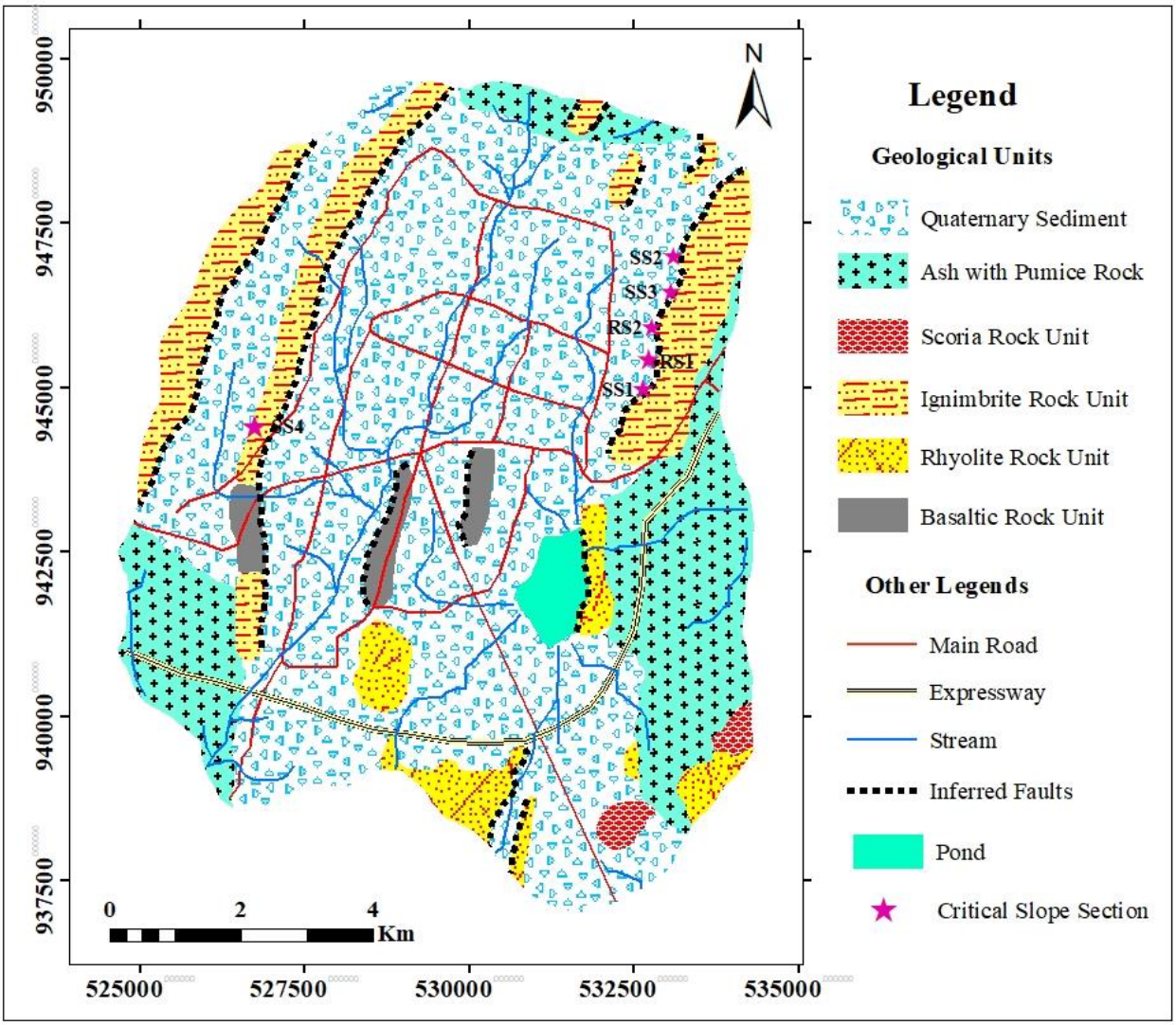

Figure 4. 7 Local geological map of the study area at a scale of 1: 10000 (After Chemeda, 2020).

CHAPTER FIVE

5. RESULTS AND DISCUSSION

5.1 Identification of Critical Slope Sections

A detailed field investigation was conducted to identify critical slope sections and acquire data that can be used for slope stability analysis. The critical slope sections were identified based on field manifestation such as the removal of slope toe, development of tension cracks, bulging of slope face, and adversely oriented discontinuity that favors rock slope failures. Accordingly, about two structurally controlled and four non-structural controlled slope sections were identified (Table 5.1).

Table 5. 1 Critical slope sections identified during a detailed field investigation.

Slope Section	Location		Brief Description of the Identified Critical Slope Section
	E	N	
Structural Controlled Slope Sections			
RS1	532996	945491	A slope section constituted by moderately weathered ignimbrite
RS2	533004	945559	A slope section constituted by moderately weathered ignimbrite
Non-Structural Controlled Slope Sections			
SS1	532998	945418	A slope section with a relatively large scarp face with a nearly circular shape constituted by eluvium deposit on top of ignimbrite
SS2	533241	946570	A critical slope section constituted by eluvium soil deposited on top of ignimbrite rock
SS3	533048	945862	A critical slope section constituted by eluvium soil, pumice, and ignimbrite rocks.
SS4	527164	944594	A critical slope section constituted by moderately to highly weathered ignimbrite rock

5.2 Engineering Geological Characterization of Rocks

5.2.1 Uniaxial Compressive Strength (UCS)

The Uniaxial Compressive Strength (UCS) of the rocks of the critical slope sections was determined from rebound values acquired from the N-type Schmidt hammer test in the field. The UCS was determined from representative rebound value using Eq. 3.1 forwarded by Barton and Choubey (1977). Table 5.2 below presents some representative UCS of rocks in the study area.

Table 5. 2 Average Schmidt hammer rebound value (R) at critical sections of rock slope and their corresponding UCS

Slope Section	Joint Sets	Average or representative rebound value as per ASTM C 805 (2018)	Unit Weight kN/m^3	UCS (MPa)	JCS (MPa)
Structural Controlled Slope Section					
RS1	JS1	52.0	26.40	165.22	82.610
	JS2	49.3	26.40	143.00	71.500
	JS3	50.0	26.40	148.45	74.225
RS2	JS1	50.5	25.03	132.54	66.270
	JS2	48.0	25.03	116.75	78.375
Non-structural controlled Slope sections					Average UCS (MPa)
SS1	HW Ignimbrite	24.5	22.88	31.84	29.32
		20.8	22.88	26.79	
SS2	HW Ignimbrite	20.8	20.59	24.37	22.76
		17.4	20.59	21.14	
SS3	HW to MW Ignimbrite	34.2	20.87	43.45	43.90
		34.7	20.87	44.36	
SS4	HW Ignimbrite	18.6	21.50	23.01	24.97
		22.2	21.50	26.92	
	HW to MW Ignimbrite	25.8	22.26	32.73	43.15
		36.7	22.26	53.57	
MW-Moderately Weathered, HW- Highly Weathered					

The study results showed that the UCS of rocks of structurally controlled slope sections ranges from 116.75 MPa to 165.22 MPa for the ignimbrite rock and from 21.14 MPa to 53.57 MPa for non-structural controlled slope section Moreover, based on the classification of rocks from UCS forwarded by ISRM (1978), the rocks in the structurally controlled slope section are classified as a very strong rock.

5.2.2 Rock Quality Designation (RQD)

In this study, since there are no core rock samples, the RQD was determined in the field based on the Volumetric Joint Count Method. In the study area, the rocks of non-structural controlled slope sections are mainly covered by colluvium soils. Hence, the RQD was only determined for rocks' structural controlled slope sections. Accordingly, the Volumetric Joint Count (Jv) of rocks' of structurally controlled slope sections was first determined from the average spacing of joint sets using Eq. 2.3. Afterward, the RQD of rocks was determined using Eq. 2.2 suggested by Palmstrom (2005). The result showed that the ignimbrite at the critical slope sections has RQD values in the order of 72.25 % to 82.00% respectively (Table 5.3).

Table 5. 3 RQD of rocks of the study area at structural controlled slope sections.

Slope Section	Rock Type	Jv	RQD (%)	Deer and Deere(1988) RQD Classification
RS1	Ignimbrite	11.2	82.00	Good
RS2	Ignimbrite	15.1	72.25	Good

5.2.3 Unit Weight of Rocks

The unit weight of the rock is one of the major parameters in slope stability analysis. Moreover, it is one of the parameters during the determination of UCS of intact rocks from Schmidt hammer rebound value. In this study, the unit weight of rocks in the study area was determined using the buoyancy technique in the laboratory. Accordingly, the test result showed that the unit weight of rocks in the study area varies from 24.75 kN/m^3 to 25.30 kN/m^3 (Table 5.4).

Table 5. 4 A Unit weight of rocks in the study area

	Structural Controlled							
Slope section	Rock Type	Unit weight	Mass(g)	V1(ml)	V2 (ml)	V2-V1 (ml)	ρ= (g/cm^3)	Average γ (kN/m^3)
RS1	Ignimbrite	γ_{dry}	86.4	150.0	186.0	36.0	2.400	24.75
			102.2	150.0	190.0	40.0	2.550	
		γ_{sat}	105.7	150.0	192.0	42.0	2.520	25.30
			120.5	200.0	247.5	47.5	2.540	
RS2	Ignimbrite	γ_{dry}	90.5	150.0	186.5	36.5	2.479	24.79
			110.4	200.0	244.5	44.5	2.480	
		γ_{sat}	92.6	150.0	187.0	37	2.503	25.13
			85.8	150.0	184.0	34	2.523	
Non-Structural Controlled								
SS1	Ignimbrite	γ_{dry}	80.8	150.0	184.5	34.5	2.342	22.88
			115.0	150.0	201.5	51.5	2.233	
		γ_{sat}	96.8	150.0	192.0	42.0	2.304	23.31
			82.5	150.0	185.0	35.0	2.357	
SS2	Ignimbrite	γ_{dry}	75.0	150.0	186.0	36.0	2.083	20.59
			87.5	150.0	193.0	43.0	2.034	
		γ_{sat}	68.5	150.0	182.0	32.0	2.140	21.85
			75.8	150.0	184.0	34.0	2.229	
SS3	Ignimbrite	γ_{dry}	110.0	150.0	199.0	49.0	2.244	20.87
			125.5	150.0	215.0	65.0	1.930	
		γ_{sat}	74.5	150.0	185.0	35.0	2.128	22.07
			64.0	150.0	178.0	28.0	2.285	
SS4	Ignimbrite-A	γ_{dry}	130.0	200.0	258.4	58.4	2.226	22.26
		γ_{sat}	95.6	200.0	239.2	39.2	2.438	24.38
	Ignimbrite-B	γ_{sat}	105.8	200.0	249.2	49.2	2.150	21.50
		γ_{dry}	117.3	200.0	250.4	50.4	2.327	23.27
Note: At SS4, Ignimbrite-A (moderately to highly weathered) was taken from the bottom slope profile while Ignimbrite-B (Highly Weathered) was taken from the middle slope profile								

5.2.4 Rock Mass Rating (RMR)

The quality of rock mass at structurally controlled slope sections was determined using Bieniawski's (1989) basic Rock Mass Rating (RMR) system. The Schmidt hammer-based UCS of intact rocks (Table 5.2), Volumetric Joint Method derived RQD (Table 5.3), field-determined condition and spacing of discontinuities, and groundwater were used as input parameters following the guidelines of this system. The analysis of the result showed that the ignimbrite rock of the study area is classified as Good rock at RS1 while it is classified as Fair rock at RS2 (Table 5.5).

Table 5. 5 Rock mass classification based on RMR system at structural controlled slope sections.

Parameters		Structural Controlled Slope Sections			
		RS1	Rating	RS2	Rating
UCS (MPa)		152.07	12	124.65	12
RQD (%)		82.00	17	72.25	13
Joint spacing (cm)		250	20	20	10
Condition of Joints	Persistence(m)	>20	0	>20	0
	Aperture(mm)	75	0	16.5	0
	Filling	Partially open	0	Partially filled with soil	0
	Roughness	Slightly rough	3	Slightly rough	3
	Degree weathering	Moderately	3	Moderately	3
Groundwater Condition.		Damp	10	Damp	10
RMR		65		51	
Class		Good Rock		Fair Rock	

5.3 Slope Stability Analysis of Rock Slope (Structural Controlled)

5.3.1 Kinematic Analyses

Slope stability modeling of structurally controlled slope sections was first determined using kinematic analysis via pole data stereographic projections to determine the mode of rock failure. This modeling was conducted using Dips 6.0 software (Dips 6.0 Rocscience, 2004) based on procedures forwarded by Hoek & Bray (1981) and Wyllie & Mah (2004) from input parameters listed in Table 5.6. The input data for the analysis such as the orientation of discontinuities and slope face were determined during detailed fieldwork. Similarly, the friction cone (Table 5.6 and Appendix 1) was determined using Rockdata 3.0 software (Rocdata 3.0 Rocscience, 2004).

Table 5. 6 Input parameters for kinematics analysis.

Slope sections	Joint set and its parameter						Slope face parameters		Friction cone
	JS1		JS2		JS3				
	D	DD	D	DD	D	DD	D	DD	
RS1	46	320	58	130	76	262	80	257	39.02
RS2	64	115	48	255			78	240	28.69
D= Dip Amount, DD= Dip Direction									

From the modeling results, both RS1 and RS2 are admissible for both planar and wedge modes of failures. The planar mode of failure was distinguished in the Dip 6.0 software by determining the pole of joint sets that fall in the critical zone of planar failure as highlighted in red color in Figure 5.1. According to modeling results, the planar mode of failure was identified at slope section RS1 due to JS3 whereas it occurred due to JS2 at RS2 (Figure 5.1 A). Similarly, the wedge mode of failure was identified in the Dips 6.0 software by differentiating the intersection of joints that fall in the critical zone of wedge failure. Accordingly, this mode of failure was identified due to the intersection of JS1 and JS3, and JS2 and JS3 at slope section RS1. Similarly, this mode of failure was identified due to the intersection of JS1 and JS2 with potential failure along 174^0 at RS2.

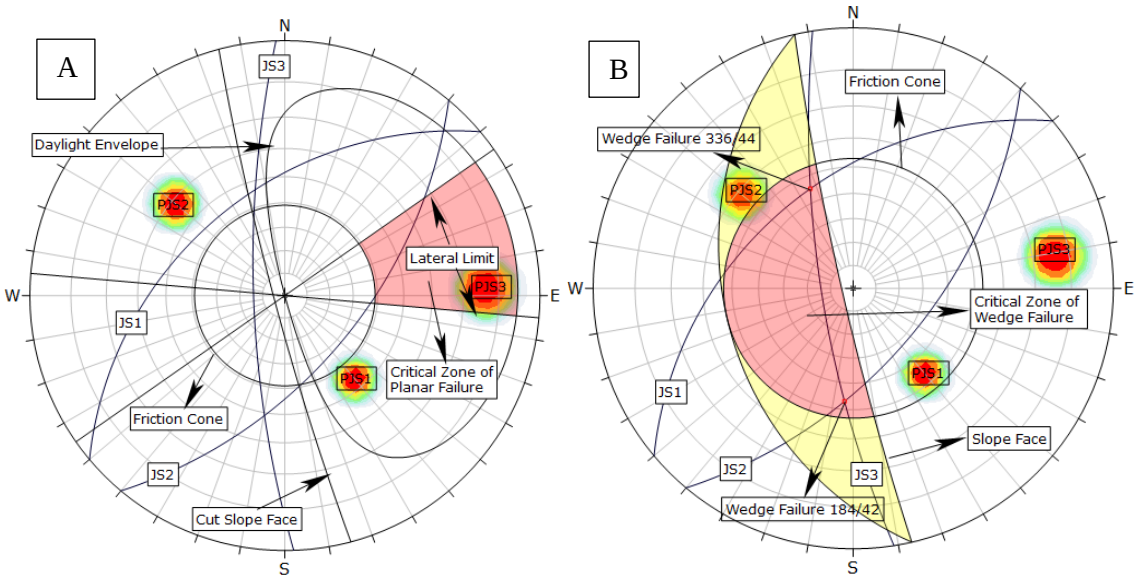

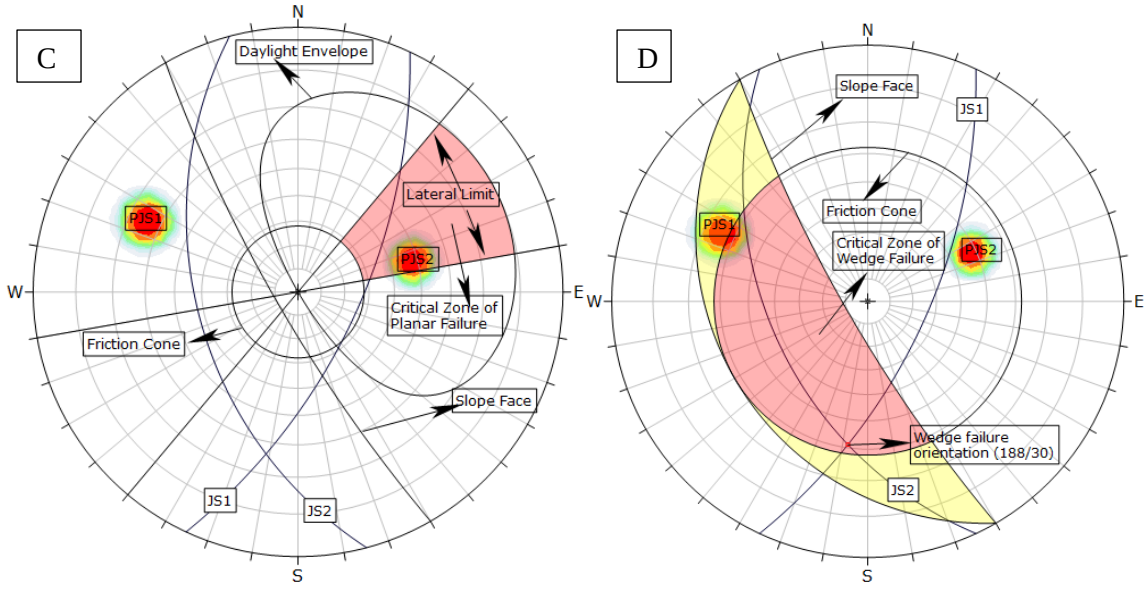

Figure 5. 1 Stereographic projection that shows a different mode of rock slope failures. A) Planar failure, B) Wedge failure at RS1, C) planar failure, and D) wedge failure at RS2.

Table 5. 7 The result of the kinematic analysis

Slope Sections	Possible mode failure based on kinematic analysis
RS1	Planar mode of failure due to JS3
	Wedge mode of failure due to the intersection of JS1 and JS3
	Wedge mode of failure due to the intersection of JS2 and JS3
RS2	Planar mode of failure due to JS2
	Wedge mode of failure due to the intersection of JS1 and JS2

5.3.2 Rock Slope Stability Modeling Using LEM

The kinematic modeling revealed that the identified critical rock slope sections are subjected to planar and wedge modes of failure (Figure 5.1 and Table 5.7). In this section, further stability analysis of these two modes of failure will be conducted by using LEM to determine the stability of the slope in terms of FOS.

5.3.2.1 LEM Modeling of Planar Failure

The kinematic modeling revealed that RS1 and RS2 are unstable for planar failure due to JS3 and JS3, respectively (Figure 5.1). The modeling of this mode of failure in terms of FOS was done by using LEM-based Rocplane 2.0 software (Rocplane 2.0 Rocscience, 2004) based on the study by Hoek & Bray (1981) and Sharma et al. (1995). The analysis was done under four projected conditions (i.e. static dry, dynamic dry, static saturated, and dynamic saturated conditions) from input parameters listed in Table 5.8.

Table 5. 8 Input parameters for RocPlane software based on Barton- Bandis (1990) failure criterion.

Slope section	Input parameters for RocPlane V. 2.0										
	JS	Slope geometry						Strength		Force	
		Sa (^{0})	Sh (m)	γ (t/m^3) d/s	Fpa (^{0})	W (^{0})	Ufa (^{0})	C (t/m^2)	Φ (^{0})	γw (t/m^3)	αs
RS1	JS3	80	30	2.52/2.58	76	4	15	2.243	36.74	1	0.1
RS2	JS2	78	32	2.53/2.56	48	6	10	1.019	27.57	1	0.1
JS= Joint set, Sa= slope angle, Sh= slope height, γ= unit weight, Fpa= failure plane angle, W= waviness, Ufa=upper face angle, c= cohesion, Φ= friction angle, γw= unit weight of water,s=saturated, d=dry αs = seismic coefficient.											

LEM-based Rocplane 2.0 software revealed that JS3 of RS1 has FOS in the order of 1.07, 0, 0.96, and 0 during static dry, static saturated, dynamic dry, and dynamic saturated conditions, respectively (Table 5.9 and Figure 5.2). According to Wyllie and Norrish (1996), Wyllie & Mah (2004), and Christian (2004), FOS less than 1, greater than 1, and equal to 1 indicate unstable, stable, and slope in the brink of failure, respectively. Hence, JS3 of RS1 is only stable (i.e. FOS > 1) during current or static dry condition, and unstable (i.e. FOS < 1) during remaining conditions. The modeling results have also shown that saturated conditions have much lower FOS than dry conditions (Table 5.9). According to Raghuvanshi et al. (2017), intensive rainfall or saturation can significantly increase pore water pressure along the failure planes thereby leading to slope failure with much lower FOS during wet seasons as compared to dry seasons. Thus, the low FOS of planar failure of RS1 during saturated conditions is attributable to the high pore-water pressure generated during rainy seasons.

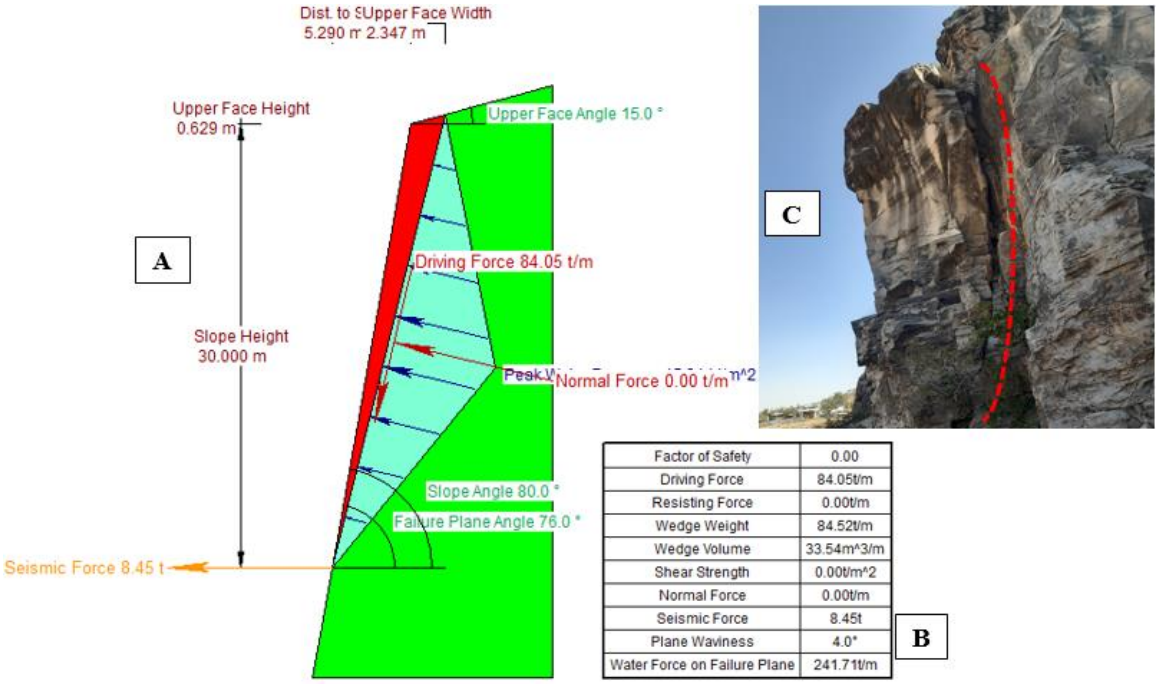

Factor of Safety	0.00
Driving Force	84.05t/m
Resisting Force	0.00t/m
Wedge Weight	84.52t/m
Wedge Volume	33.54m^3/m
Shear Strength	0.00t/m^2
Normal Force	0.00t/m
Seismic Force	8.45t
Plane Waviness	4.0°
Water Force on Failure Plane	241.71t/m

Figure 5. 2 A) 2D view of the planar mode of failure due to JS3 dipping at RS1, B) Summary of Rocplane 2.0 software for JS3 during dynamic saturated conditions, and C) Existing field condition

Moreover, the planar modeling revealed that JS2 of RS2 is unstable (i.e. FOS < 1) during all projected conditions (Table 5.9 and Figure 5.3). According to Raghuvanshi (2017) and Tesfaye et al. (2023), the majority of slope failure takes place during intensive rainfall/or saturation and during the presence of seismic activity. Nevertheless, the planar failure due to JS2 of RS2 is unstable even with the absence of saturation and seismic activity. Hence, apart from saturation, planar instability of this slope section is also primarily controlled by factors such as slope geometry and failure plane properties.

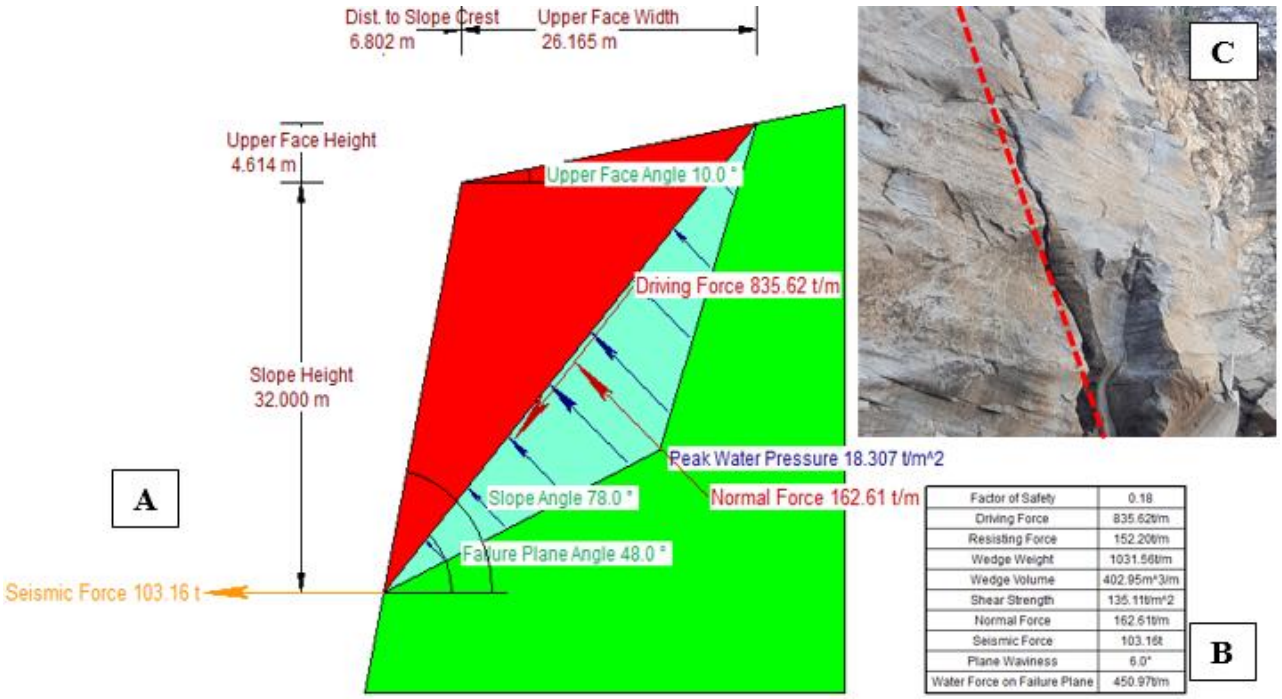

Figure 5. 3 A) 2D view of the planar mode of failure due to JS2 dipping at RS2, B) Summary of Rocplane 2.0 software for JS2 during dynamic saturated conditions, and C) Existing field condition

Table 5. 9 Summary of FOS obtained for RSS1 under different anticipated conditions.

Slope section	Joint Set	FOS results under different anticipated conditions			
		Static dry	Static saturated	Dynamic dry	Dynamic saturated
RS1	JS3	1.07	0.00	0.96	0.00
RS2	JS2	0.63	0.26	0.52	0.18

5.3.2.2 Sensitivity Analysis of Planar Mode of Failure

The LEM Modeling has shown that water force/or saturation is a major factor that controls the stability of planar failure in both slopes as saturation resulted in a significant reduction in the FOS (Table 5.9). Hence, in this study, water force is not considered for the sensitivity analysis. For all remaining parameters, sensitivity analysis was conducted by changing the value of one input parameter over a certain range (i.e. original value + or – 5) while keeping the original value as the mean value. The sensitivity curves indicate that the parameter with the steepest curve strongly influences the stability as compared to parameters with a gentler curve (Lamessa and Meten 2021). Accordingly, the analysis has shown that the planar failure due to JS3 at RS1 is strongly influenced by slope angle followed by failure plane angle, cohesion, unit weight, seismic coefficient, friction angle, and slope height (Figure 5.4A). Similarly, this sensitivity analysis has also shown that planar failure due to

JS2 at RS2 is dominantly affected by failure plane angle followed by friction angle, slope angle, cohesion, seismic coefficient, unit weight, and slope height (Figure 5.4B). In general, sensitivity analysis of both planar failures has shown that slope and failure plane angles significantly influence slope failure while unit weight, slope height, and seismic coefficient slightly influence the stability of the slope.

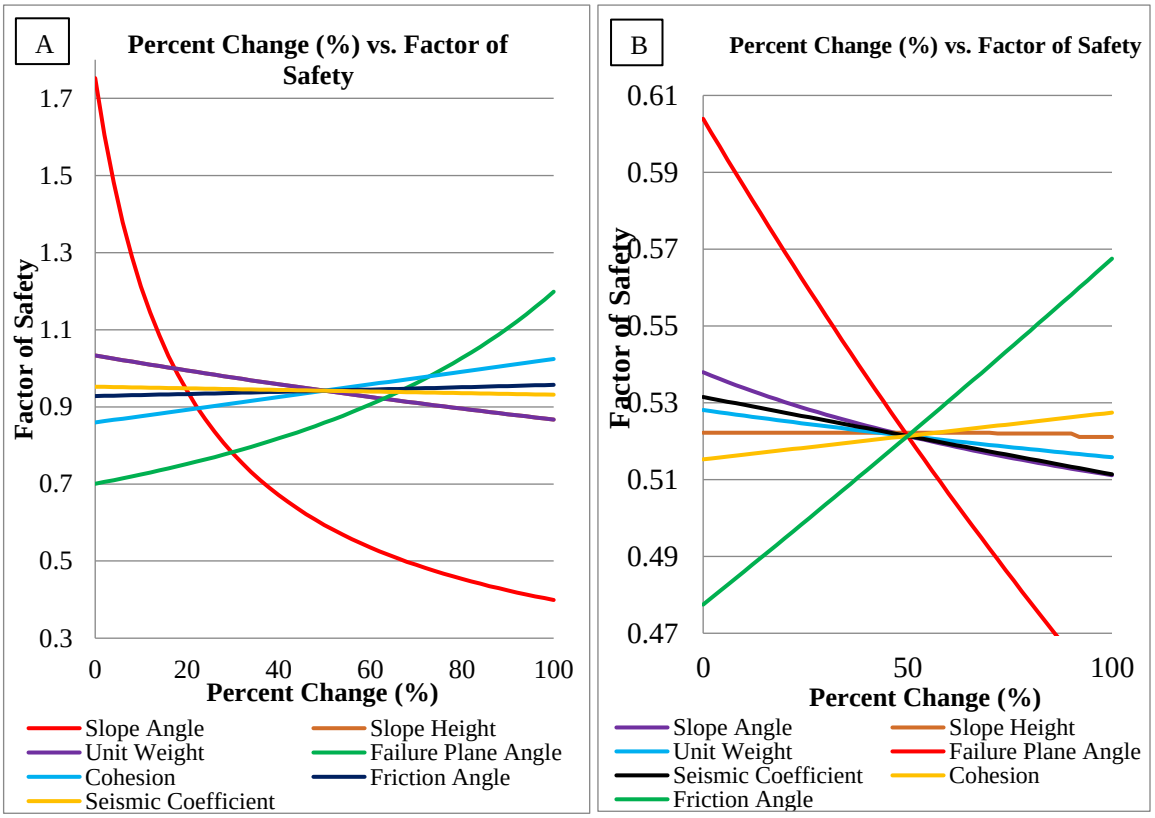

Figure 5. 4 Sensitivity analysis of the planar mode of failure A) at RS1 and B) at RS2.

5.3.2.3 LEM Modeling of Wedge Failure

The stability modeling of wedge failure in terms of FOS was undertaken using LEM based approach following the procedure forwarded by Hoek & Bray (1981) using Swedge 4.0 software (Swedge 4.0 Rocscience 2004). This analysis was conducted for wedge identified at both RS1 and RS2 from input parameters given in Table 5.10.

Table 5. 10 Input parameters used for determination of FOS for Swedge software.

Slope section	Input parameters for Swedge V. 4.0									
	JS	Slope geometry					Strength		Force	
		JS D/DD(^{0})	Sh (m)	γ (t/m^3) s/d	Sa (D/DD^0)	UF (D/DD^0)	C (t/m^2)	Φ (^{0})	γw (t/m^3)	αs
RS1	JS1	46/320	30	2.58/2.52	80/257	15/240	5.506	41.73	1	0.1
	JS2	58/130	30	2.58/2.52	80/257	15/240	3.467	38.20	1	0.1
	JS3	76/262	30	2.58/2.52	80/257	15/240	2.423	36.74	1	0.1
RS2	JS1	64/115	32	2.56/2.53	78/240	10/230	1.427	28.76	1	0.1
	JS2	48/255	32	2.56/2.53	78/240	10/230	1.019	27.57	1	0.1
JS= joint set, Sh=slope height, γ=unit weight, s/d=saturated/dry, Sa=slope angle, UF=upper face, c=cohesion, Φ=friction angle, γw= unit weight of water, αs= seismic coefficient.										

From the kinematic modeling, slope section RS1 is subjected to wedge failure due to the intersection of JS1 and JS3, and JS2 and JS3 (Figure 5.1 and Table 5.7). LEM modeling using Swedge V. 4.0 has revealed that the wedge formed due to JS1 and JS3 has FOS in the order of 1.147, 1.007, 0.292, and 0.276 (Figure 5.5 and Table 5.11). Similarly, the wedge formed due to JS2 and JS3 has FOS in the order of 2.607, 2.271, 0.841, and 0.786 under static dry, dynamic dry, static saturated, and dynamic saturated conditions, respectively (Figure 5.6 and Table 5.11). Thus, based on the interpretation of FOS given by Wyllie and Norrish (1996) and Wyllie & Mah (2004), both wedges are unstable during saturated and stable during dry conditions. As per Raghuvanshi et al. (2017), Hossain (2011), and Tesfaye et al. (2023), this signifies that wedge instability of this slope is attributable to failure surface lubrication and pore water pressure induced by rainfall.

Similarly, the LEM modeling of wedge-formed at RS2 has shown that a wedge formed due to JS1 and JS2 has a FOS in the order of 1.902, 1.550, 1.300, and 1.060 during static dry, dynamic dry, static saturated, and dynamic saturated conditions, respectively (Figure 5.7 and Table 5.11). This signified that wedge formed at this slope section is stable during all anticipated conditions.

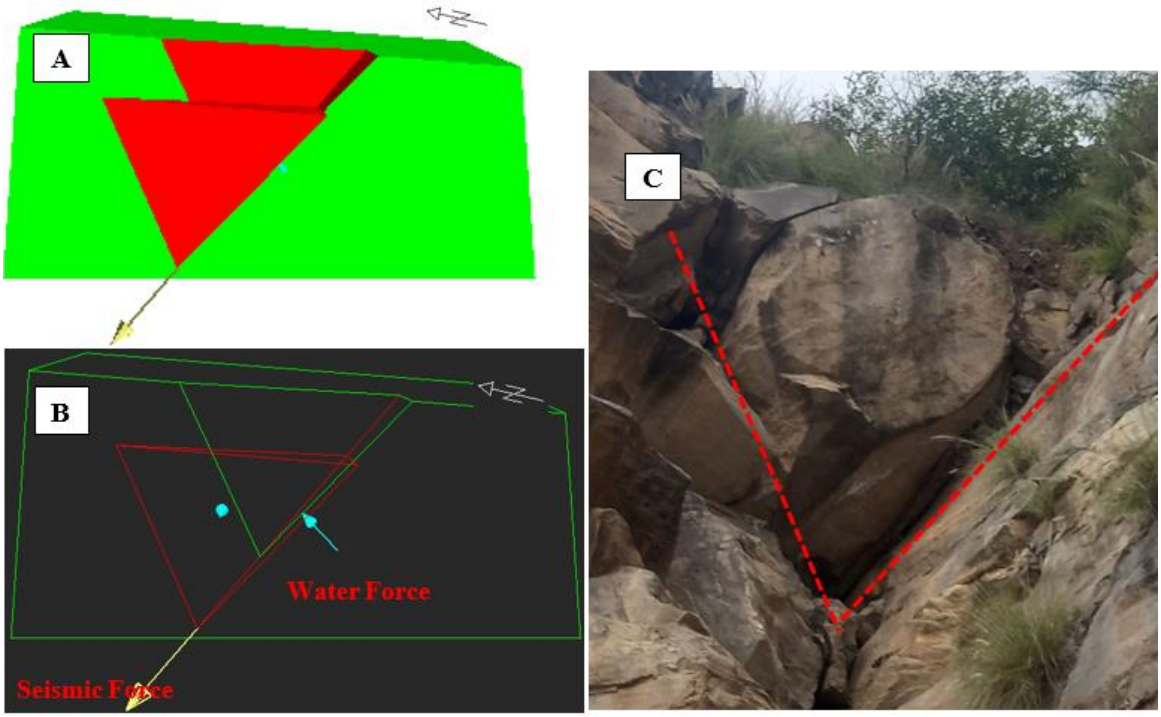

Figure 5. 5 A) 3D view of the slope geometry of JS1 and JS3 of RS1 with shaded draw mode under dynamic saturated condition, B) 3D view of geometry with wireframe draw mode, and C) Actual field condition

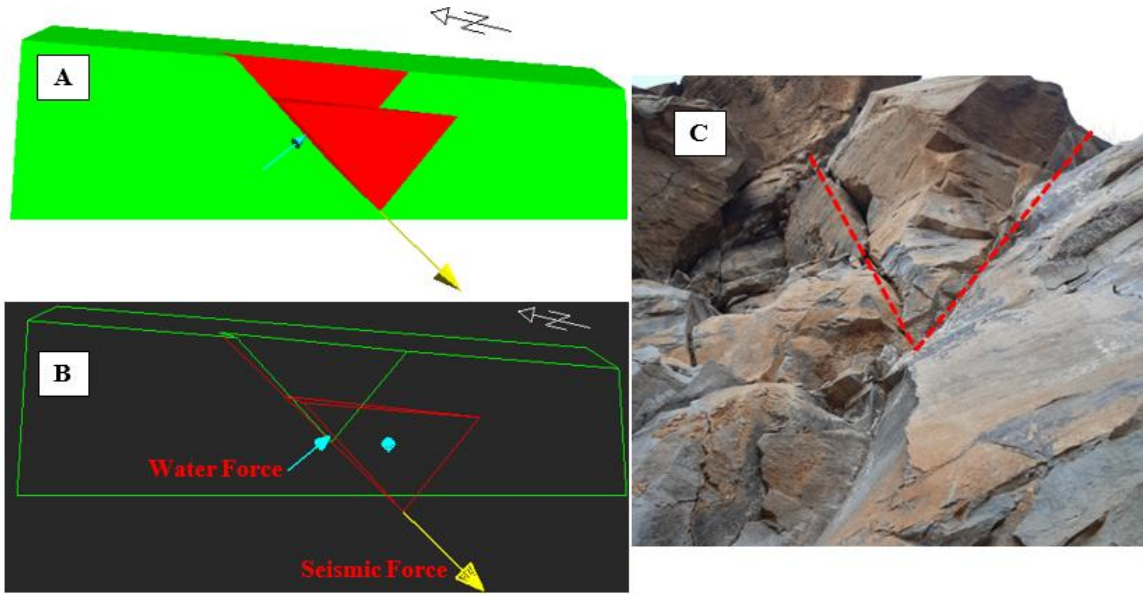

Figure 5. 6 A) 3D view of the slope geometry of JS2 and JS3 of RS1 with shaded draw mode under dynamic saturated condition, B) 3D view of geometry with wireframe draw mode, and C) Actual field condition

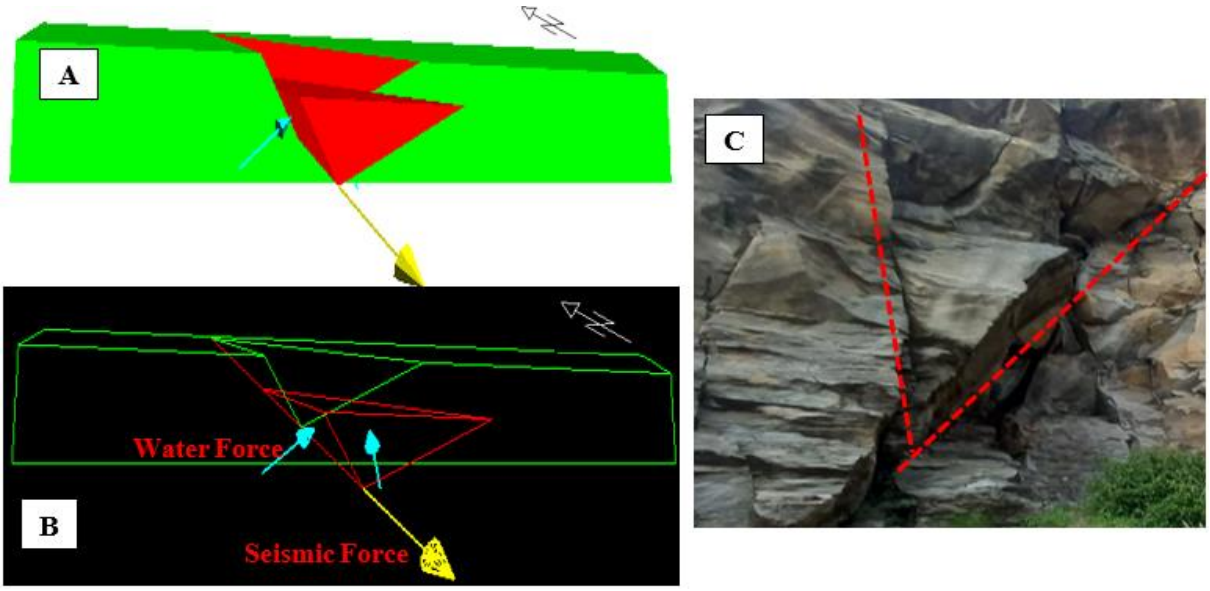

Figure 5. 7 A) 3D view of the slope geometry of JS1 and JS2 of RS2 with shaded draw mode under dynamic saturated condition, B) 3D view of geometry with wireframe draw mode, and C) Actual field condition

Table 5. 11 The FOS under different anticipated conditions for wedge mod of failure.

Slope section	JS (intersection)	FOS results under different anticipated conditions			
		Static dry	Static saturated	Dynamic dry	Dynamic saturated
RS1	JS1 & JS3	1.147	0.292	1.007	0.276
	JS2 & JS3	2.607	0.841	2.271	0.786
RS2	JS1 & JS2	1.902	1.300	1.550	1.060

5.4 Soil Characterization

Some identified critical slope sections are partly constituted by soils. Hence, properties of soils such as unit weight and shear strength parameters will have a significant impact on controlling the stability of these slopes. Accordingly, tests such as unit weight and direct shear tests were conducted on representative soil samples to acquire these two parameters.

5.4.1 Unit Weight

Unit weight test of soil is conducted at Engineering Corporation of Oromia (ECO). The test result showed that the dry unit weight of soils of the study area varies from 13.24 to 19.28 kN/m^3. Similarly, the test results also showed that the saturated unit weight of soils in the study area ranges from 14.35 to 21.42 kN/m^3 (Table 5.12).

Table 5. 12 Unit weight test results of soils of the study area

No.	Sample Code	Slope Section	Dry Unit Weight (γ_{dry})	Saturated Unit Weight (γ_{sat})
1	SS1	SS1-A	18.70	19.66
		SS1-B	19.28	21.42
2	SS2	SS2-A	16.24	17.33
		PS1	13.24	14.35
3	SS3	SS2-A	14.65	15.21

5.4.2 Shear Strength Test

The shear strength parameters (i.e. cohesion and friction angle) of slope-forming materials are one of the major input parameters for determining the stability of the slope. Hence, in this study, the shear strength parameters of soils forming the critical slope sections were determined using a direct shear test. The test results showed that the cohesion of soils of the study area varies from 0.140 MPa to 8.54 MPa while the friction angle ranges from 17.224^0 to 29.500^0 (Table 5.13 and Figure 5.8).

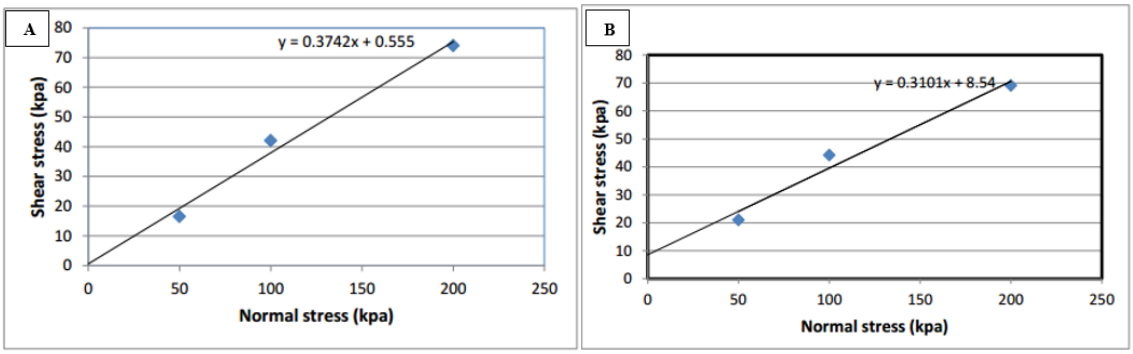

Figure 5. 8 A Sample of normal versus shear stress curve of direct shear test on the soil A) at SS1 and B) at SS3

Table 5. 13 The shear strength parameters of soils of the study area

Sample ID	Slope Section Description	Shear Strength Parameters	
		C(kN/m^2)	ϕ (^{0})
SS1-A	SS1 (Eluvium soil deposited on ignimbrite rock)	0.555	20.516
SS1-B		0.140	29.500
SS2-A	SS2 (Eluvium soil deposited on pumice and ignimbrite rock)	6.244	21.550
PS-1		8.54	17.224
SS2-A	Eluvium Soil deposited on Ignimbrite	8.142	19.84

5.5 Stability Analysis of Non-Structural Controlled Slope Section

For non-structural controlled slope sections (i.e. slope sections constituted by soils and weathered rocks), the stability modeling was conducted using LEM and FEMs. In the following sections, the analysis results obtained from both of these methods will be discussed.

5.5.1 Stability Modeling Using LEM

For modeling the stability of the slope using LEM, Slide 6.0 software was used to determine FOS through Hoek-Brown Failure Strength Criteria. This technique/software uses shear strength parameters, unit weight, slope geometry, horizontal seismic acceleration, and degree of saturation as input parameters. In this study, shear strength parameters for rocks were determined from Hoek-Brown Failure Strength Criteria using Rockdata software (Rocdata 3.0 Rocscience, 2004) while for soils these parameters were determined using direct shear test. Moreover, the unit weight of both rocks and soils was determined in the laboratory while the slope geometry was determined in the field using a tape meter. Furthermore, the horizontal seismic acceleration of the study area (0.1 g) was obtained from a seismic hazard map of Ethiopia forwarded by EBCS (1995). The modeling was then done from the input parameter given in Table 5.14 using the Morgenstern–Price method as it considers both force and moment equilibrium acting on the failure surface (Koca 2020).

Table 5. 14 Input Parameters for the Slide 6.0 Software.

Slope Section	Geology	C (KN/m^2)	ϕ (^{0})	γ_{dry} (kN/m^3)	γ_{sat} (kN/m^3)	Slope height (m)	Average Slope angle (^{0})	
SS1	Eluvium Soil (SS1-A)	0.555	20.516	18.70	19.66	35	Top	17
	Eluvium Soil (SS1-B)	0.140	29.500	19.28	21.42		Middle	75
	HW Ignimbrite	110.0	30.61	22.88	23.31		Bottom	53
SS2	Eluvium Soil	6.244	21.550	16.24	17.33	42	Top	59
	Pumice	8.54	17.224	13.24	14.35		Middle	45
	HW Ignimbrite	141.0	33.15	20.59	21.85		Bottom	28
SS3	Eluvium soil	8.142	19.84	14.65	15.21	30	Top	68
	MW to HW Ignimbrite	91.0	33.16	20.87	22.07		Middle	45
							Bottom	73
SS4	HW Ignimbrite	115.0	29.21	21.50	23.27	42	Top	51
	MW to HW Ignimbrite	211.0	38.87	22.26	24.38		Middle	70
							Bottom	48

The slope section SS1 is characterized by three slope profiles with bottom, middle, and top profiles having dip angles of 53^0, 75^0, and 16^0, respectively. The slope is constituted by eluvium and highly weathered ignimbrite rock (Figure 5.9). Based on the field manifestation, two soil samples (i.e. one each from eluvium 1 and eluvium 2) were taken from this slope section for better engineering geological representation of the slope. The stability modeling was done from input parameters shown in Table 5.14 and the analysis results were shown in Table 5.15 and Figure 5.10.

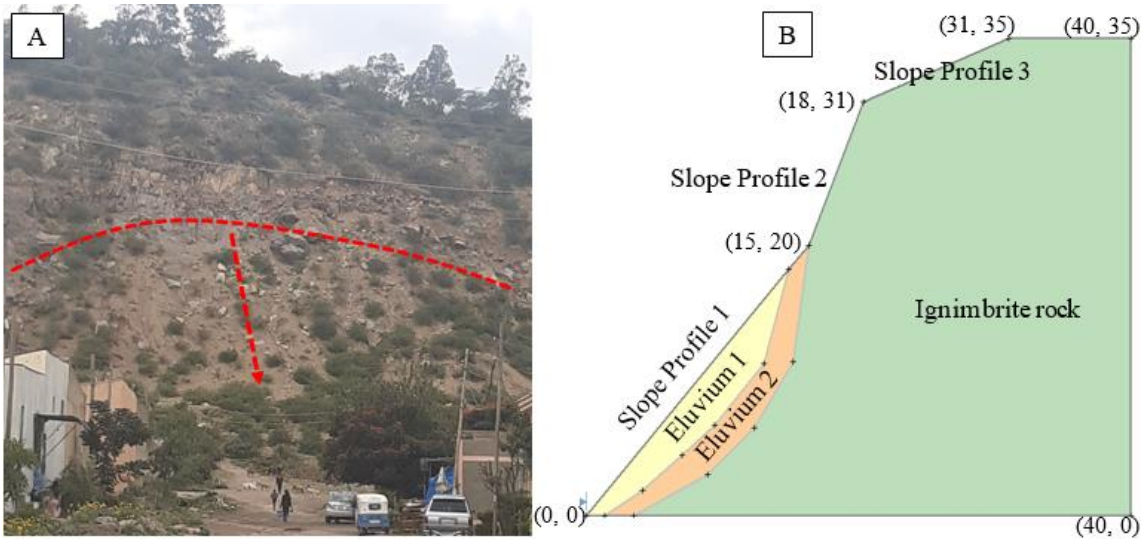

Figure 5. 9 A) Existing field condition of slope section SS1 and B) Slope geometry

The modeling results showed that the FOS corresponding to the critical slip surface for SS1 is in the order of 0.364, 0.305, 0.225, and 0.194 under static dry, dynamic dry, static saturated, and dynamic saturated conditions, respectively (Table 5.15 and Figure 5.10). Hence, based on the interpretation of FOS given by Wyllie and Norrish (1996), Wyllie & Mah (2004), and Christian (2004), this slope is unstable under all anticipated conditions. The results showed that this slope is unstable even without the presence of any external force suggesting that the shear strength of geological materials and slope geometry have significantly contributed to destabilizing this slope. Moreover, the modeling also showed that the potential failure only involves the eluvium soil as shown in yellow color in Figure 5.10.

Table 5. 15 LEM modeling results of Slide software as determined using the GLE technique for SS1

Global minimums	GLE/Morgenstern-Price Technique Result			
	Static Dry	Dynamic Dry	Static Saturated	Dynamic Saturated
FOS	0.3640	0.3050	0.2250	0.1943
RM (kN-m)	5706.09	5172.88	2082.8	2654.98
DM(kN-m)	15675.2	16964.9	9271.14	13663.2
RHF(kN)	74.6596	67.974	29.3271	44.5383
DHF(kN)	205.098	222.927	130.543	229.204
C	29.645, 40.029	29.645, 40.029	27.440, 35.619	20.825, 35.619
R	49.737	49.737	44.906	40.214
RM = resisting moment, DM = driving moment, RHF = resisting horizontal force, DHF = driving horizontal force, C =c enter, R = radius.				

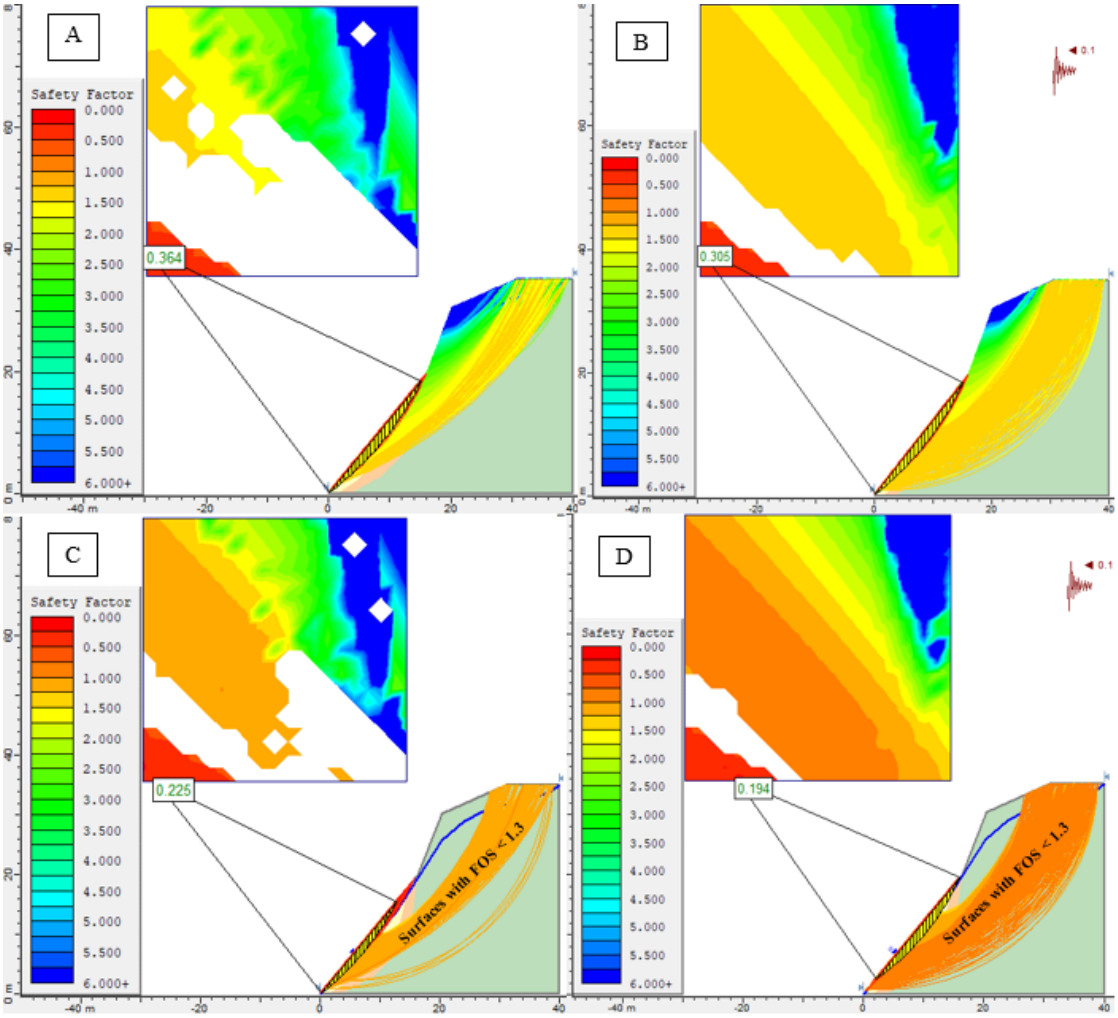

Figure 5. 10 LEM modeling result of SS1 using Slide 6.0 software under A) static dry, B) dynamic dry, C) static saturated, and D) dynamic saturated conditions.

The slope section SS2 is also multi-sloped with three slope profiles. The bottom profile dips at an angle of 28^0 while the middle and top profiles dip at angles of 45^0 and 59^0, respectively (Table 5.14). In terms of geology, eluvium soil, pumice, and ignimbrite rocks constitute this slope. The pumice is sandwiched between blocks of ignimbrite rock while the eluvium soil is deposited on the bottom half of the ignimbrite itself. The stability modeling was then conducted upon determination of all required parameters and analysis results were shown in Table 5.16 and Figure 5.11. The results of the modeling showed that this slope is only stable during static dry condition with the FOS of 1.117 (Table 5.16 and Figure 5.11). During the remaining conditions, this slope is unstable with potential failure involving eluvium soil and pumice. Hence, the potential failure is likely to involve the bottom and middle slope profiles. During dynamic saturated conditions in particular, driving horizontal force with a magnitude of 1309.94 kN and resisting horizontal force of

574.866 kN were applied to the slope which decreased FOS from 1.117 from static dry to dynamic saturated condition (Table 5.16). The modeling showed that the external triggering factors of the slope (i.e. seismic activity and rainfall) are the major factors controlling the stability of this slope as this slope became unstable during dynamic and saturated conditions.

Table 5. 16 LEM modeling results of Slide software as determined using the GLE technique for SS2

Global minimums	GLE/Morgenstern-Price Technique Result			
	Static Dry	Dynamic Dry	Static Saturated	Dynamic Saturated
FOS	1.1173	0.9081	0.4592	0.4390
RM (kN-m)	54135.3	52446.9	28254.9	26915.0
DM(kN-m)	48450.7	57748.5	51441.7	61330.7
RHF(kN)	1133.03	1102.18	596..744	574.866
DHF(kN)	1014.06	1213.6	1086.45	1309.94
C	5.339, 43.816	5.339, 43.816	5.339, 43.816	5.339, 43.816
R	41.848	41.848	41.848	41.848
RM=resisting moment, DM=driving moment, RHF=resisting horizontal force, DHF=driving horizontal force, C=center, R=radius.				

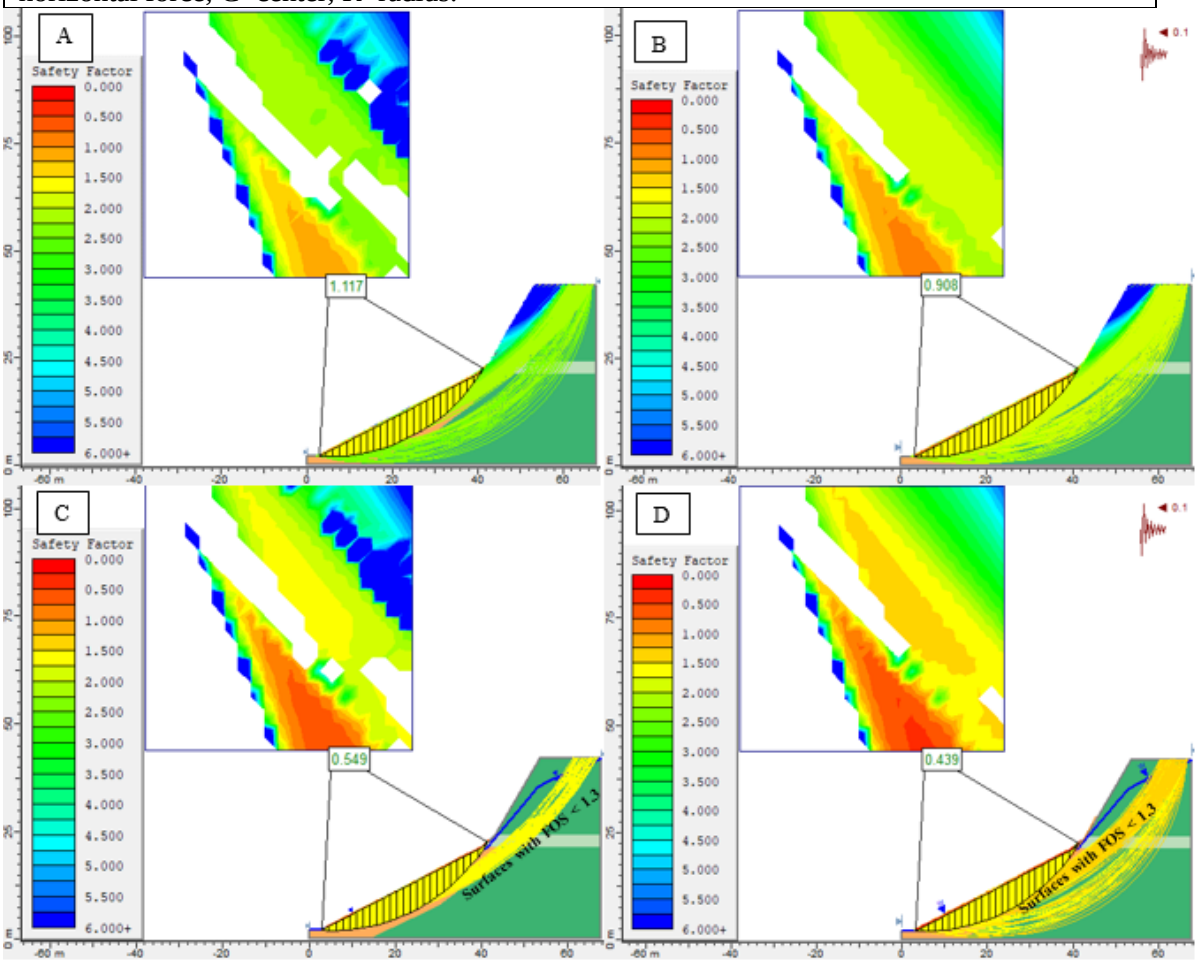

Figure 5. 11 LEM modeling result of SS2 using Slide 6.0 software under A) static dry, B) dynamic dry, C) static saturated, and D) dynamic saturated conditions.

Likewise SS1 and SS2, slope section SS3 is also multi-sloped with three slope profiles designated as bottom, middle, and top slope profiles dipping at an angle of 73^0, 45^0, and 68^0, respectively (Table 5.14). In this slope, eluvium soil is deposited on ignimbrite rock forming the bottom slope profile that dips at an angle of 73^0 towards the residential area (Figure 5.12). The modeling results showed that this slope is stable during static dry and dynamic dry conditions with FOS of 1.443 and 1.271, respectively (Table 5.17 and Figure 5.13A and B). However, this slope is unstable during static saturated and dynamic saturated conditions with corresponding FOS of 0.522 and 0.467. This showed that rainfall/or saturation is the major factor contributing to the instability of this slope.

Figure 5. 12 Existing field condition of slope section SS3.

Table 5. 17 LEM modeling results of Slide software as determined using the GLE technique for SS3

Global minimums	GLE/Morgenstern-Price Technique Result			
	Static Dry	Dynamic Dry	Static Saturated	Dynamic Saturated
FOS	1.4433	1.2716	0.5223	0.4672
RM (kN-m)	100812.0	97045.6	2648.44	2028.24
DM(kN-m)	69846.3	76316.2	5069.98	4340.62
RHF(kN)	1719.95	1593.27	51.6254	43.1938
DHF(kN)	1191.64	1252.94	98.828	92.4387
C	8.347, 38.132	9.876, 39.662	11.406, 28.953	11.406, 28.953
R	33.787	35.666	26.162	25.926

RM=resisting moment, DM=driving moment, RHF=resisting horizontal force, DHF=driving horizontal force, C=center, R=radius.

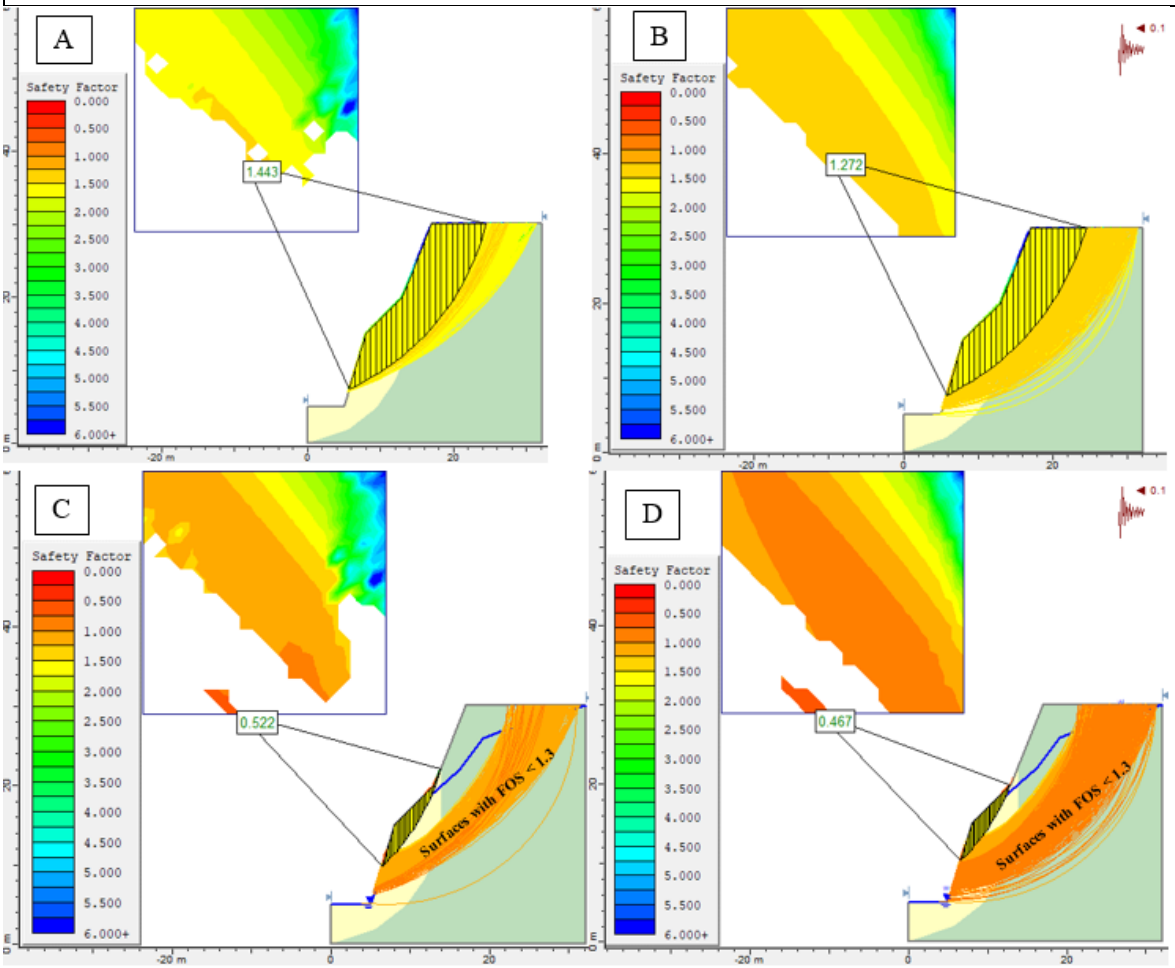

Figure 5. 13 LEM modeling result of SS3 using Slide 6.0 software under A) static dry, B) dynamic dry, C) static saturated, and D) dynamic saturated conditions.

Another critical slope section identified in the study area, SS4, is located following the Aba-Geda ridge and it strikes in a relatively N-S direction. Unlike other identified slope sections, this slope is facing eastward. Moreover, likewise other identified critical slope sections of the study area, this slope is also characterized by three slope profiles (bottom, middle, and top slope profiles). The bottom slope profile dips at an angle of 48^0 and is

constituted by moderately to highly weathered ignimbrite. On the other hand, the middle and top slope profiles dip at angles of 70^0 and 51^0, respectively, and are constituted by highly weathered ignimbrite. The LEM modeling of this slope, as executed from input parameters listed in Table 5.14, revealed this slope is stable under all projected slope conditions (Table 5.18 and Figure 5.14).

Table 5. 18 LEM modeling results of Slide software as determined using the GLE technique for SS4

Global minimums	GLE/Morgenstern-Price Technique Result			
	Static Dry	Dynamic Dry	Static Saturated	Dynamic Saturated
FOS	2.0450	1.7371	1.5972	1.3120
RM (kN-m)	456304.0	227669.0	378043.0	182738.0
DM(kN-m)	223146	131060.0	236683.0	139314.0
RHF(kN)	4166.16	4077.29	3450.7	3271.8
DHF(kN)	2037.37	2347.12	2160.4	2494.33
C	66.416, 90.470	39.741, 58.459	66.416, 90.470	39.741, 58.459
R	81.684	41.170	81.684	41.170

RM=resisting moment, DM=driving moment, RHF=resisting horizontal force, DHF=driving horizontal force, C=center, R=radius.

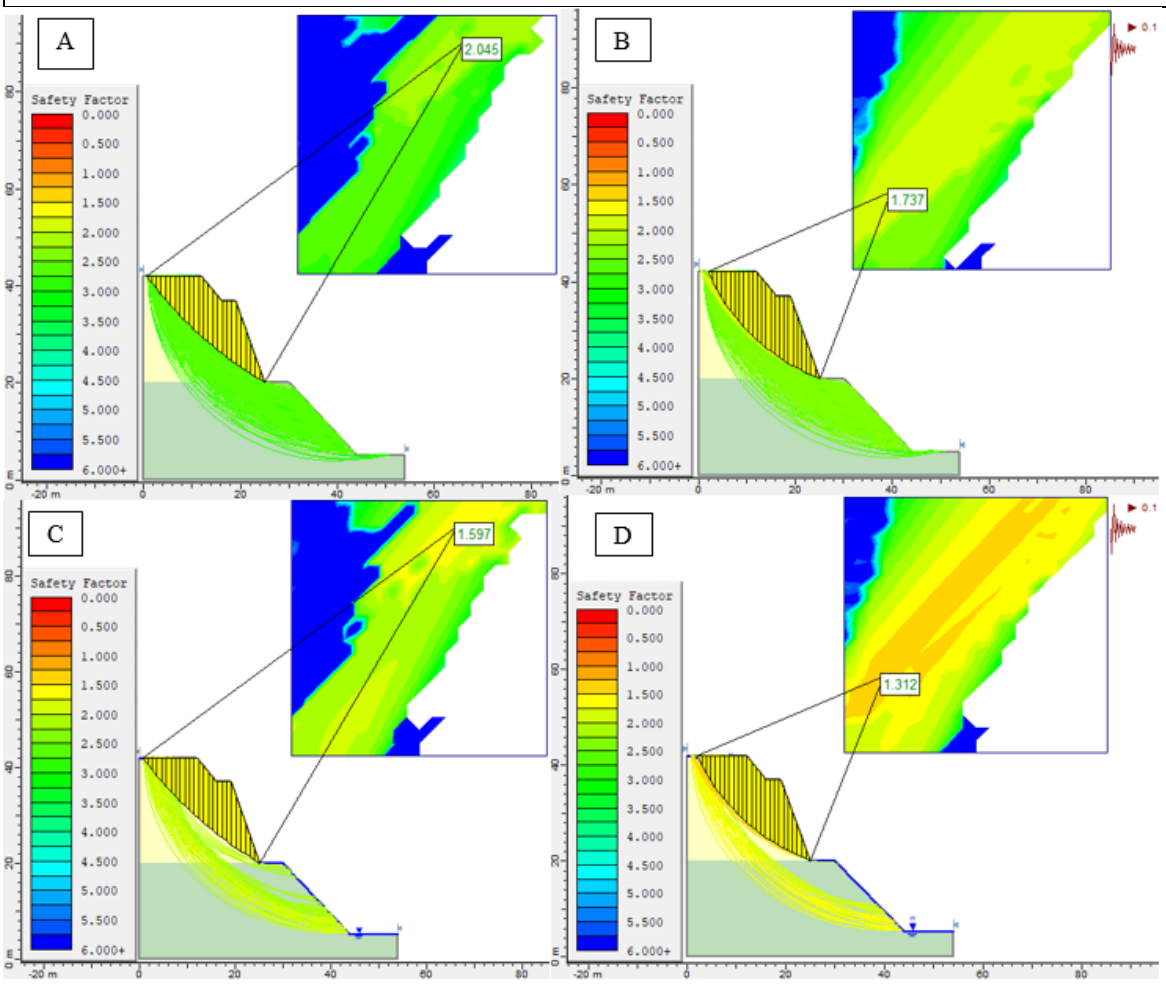

Figure 5. 14 LEM modeling result of SS4 using Slide 6.0 software under A) static dry, B) dynamic dry, C) static saturated, and D) dynamic saturated conditions.

5.5.2 Stability Modeling Using the FEM Method

To compare and validate the results of LEM modeling, further stability analysis was also conducted for non-structural controlled slope sections using FEM-based Phase V 2.0 software. During this FEM slope modeling via Phase V 2.0 software, the same material properties and slope geometry used during LEM modeling were used except for the addition of two other parameters. These two parameters are poison ratio (V) and Young's modulus and they were determined via equations stated in section 3.5.2. Finally, the modeling was executed from the input parameters listed in Table 5.19.

Table 5. 19 Input parameters for FEM-based Phase V 2.0 software for slope modeling

Slope Section	Geology	C (KN/m^2)	V	E (kPa)	ϕ (^{0})	γ_{dry} (kN/m^3)	γ_{sat} (kN/m^3)	Slope height (m)	Average Slope angle (^{0})	
SS1	Eluvium Soil (SS1-A)	0.555	0.033	10438.8	20.516	18.70	19.66	35	Top	17
	Eluvium Soil (SS1-B)	0.140	0.168	24000.0	29.500	19.28	21.42		Middle	75
	HW Ignimbrite	110.0	0.373	936470.0	30.61	22.88	23.31		Bottom	53
SS2	Eluvium Soil	6.244	0.048	10632.0	21.550	16.24	17.33	42	Top	59
	Pumice	8.54	0.016	7594.8	17.224	13.24	14.35		Middle	45
	HW Ignimbrite	141.0	0.355	1385160.0	33.15	20.59	21.85		Bottom	28
SS3	Eluvium soil	8.142	0.022	9073.2	19.84	14.65	15.21	30	Top	68
	Ignimbrite	91.0	0.381	910220.0	33.16	20.87	22.07		Middle	45
									Bottom	73
SS4	HW Ignimbrite	115.0	0.371	915420.0	29.21	21.50	23.27	42	Top	51
	MW to HW Ignimbrite	211.0	0.349	2266750.0	38.87	22.26	24.38		Middle	70
									Bottom	48
C-Cohesion, ϕ-Friction angle, V-Poison ratio, E- Young's modulus, γ_{dry}, Dry unit weight, γ_{sat}, Saturated unit weight										

FEM modeling using Phase V 2.0 software revealed that SS1 is unstable under all projected conditions including under the absence of any external seismic and water force (Figure 5.15). Hence, following the studies of Bushira et al. (2018), and Bekele and Meten (2022), the stability of this slope is primarily controlled by factors other than external forces such as slope geometry and shear strength of slope-forming materials. Thus, any remedial measures concerning this slope should be directed at either strengthening the materials of the slope or modifying the slope geometry.

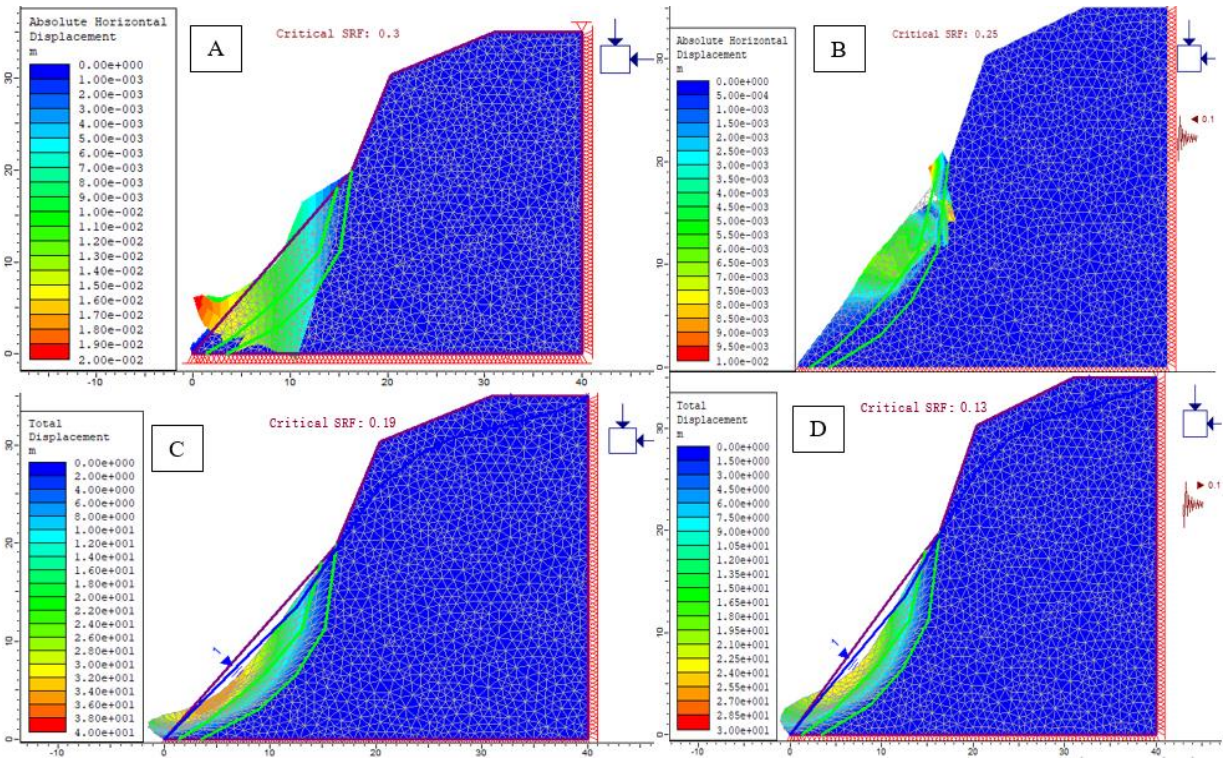

Figure 5. 15 SRF as determined for SS1 using FEM-based Phase V 2.0 software under A) static dry, B) dynamic dry, C) static saturated, and D) dynamic saturated conditions.

Furthermore, the FEM modeling has shown that SS2 is marginally stable during static dry condition with an SRF of 1.03 and unstable during all remaining conditions with an SRF of less than 1 (Figure 5.16). There is a significant reduction in SRF from static dry condition (SRF = 1.03) to dynamic dry (SRF = 0.67) to static and dynamic saturated (Figure 5.16). Agreeing with studies by Song et al. (2020) and Raghuvanshi (2017), this showed that external triggering factors such as seismic and water forces significantly contribute to destabilizing this slope. Moreover, likewise the LEM modeling, FEM modeling has also shown that the potential failure surface is likely to affect the bottom and middle slope profiles (i.e. eluvium soil and pumice layers) (Figure 5.16).

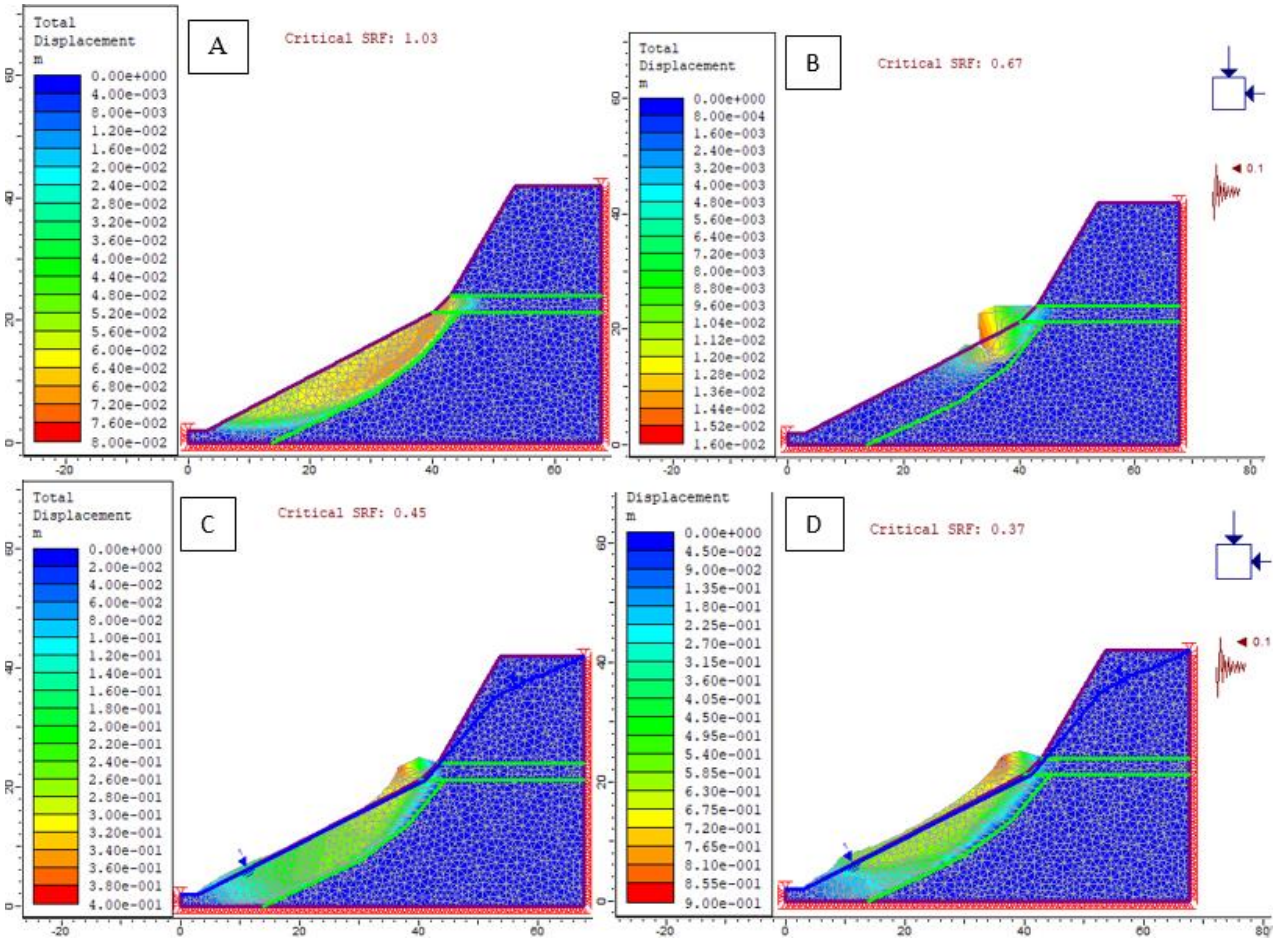

Figure 5. 16 SRF as determined for SS2 using FEM-based Phase V 2.0 software under A) static dry, B) dynamic dry, C) static saturated, and D) dynamic saturated conditions.

Moreover, the FEM modeling has shown that SS3 is also unstable under all anticipated conditions likewise SS1 (Figure 5.17). Hence, the unstable nature of this slope is greatly attributed comparison between the slope geometry and shear strength parameters of materials of the slope. This modeling has also revealed that the potential failure surface of this slope affects the bottom, middle, and partly smaller parts of the upper slope profile. Thus, the eluvium soil deposit and the uppermost of this slope that constitutes the aforementioned slope profiles will be removed because of this slope failure.

On the contrary, the FEM modeling has illustrated that SS4 is stable under all project slope conditions with SRF greater than 1.13 (Figure 5.18). The stability of this slope is mainly due to the strength of the geological materials that constitute this slope, which is ignimbrite rock.

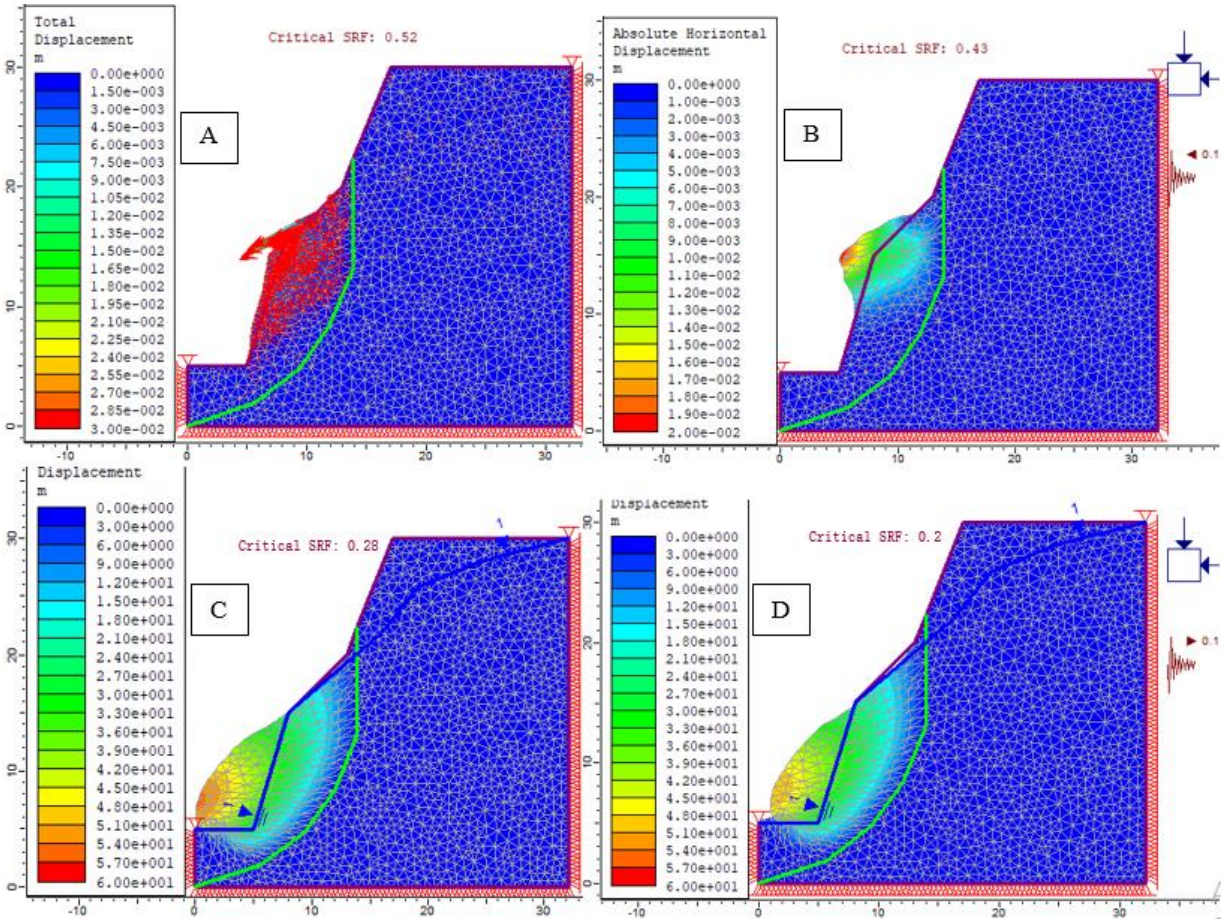

Figure 5. 17 SRF as determined for SS3 using FEM-based Phase V 2.0 software under A) static dry, B) dynamic dry, C) static saturated, and D) dynamic saturated conditions.

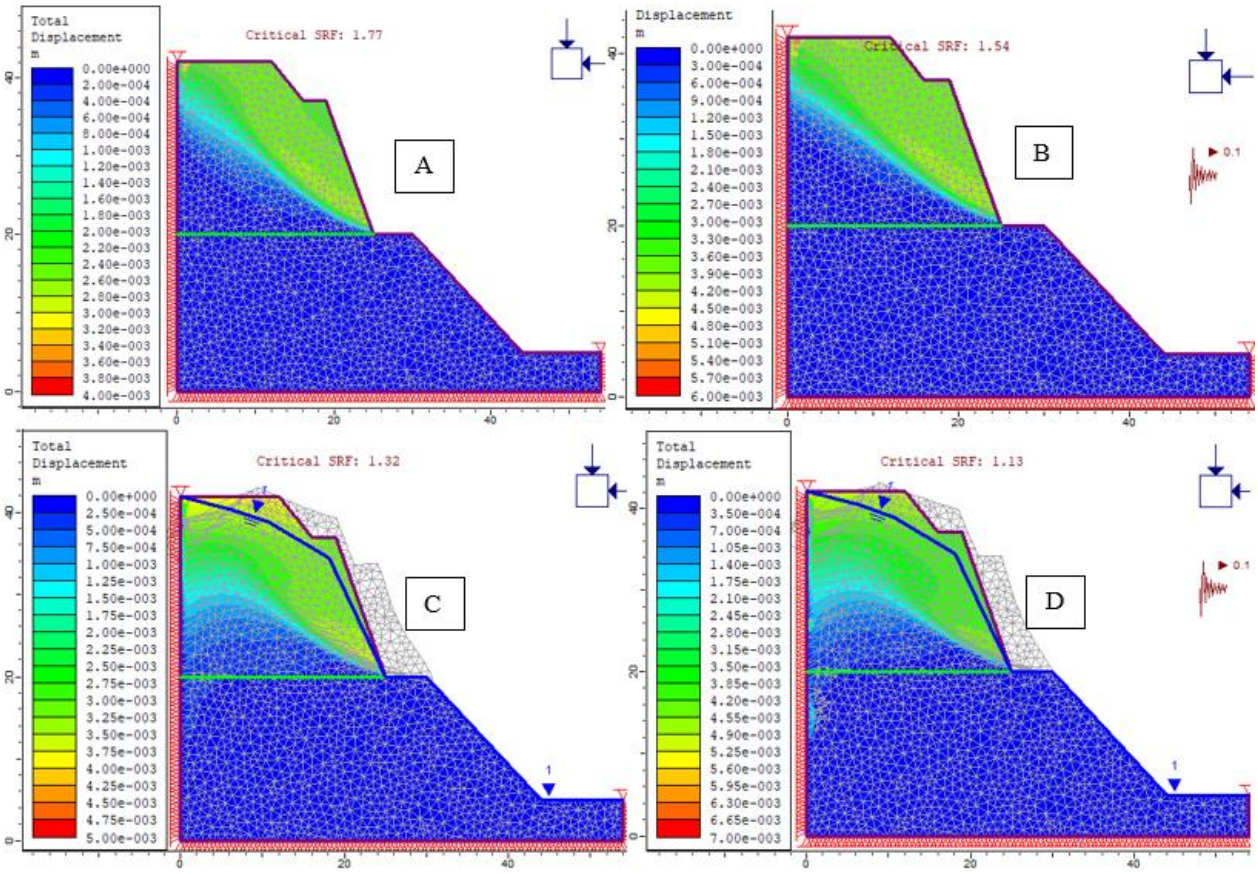

Figure 5. 18 SRF as determined for SS4 using FEM-based Phase V 2.0 software under A) static dry, B) dynamic dry, C) static saturated, and D) dynamic saturated conditions.

5.6 Comparison of LEM and FEM Results for Non-Structural Controlled Slope Sections

A comparison of FOS obtained from LEM-based Slide 6.0 software and SRF obtained from FEM-based Phase V 2.0 software revealed that the results are in close agreement for slope section SS1, SS2, and SS4 while the results show variation for slope section SS3 (Table 5.20). The difference in FOS obtained from LEM and SRF obtained from FEM is less than 0.08 in all conditions except between dynamic dry condition of SS2 where the difference is 0.238. Similarly, the difference is less than 0.3 for SS4. This showed that the results of both methods are in very close agreement for SS1, SS2, and SS4. Moreover, the potential slip surface obtained from both LEM-based Slide 6.0 software and FEM-based Phase V 2.0 software is also in very close agreement.

On the contrary, the results obtained from LEM and FEM techniques show a clear variation for slope section SS3. For example, LEM yielded stable slope conditions during static and dynamic dry conditions for SS3 while FEM yielded unstable slope conditions under all

conditions for this slope (Table 5.20). Moreover, the difference in FOS of LEM and SRF of FEM of this slope is as high as 0.9233. The difference between the LEM and FEM results is evident when a heterogeneous and complex slope geometry is analyzed (Mebrahtu et al., 2022). In the study area, however, all slope sections are constituted by heterogeneous materials, and all slopes are characterized by related slope geometry. Hence, the variation of results of LEM and FEM of SS3 is not attributable to heterogeneity and slope complexity. This study depicted that variation of the results is related to slip surface as inferred failure surface involved two materials in the SS3 and just one material in the remaining slope sections.

Table 5. 20 Correlation of FOS and SRF obtained between Slide 6.0 and SRF, respectively

Slope Section	LEM (Slide 6.0 Software)				FEM (Phase 2.0 Software)			
	Static Dry	Dynamic Dry	Static Saturated	Dynamic Saturated	Static Dry	Dynamic Dry	Static Saturated	Dynamic Saturated
SS1	0.3640	0.3050	0.2250	0.1943	0.30	0.25	0.19	0.13
SS2	1.1173	0.9081	0.4592	0.4390	1.03	0.67	0.45	0.37
SS3	1.4433	1.2716	0.5223	0.4672	0.52	0.43	0.28	0.20
SS4	2.0450	1.7371	1.5972	1.3120	1.77	1.54	1.32	1.13

5.7 Possible Remedial Measures

5.7.1 Possible Remedial Measures for Planar and Wedge Failures

LEM modeling has shown that the identified planar failures of the study area are unstable under all anticipated seismic and saturated conditions. Moreover, the LEM has also shown that the identified wedges of the study area are all unstable under saturated conditions. Thus, possible counteractive measures are needed for these unstable slopes so that they can be stable even under the worst condition (i.e. dynamic saturated condition). This study used Rocplane (Rocplane 2.0 Rocscience, 2004) and Swedge software (Swedge 4.0 Rocscience, 2004) to design and provide the possible remedial measures for planar and wedge mode of failures, respectively. For the stabilization of planar failure, rock bolts were used as stabilizing tools whereas combined rock bolts and shotcrete were used as stabilizing tools for wedge failures. The designed rock bolts are all systematically designed to cross the failure surface so that FOS can be increased. Moreover, all stabilization analyses were done for the worst possible slope condition (i.e. dynamic saturated condition).

Accordingly, two rock bolts each with 125 ton/m bolt capacity were designed to stabilize planar failure at RS1 due to JS3 (Table 5.21 and Figure 5.19). The bolts have a length ranging from 5 to 8m and were applied at an angle of 10^0 to the slope. This stabilization measure has increased the FOS of this planar mode of failure from 0.00 to 1.27. Moreover, three rock bolts each with 250 ton/m bolt capacity were installed at an angle of 12^0 to the slope to stabilize planar failure due to JS2 at RS2 (Table 5.21 and Figure 5.20). This remedial measure has increased the FOS of this slope due to planar failure from 0.00 to 1.21. A FOS of greater than 1.2 has been recommended for slope stability safety of cut slopes by Hoek & Bray (1981), Duncan (2000), Bushira et al. (2018), Lamessa and Meten (2021), and Tesfaye et al. (2023). Hence, the above-designed rock bolts can be used as stabilizing measures in both slope sections.

Table 5. 21 Stabilization of planar mode of failure at RS1 and RS2 via application of Rock Bolt.

Slope section	Joint set	Bolt Parameters					FOS
		Bolt angle (^{0})	Bolt Length (m)	Single Bolt Capacity (ton/m)	Number of Bolt applied	Total Bolt Capacity (ton/m)	
RS1	JS3	10	5m to 8m	125	2	250	1.27
RA2	JS2	12	22m to 24m	250	3	750	1.21

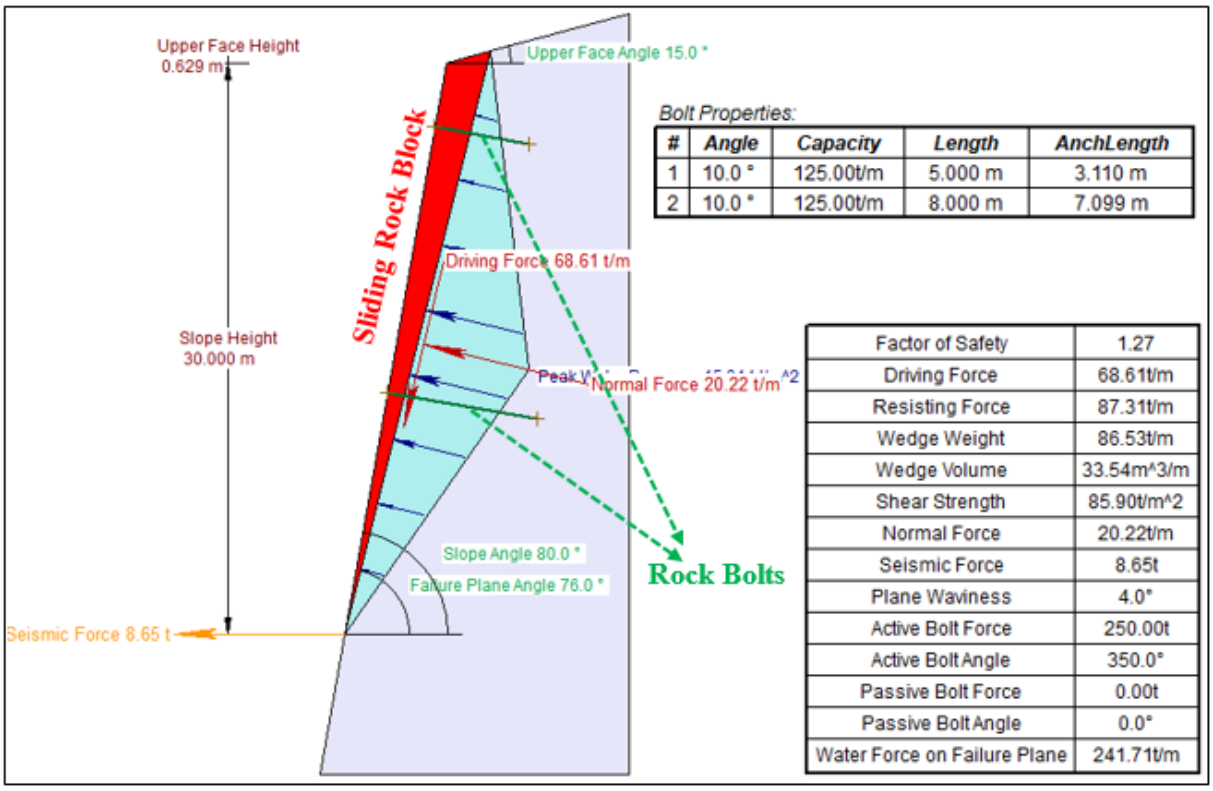

Figure 5. 19 Rocplane 2.0 designed and installed rock bolts for JS3 at RS1.

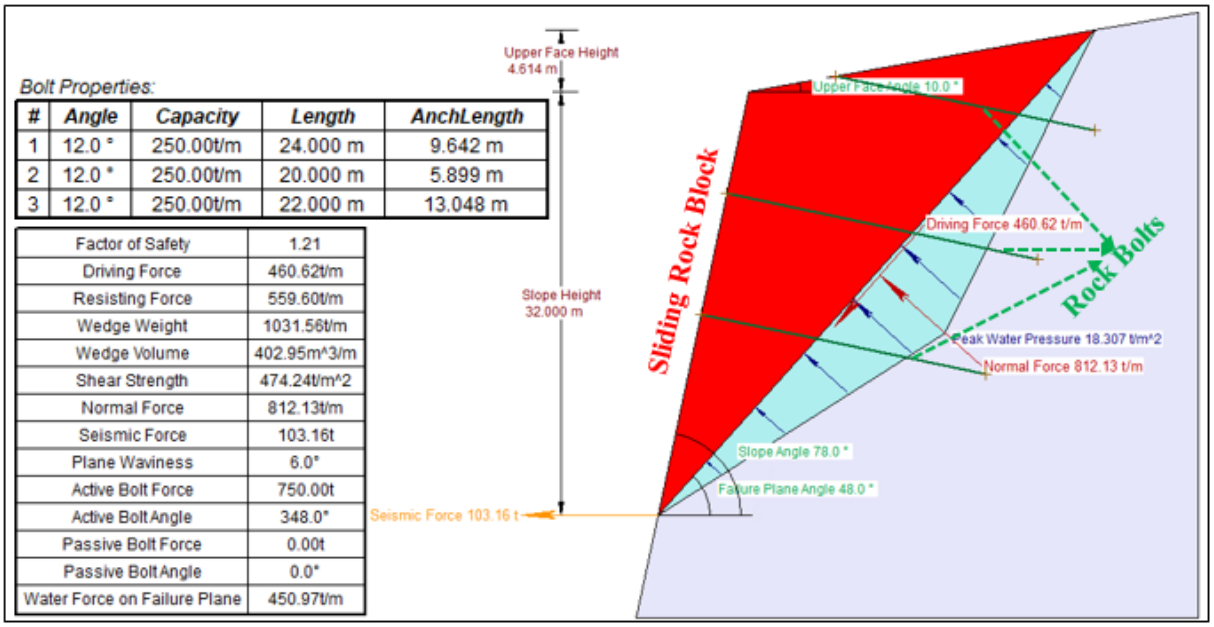

Figure 5. 20 Rocplane 2.0 designed and installed rock bolts for JS2 at RS2.

Furthermore, the shotcrete with a shear strength capacity of 320 ton/m^2 to the slope face and four rock bolts with single bolt capacity of 500 ton/m at a trend direction of 077^0 were designed to stabilize the wedge formed due to JS1 and JS3 at RS1 (Table 5.22 and Figure 5.21A). This combined bolt and shotcrete stabilization has increased the FOS of the wedge of this slope from 0.276 to 1.227. Similarly, four rock bolts plunging 15^0 to the slope with a trend direction of 070^0 each having 250 ton/m bolt capacity were designed with 600 ton/m^2 shear strength shotcrete to stabilize the wedge formed at RS1 due to JS2 and JS3 (Table 5.22 and Figure 5.21B). As a result, the FOS of this wedge has increased from 0.786 during normal dynamic saturated condition to 1.230 by this stabilization mechanism. Hence, as both stabilization measures for both wedges yielded a FOS greater than 1.2, they can be used to remediate wedges of this slope.

Table 5. 22 Stabilization of wedge mode of failure at RSS2 and RSS3 through the application of Rock Bolt and Shotcrete.

Slope section	Bolt Parameters								FOS
	Joint	Bolt plunge (^{0})	Bolt trend direction (^{0})	Average Bolt Length (m)	Single Bolt (ton/m) capacity	Number of Bolt applied	Total Bolt Capacity (ton/m)	Shotcrete shear strength (t/m2)	
RS1	JS1 & JS3	10	077	10	500	4	2000	320	1.227
	JS2 & JS3	15	070	8	250	4	1000	600	1.230

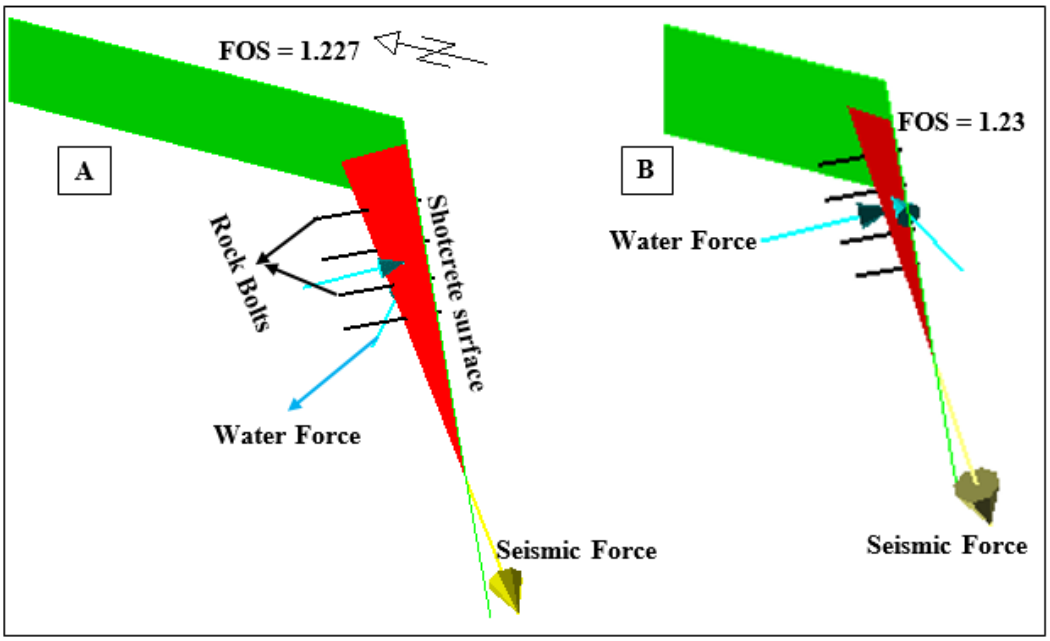

Figure 5. 21 A designed and installed rock bolt and shotcrete for wedge formed due to the intersection of A) JS1 and JS3 and B) JS2 and JS3 at RS1.

5.7.2 Possible Remedial Measures for Non-Structural Controlled Slope Sections

The stability modeling using both LEM and FEM has shown that slope sections SS1, SS2, and SS3 are all unstable under saturated conditions. In this study, slope flattening, benching, and combined slope flattening and benching were designed to determine the most suitable remedial measures for these slopes.

5.7.2.1 Flattening Slope Angle

The potential for slope failure increases with an increase in the steepness of the slope as the main driving force acting on the slope (i.e. gravitational force) is proportional to the slope inclination (Hamza and Raghuvanshi 2017). Hence, as the slope angle increases gravitational forces increase, which aggravates slope failure. Thus, flattening the slope angle is one of the major remedial measures used for minimizing slope failure.

Accordingly, slope-flattening analysis is carried out for SS1, SS2, and SS3 considering the worst possible condition (i.e. dynamic saturated condition). The analysis is conducted via LEM-based Slide 6.0 software first by modeling the existing slope condition as 1H: 1V and then by progressively reducing the slope angle to 1.5H: 1V, 2H: 1V, and 2.5H: 1V.

For slope section SS1, the failure surface involves the bottom and a small portion of upper slope profiles with failure only involving eluvium soil deposit (Figure 5.9, 5.10, and 5.15).

Hence, the slope flattening was done only for the bottom and middle slope profiles for this slope. The analysis has shown that this slope will be stabilized by reducing the bottom profile from 53^0 (1H: 1V) to 26.57^0 (2.5H: 1V) and the middle profile from 75^0 (1H: 1V) to 55.71^0 (2.5H: 1V) which leads to increase in FOS from 0.194 to 2.05 (Table 5.23 and Figure 5.22). However, a detailed analysis has also shown that this slope can be stabilized by reducing the slope angle to 2H: 1V and then by removing the remaining soil deposit.

Similarly, the analysis has also shown that SS2 will be stabilized by reducing bottom, middle, and upper slope profiles to angles of 14.4^0, $26.57^{0,}$ and 39.30^0, respectively (Table 5.23). This stabilization measure has increased the FOS of this slope from 0.439 during 1H: 1V to 1.741 during 2H: 1V (Table 5.23 and Figure 5.23). The detailed analysis has also shown that this slope can also be stabilized by reducing the slope angle to just 1.5H: 1V and then removing the remaining eluvium soil deposit. Moreover, the modeling also showed that slope section SS3 will become stable with a reduction in slope angle from 1H: 1V to 2.5H: 1V which resulted in an increase in FOS from 0.467 to 1.585 (Table 5.23 and Figure 5.24).

Table 5. 23 The results of slope flattening analysis for slope sections SS1, SS2, and SS3 as determined from the dynamic saturated conditions.

Slope Section and Failure Slope Face		1H:1V		1.5H:1V		2H:1V		2.5H:1V	
		Eqv. Angle	FOS	Eqv. Angle	FOS	Eqv. Angle	FOS	Eqv. Angle	FOS
SS1	Top Slope Profile	17	0.194	------	0.233	------	0.284	------	***2.05***
	Middle slope profile	75		68.0		61.4		55.71	
	Bottom slope profile	53		40.0		32.0		26.57	
SS2	Top Slope Profile	59	0.439	47.49	0.882	39.30	***1.741***	------	------
	Middle slope profile	45		33.69		26.57		------	
	Bottom slope profile	28		19.90		14.4		------	
SS3	Top Slope Profile	68	0.467	59.04	0.645	51.34	0.819	45.00	***1.585***
	Middle slope profile	45		33.69		26.57		21.80	
	Bottom slope profile	73		65.77		59.04		53.13	

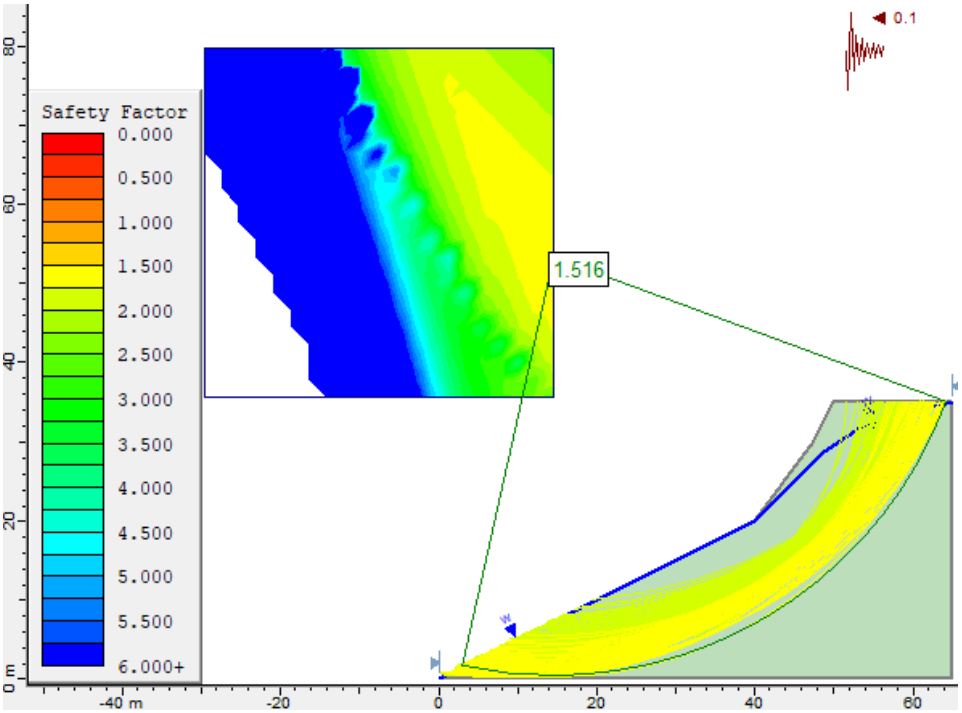

Figure 5. 22 A sample of stabilized slope model after slope flattening to 2.5H: 1V for slope section SS1

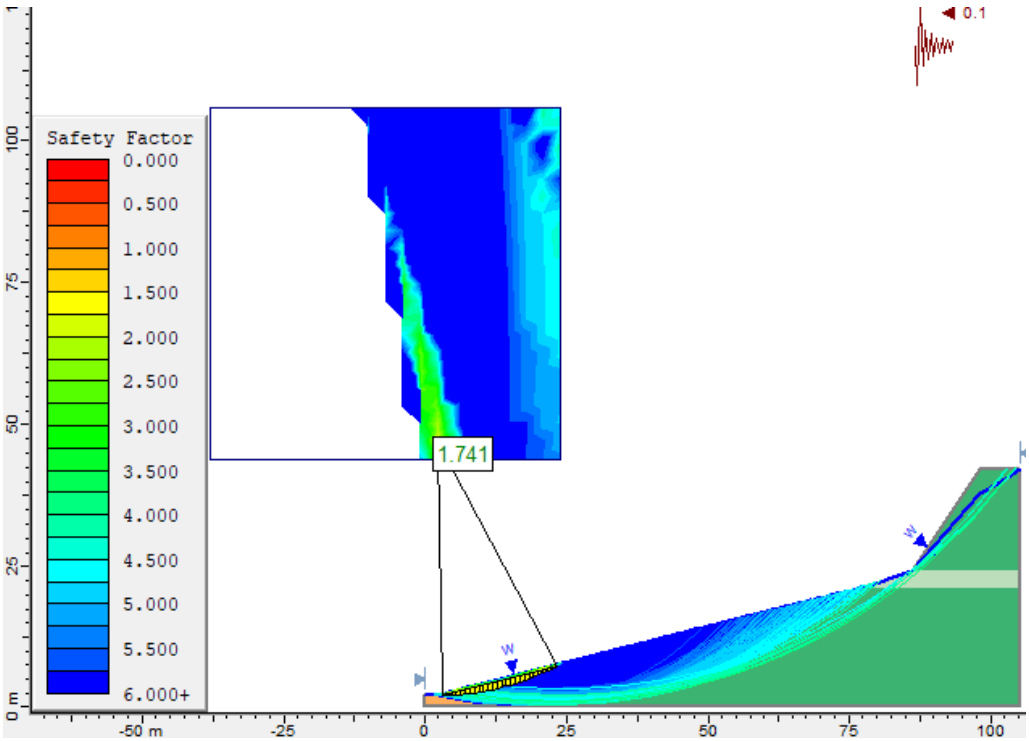

Figure 5. 23 A sample of stabilized slope model after slope flattening to 2H: 1V for slope section SS2

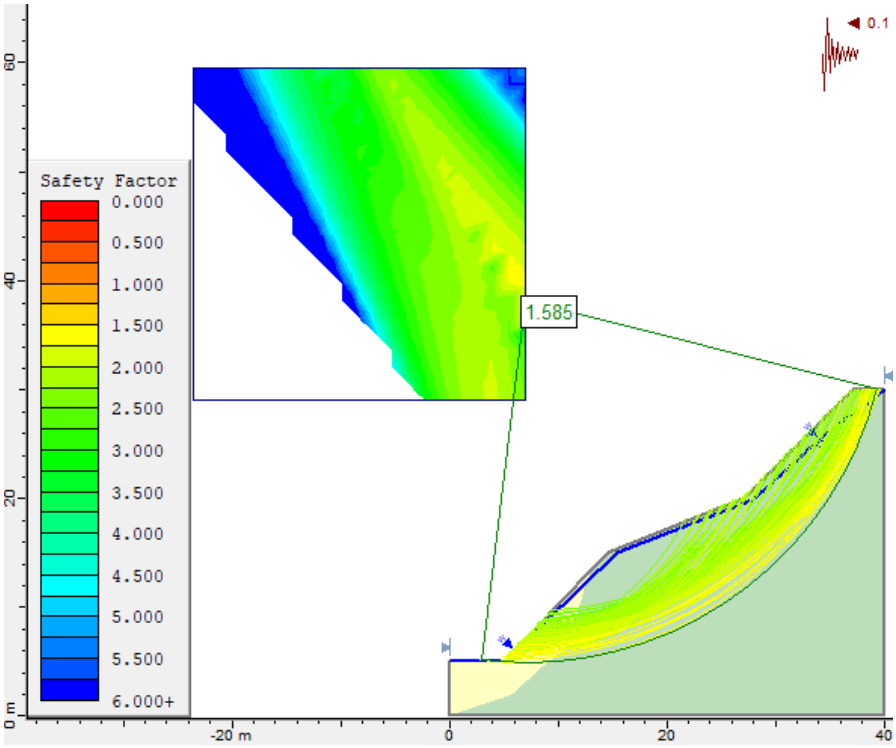

Figure 5. 24 A sample of stabilized slope model after slope flattening to 2.5H: 1V for slope section SS3

5.7.2.2 Benching

Benching is one of the most common slope stabilization techniques. It is a mechanism by which a steep slope can be differentiated into lower ones thereby potentially increasing the stability of the slope (Bushira et al., 2018; Abramson, 2002). In this study, 4 to 6 m long benches have been along the potential failure surface by progressively increasing the number of benches. The analysis of the results showed that the FOS of all slopes slightly increases as the number of benches increases (Table 5.24). Moreover, the analysis has also shown that benching will not stabilize the slopes of the study area as all benching analysis has yielded a FOS of less than 1 for all slopes (Table 5.24, Figures 5.25, 5.26, and 5.27).

Table 5. 24 The results of slope benching for SS1, SS2, and SS3.

Slope Section	SS1		SS2		SS3	
Bench Number	Bench Height (m)	FOS	Bench Height (m)	FOS	Bench Height (m)	FOS
Bench 1	10.0	0.289	13.1	0.554	17.0	0.679
Bench 2	6.1	0.378	8.5	0.583	17.5	0.673
	11.8		15.0		10.2	
Bench 3	6.0	0.318	5.0	0.735	17.0	0.519
	12.0		10.0		11.5	
	18.0		15.5		8.0	

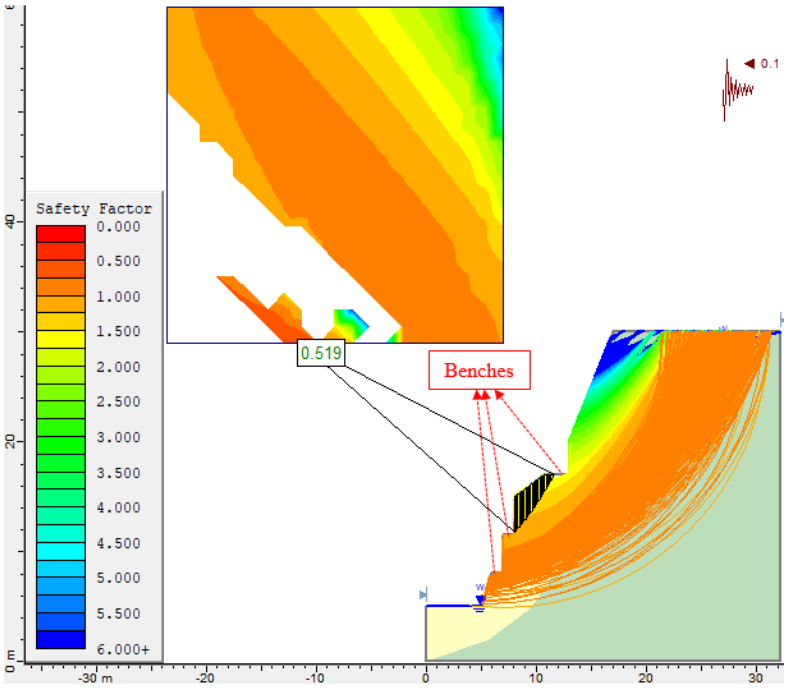

Figure 5. 25 A sample of the slope model after three benches at 8.0 m, 11.5 m, and 17.5 m for SS1

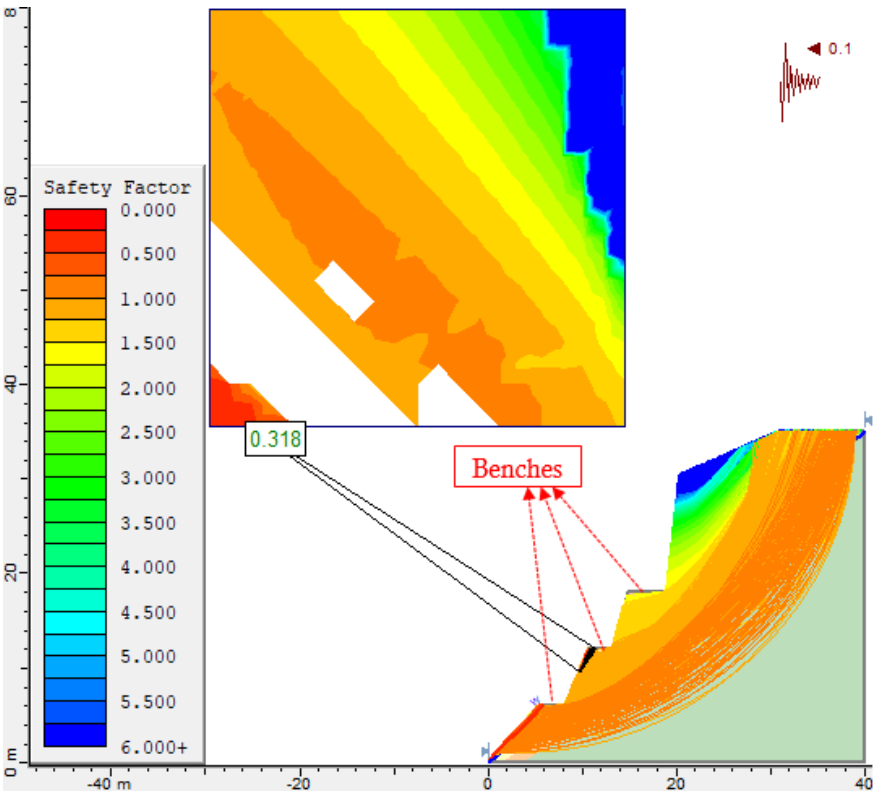

Figure 5. 26 A sample of the slope model after three benches at 6.0 m, 12.0 m, and 18.0 m for SS1

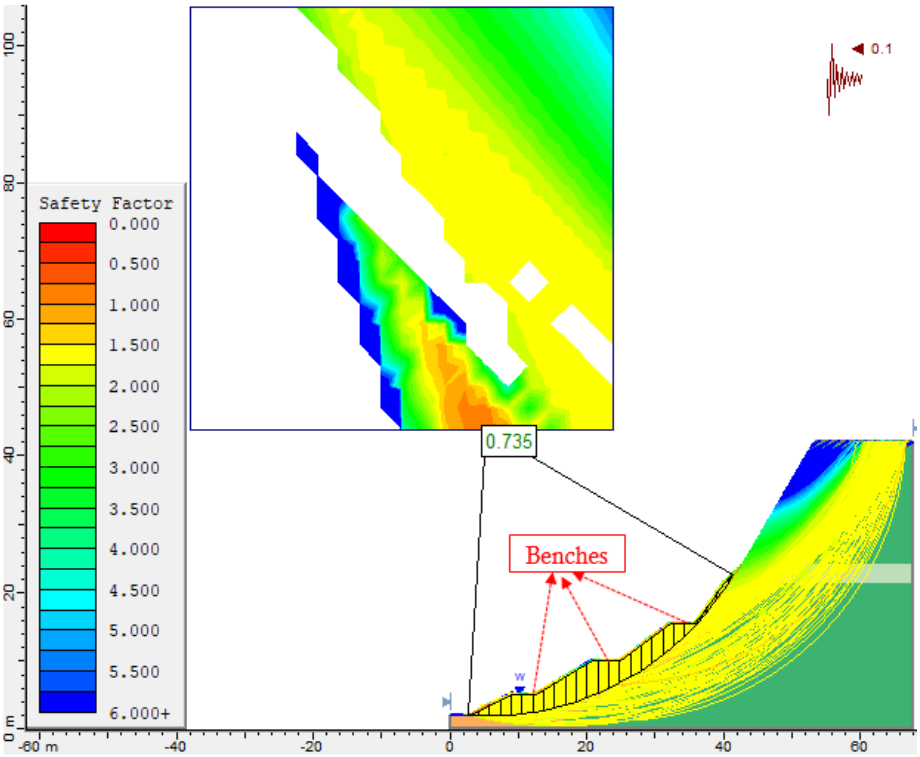

Figure 5. 27 A sample of the slope model after three benches at 5.0 m, 10.0 m, and 15.5 m for SS2

5.7.2.3 Combined Slope Flattening and Benching

In some slopes, benching alone is not effective for stabilizing the slope (Abramson, 2002). Jampani and Bhupathi (2017) stated that a combination of slope flattening and benching is one of the most effective slope stabilization mechanisms. Hence, in this study, slope stabilization analysis has been conducted by progressively flattening the slope angles from 1H: 1V to 1.5H: 1V, 2H: 1V, and 2.5H: 1V, and by providing 4 to 6 m long benches at different height intervals.

The analysis has shown that SS1 can be stabilized with slope flattening to 2H: 1V and with the introduction of 3 benches at lower slope profile at heights of 3 m, 6.2 m, and 9.2 m which increase the FOS of this slope to 1.355 (Table 5.25 and Figure 5.28). On the contrary, slope flattening has yielded a FOS of 0.284 at 2H: 1V for this slope (Table 5.23) while the application of three benches has produced a FOS of just 0.318 (Table 5.24). Hence, the results have shown that coupled slope flattening and benching is a more effective slope stabilization technique than just slope flattening or benching.

Moreover, this analysis has shown that SS2 can also be stabilized with slope flattening to just 1.5H: 1V and one bench at a height of 8.1 m (Table 5.25 and Figure 5.29). In addition,

SS3 can also be stabilized with slope flattening to 2H: 1V and with the introduction of two benches at 10.3 m and 17.3 m (Table 5.25 and Figure 5.30).

Table 5. 25 The results of combined slope flattening and benching analysis for slope sections SS1, SS2, and SS3 as determined from the dynamic saturated conditions.

Slope Section and Failure Slope Face		1H:1V			1.5H:1V			2H:1V		
		Eqv. Angle	Bench Height	FOS	Eqv. Angle	Bench Height	FOS	Eqv. Angle	Bench Height	FOS
SS1	Top face	17	-----	0.274	11.6	------	0.355	------	Three benches at the bottom profile at heights of 3m, 6.2m & 9.2m	***1.355***
	Middle face	75	-----		68.0	------		61.4		
	Bottom Face	53	-----		40.0	10.0		32.0		
SS2	Top layer	59	-----	0.535	47.49	------	***1.270***	------	------	------
	Middle face	45	22.1		33.69	------		------	------	
	Bottom Face	28	14.0		19.90	8.1		------	------	
SS3	Top Slope face	68	------	0.704	59.04	------	0.793	51.34	------	***1.238***
	Middle face	45	14.0		33.69	17.5		26.57	17.3	
	Bottom Face	73	9.5		65.77	9.1		59.04	10.3	

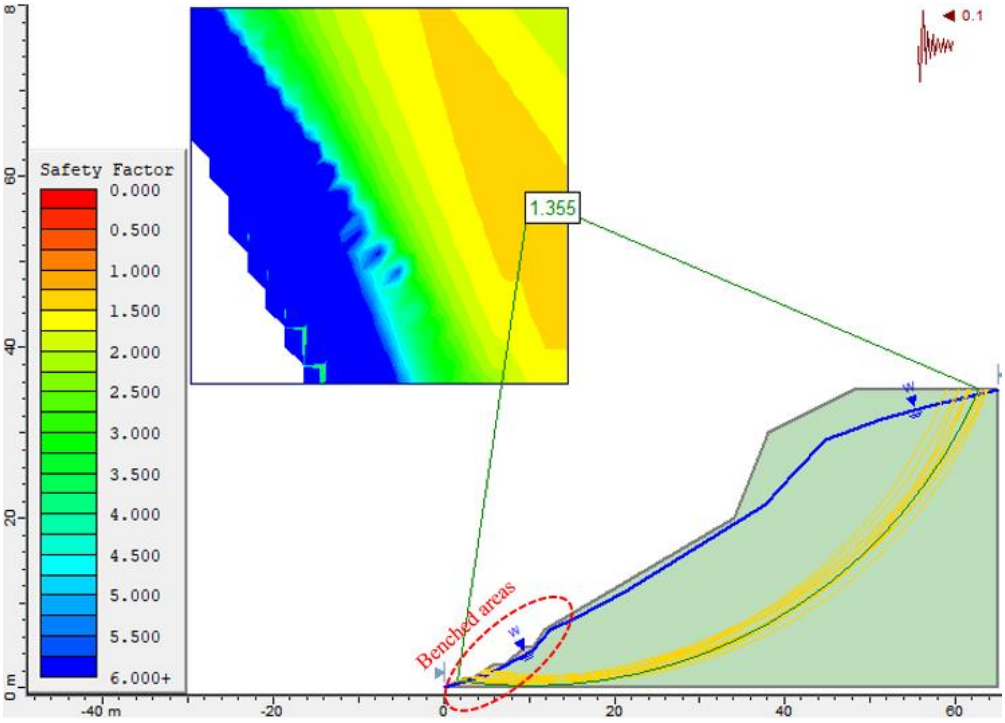

Figure 5. 28 A sample of stabilized slope model after combined slope flattening at 2H: 1V with 3 benches for slope section SS1

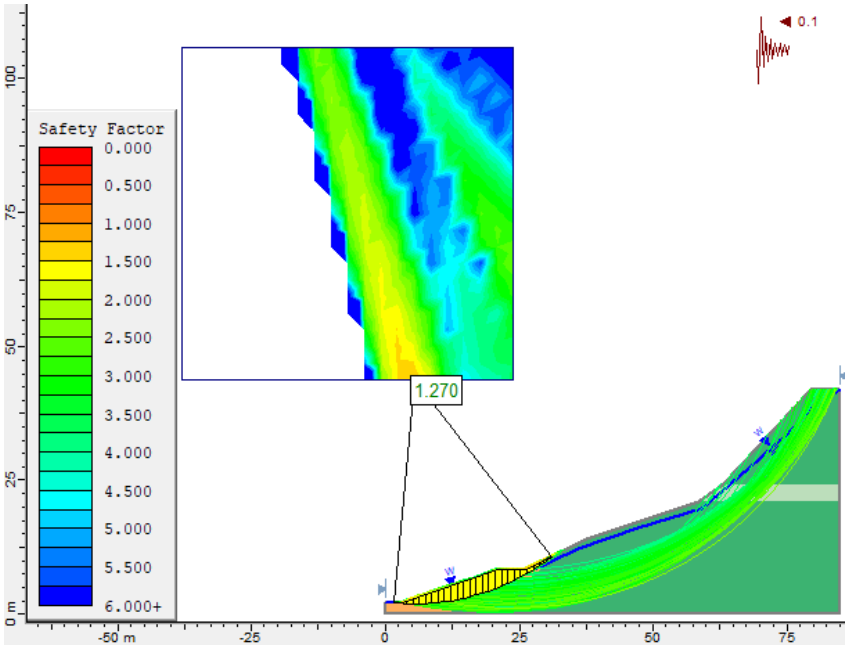

Figure 5. 29 A sample of a slope model after combined slope flattening at 1.5H: 1V with a 3m bench at a height of 8.1 m for slope section SS2

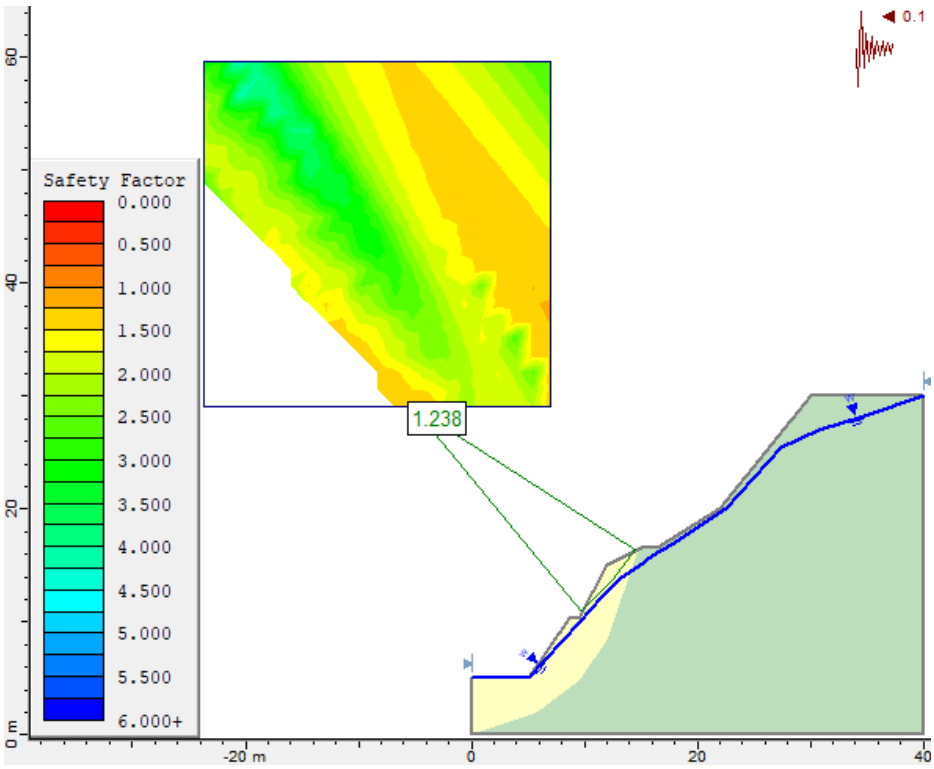

Figure 5. 30 A sample of a slope model after combined slope flattening at 2H: 1V with a 3m bench at a height of 10.3 m and 17.3 m for slope section SS3.

CHAPTER SIX

CONCLUSIONS AND RECOMMENDATIONS

6.1 Conclusions

In this study, slope stability modeling was conducted to locate and analyze the critical slope sections around the ridges of Adama town, central Ethiopia. The data used for modeling were generated via a detailed field survey, laboratory testing, and a thorough literature review. The stability modeling was then conducted via Kinematic, LEM, and FEMs. Finally, the following concluding remarks were generated:

- Based on field observation, two critical structural controlled and four non-structural controlled slope sections were identified. The Ignimbrite rock constitutes the structurally controlled slope sections while the non-structural controlled slope sections are constituted by eluvium soil, pumice, and ignimbrite rocks.
- The UCS ranges from 116.75 to 165.22 MPa for rocks structurally controlled and from 21.14 to 53.57 MPa for rocks of non-structural controlled slope sections.
- Rock Mass Rating (RMR) revealed that slope section RS1 is classified as Good rock while RS2 is classified as Fair rock.
- The Kinematic Modeling revealed that slope section RS1 is subjected to planar failure due to JS3 and wedge failure due to the intersection of JS1 and JS3, and JS2 and JS3. Similarly, this modeling also depicted that RS2 is subjected to planar failure due to JS2 and wedge mode of failure due to the intersection of JS1 and JS3.
- The LEM modeling has shown that planar due to JS3 of RS1 is marginally stable under static dry and unstable under remaining conditions. Similarly, this modeling has also shown that the planar failure of RS2 is unstable under all anticipated conditions.
- LEM modeling of planar failure has shown that saturation is a major factor that controls the stability of planar failure in the study area. Apart from saturation, sensitivity analysis has also shown that slope and failure angle significantly control the stability of planar failure of the study area.

- The LEM modeling has also shown that both wedges of RS1 are stable during dry conditions and unstable during saturated conditions. This indicated that rainfall is the main contributing factor to the wedge instability of this slope section. On the contrary, the modeling has shown that the wedge of RS2 is stable under all anticipated conditions.
- The LEM and FEM modeling of non-structural controlled slope sections revealed that slope sections SS1, SS2, and SS3 are all unstable under saturated conditions. This showed that saturation plays a major role in destabilizing the slopes in the study area. Both methods have also shown that SS1 is unstable under all anticipated conditions. The unstable nature of this slope even under the absence of seismicity and saturation showed that the shear strength parameters and geometry of the slope play a major role in destabilizing this slope.
- A comparison of FOS obtained from LEM-based Slide 6.0 software and SRF obtained from FEM-based Phase V 2.0 software revealed that the results are in close agreement for slope section SS1, SS2, and SS4 while the results show variation for slope section SS3.

6.2 Recommendations

Based on the results, the following remedial measures are forwarded to stabilize unstable slope sections of the study area.

- The results have shown that high rainfall/or saturation (if occurs) is the principal factor causing slope instability in the study area. Hence, providing a proper drainage system that prevents the infiltration of rainwater into the subsurface is highly recommended to stabilize the critical slope sections of the study area.
- Planar failure of RS1 due to JS3 can be stabilized by two rock bolts applied at an angle of 10^0 to the slope with each of them having 125 ton/m bolt capacity and 5 to 8 m bolt length. Moreover, planar failure of RS2 due to JS2 can also be stabilized by the application of three rock bolts at an angle of 12^0 to the slope face with each of them having 250 tons/m.
- The unstable wedge of RS1 due to JS1 and JS3 can be stabilized by shotcrete with a shear strength capacity of 320 ton/m^2 and four rock bolts with a single bolt capacity of 500 ton/m in the trend direction of 077^0. Moreover, another wedge of

this slope which is formed due to JS2 and JS3 can be stabilized with four rock bolts applied in the trend direction of 070^0 and shotcrete with a strength of 600 ton/m^2.

- Considering the close location of RS1 and RS2 to dwelling houses, the rock removal technique is not recommended to stabilize planar and wedge failures of these slopes.
- Moreover, considering the budget of rock bolts and shotcrete, this study has recommended the preparation of catch ditches and barriers at the toe of slopes to minimize and control potential damage due to unstable rock blocks.
- For non-structural controlled slope sections, the slope-flattening technique should reduce the bottom slope profile from 53.0^0 to 26.7^0 and the middle slope profile from 75.0^0 to 55.7^0 for SS1 to maintain stability. The slope section SS2 can also be stabilized by reducing the bottom, middle, and upper slope profiles to 14.4^0, $26.67^{0,}$ and 39.30^0, respectively. Similarly, SS3 can be stabilized by reducing its bottom, middle, and upper slope profiles to 53.13^0, $21.80^{0,}$ and 45.00^0, respectively.
- Benching alone should not be used as a stabilization technique in the non-structural controlled critical slope sections of the study area as all-multiple benching yielded a FOS of less than one.
- This study has recommended combined benching and slope flattening to stabilize the non-structural controlled slope sections as they become effective as compared to slope flattening or benching alone. Accordingly, it is recommended to flatten SS1 to 2H: 1V with three 4 to 5 m long benches at heights of 3 m, 6.2m, and 9.2 m. Moreover, it is recommended to flatten SS2 to 1.5H: 1V with one bench at 8.1 m and SS3 to 2H: 1V with two benches at heights of 10.3m and 17.3m
- Moreover, this study has also recommended surface drainage and plant vegetation on the non-structural controlled slope sections upon implementation of coupled slope flattening and benching.

REFERENCES

Abebe, B., Dramis, F., Fubelli, G., Umar, M. & Asrat, A. (2010). Landslides in the Ethiopian highlands and the rift margins. African Earth Science 56. Pp 131-138.

Abramson, L.W., Lee, T.S., Sharma, S and Boyce, GM. (2002). Slope Stability Concepts. Slope Stabilisation and Stabilisation Methods, Second edition, published by John Willey and Sons, Inc., 329- 461.

Ahmadi, M., Eslami, M., 2011. A new approach to plane failure of rock slope stability based on the water flow velocity in discontinuities for the Latian dam reservoir landslide. J. Mt. Sci. 8, 124–130. http://dx.doi.org/10.1007/s11629-011-2088-5.

Alzo'ubi, A. (2016). Rock slopes processes and recommended methods for analysis. International Journal of Geomate. doi: 10.21660/2016.25.34052

Anbalagan, R., Sharma, S., & Raghuvanshi, T. K. (1992, October). Rock mass stability via modified SMR approach. In Proceedings 6th Symposium on Rock Mechanics (pp. 258-268).

Aryal K.P. (2008). "Differences between LE and FE Methods used in Slope Stability Evaluations". The 12th International Conference of International Association for Computer Methods and Advances in Geomechanics (IACMAG), Goa, India 4509-4516.

ASTM C 805 (2018), Standard Test Method for Rebound Number of Hardened Concrete, ASTM International, West Conshohocken, PA, 2018. www.astm.org.

ASTM D 3080 (1998). Standard test method for the direct shear test of soils under consolidated drained conditions. Annual Book of Standards, American Society for Testing and Materials, West Conshohocken, PA, Vol. 04.08, pp.339-344.

ASTM D 5731 (1995). ASTM standard test method for determination of point load strength index of rocks. American Society for Testing and Materials, vol.04.08, Conshohocken, PA;142-148.

ASTM D 7263 (2009). Standard Test Methods for Laboratory Determination of Density (Unit Weight) of Soil Specimens, ASTM International, West Conshohocken, PA, 2009, www.astm.org

Ayalew, L.(1999).The effect of seasonal rainfall on landslides in the highlands of Ethiopia.

Bulletin of Engineering Geology and the Environment, 58(1), 9-19.

Ayalew, L., Yamagishi, H., & Ugawa, N. (2004). Landslide susceptibility mapping using GIS-based weighted linear combination, the case in Tsugawa area of Agano River, Niigata Prefecture, Japan. Landslides, 1(1), 73-81.

Aydin, A. (2009) 'ISRM suggested method for determination of the Schmidt hammer rebound hardness: Revised version', *International Journal of Rock Mechanics and Mining Sciences*, 46(3), pp. 627–634. doi:10.1016/j.ijrmms.2008.01.020.

Aydin, A. and Basu, A. (2005) 'The Schmidt Hammer in rock material characterization', *Engineering Geology*, 81(1), pp. 1–14. doi:10.1016/j.enggeo.2005.06.006.

Bar N., Yacoub TE., McQuillan A. (2019). Analysis of a large open pit mine in Western Australia using finite element and limit equilibrium methods. 53rd US Rock Mech Symp

Barton, N.R. (1976). The shear strength of rock and rock joints. Int. J. Mech. Min. Sci. & Geomech. Abstr. 13(10), 1 -24.

Barton, N., and Bandis, S. (1990). Review of predictive capabilities of JRC-JCS model in engineering practice. In: Balkema, A.A, (Ed), Proceedings of International Conference on Rock Joints, Leon, Norway, pp.603-610. Rotterdam.

Barton, N.R., and Choubey, V. (1977). The shear strength of rock joints in theory and practice. Rock Mech. 10(1-2), 1-54.

Begemann, H.K.S.P. (1974). The delft continuous soil sampler. Bulletin of the International Association of Engineering Geology 10, 35-57 https://doi.org/10.1007/BF02634629

Bell, F.G., 2007. Engineering Geology. Butterworth-Heinemann, Great Britain, p. 581.

Bekele, A. and Meten, M. (2022) 'Modeling rock slope stability using kinematic, limit equilibrium and finite-element methods along Mertule Maryam–mekane selam road, Central Ethiopia', *Modeling Earth Systems and Environment*, 9(2), pp. 1559–1585. doi:10.1007/s40808-022-01563-8.

Bieniawski, Z.T. (1973). Engineering classification of jointed rock masses. Transaction of the South African Institution of Civil Engineers, v. 15, pp. 335-344.

Bieniawski, Z.T. (1979).The geomechanics classification in rock engineering applications.

In: Proceedings of the 4th international congress on rock mechanics, Montreux, 1979, pp. 41-48.

Bieniawski, Z.T., 1989. Engineering Rock Mass Classifications. Wiley, New York, p. 251.

Bigazzi, B., Bonadonna, F.P., di Paola, G.M., Giuliani, A. (1993). K-Ar and fission track the ages of the last volcano-tectonic phase in the Ethiopian Rift Valley (Tullu Moye area). In: Geology and mineral resources of Somalia and surrounding regions. Istituto Agronomico Oltremare, Firenze, Relazioni Monografie 113, 311-322.

Bishop, A. W. (1956). The use of slip circles in stability analysis of slopes. Geotechnique, 5(1),7-17.

Boccaletti, M., Mazzuoli, R., Bonini, M., Trua, T., Abebe, B. (1999). Plio-Quaternary volcano-tectonic activity in the northern sector of the Main Ethiopian Rift (MER): relationships with oblique rifting. Journal of African Earth Sciences, 29: 679– 698.

Bommer, J., & Rodríguez, C. (2002). Earthquake-induced landslides in Central America. Engineering Geology, *63*(3-4), 189-220. doi: 10.1016/s0013-7952(01)00081-3.

Bouzid, D.A. (2022) 'Finite element analysis of slope stability by expanding the mobilized principal stress Mohr's circles – development, encoding, and validation', *Journal of Rock Mechanics and Geotechnical Engineering*, 14(4), pp. 1165–1179. doi:10.1016/j.jrmge.2022.01.016.

Brinkgreve R, Swolfs W, Engin E, Waterman D, Chesaru A, Bonnier P, Galavi V (2013) PLAXIS 3D reference manual. Plaxis bv, Delft.

Broch, E., & Franklin, J. A. (1972). The point-load strength test. In International Journal of Rock Mechanics and Mining Sciences & Geomechanics Abstracts (Vol. 9, No. 6, pp. 669-676). Pergamon.

Bushira KM, Gebregiorgis YB, Verma RK, Sheng Z (2018) Cut soil slope stability analysis along the national highway at wozeka-gidole road. Ethio Model Earth Syst Environ 4(2):591–600. https://doi. org/10.1007/s40808-018-0465-6

Chemeda Y. (2020). Engineering Geological Investigation of Adama Town: Implication to Engineering Practice. *Ethiopian Journal of Science and Sustainable Development, 7*(2), 103-116. https://doi.org/10.20372/ejssdastu:v7.i2.2020.281

Cheng, Y.M., Lau, C.K. (2014). Slope Stability Analysis and Stabilization: New Methods and Insight, second ed. CRC Press, London, UK.

Chowdhury R., Flentje P., Bhattacharya G. (2009). Geotechnical slope analysis. CRC Press.

Chowdhury, R. (2010). Geotechnical Slope Analysis. CRC Press/Balkema, The Netherlands, p. 737.

Christian, J. T. (2004). Geotechnical engineering reliability: How well do we know what we are doing? Journal of Geotechnical and Geoenvironmental Engineering, 130(10), 985-1003.

Collison, A., Wade, S., Griffiths, J., & Dehn, M. (2000). Modeling the impact of predicted climate change on landslide frequency and magnitude in SE England. *Engineering Geology*, *55*(3), 205-218. doi: 10.1016/s0013-7952(99)00121-0

Dahal, R.K., Hasegawa, S., Masuda, T., Yamanaka, M. (2006). Roadside Slope Failures in Nepal during Torrential Rainfall and their Mitigation. Disaster Mitigation of Debris Flows, Slope Failures, and Landslides, pp. 503–514.

Dai, F., Lee, C., & Ngai, Y. (2002). Landslide risk assessment and management: an overview. Engineering Geology, 64(1), 65-87. doi: 10.1016/s0013-7952(01)00093-x

Damte A., Boccaletti M., Getaneh Assefa, Mazzuoli R., Tortorici L. (1992). Geological Map of the Nazareth-Dera Region, 1:50,000 Scale. Consiglio Nazionale Delle Ricerche, Italy.

Deere U., & Deere D. (1988). The rock quality designation (RQD) index in practice. In: Kirakaldie L (ed) Rock Classification systems for engineering purposes. ASTM special publication 984. American Society for Testing Materials, Philadelphia, pp 91–101.

Duncan, J.M. (2000). Factors of Safety and Reliability in Geotechnical Engineering. Journal of Geotechnical and Geoenvironmental Engineering, ASCE, Vol. 126, No. 4, 307–316.

EBCS (1995). Design of structures for earthquake resistance.

Eberhardt, E., Stead, D., Coggan, J.S., 2004. Numerical analysis of initiation and progressive failure in natural rock slopes—the 1991 Randa rock slide. Int. J. Rock

Mech. Min. Sci. 41, 69–87

Ermias, B., Raghuvanshi, T., & Abebe, B. (2017). Landslide Hazard Zonation (LHZ) Around Alemketema Town, North Showa Zone, and Central Ethiopia - A GIS-Based Expert Evaluation Approach. International Journal of Earth Sciences and Engineering, 10(01), 33-44. doi: 10.21276/ijee.2017.10.0106.

Fellenius W. (1936). Calculation of the Stability of Earth Dams. Trans. 2nd Int. Cong. Large Dams, Washington, 445-459.

Fredlund D.G., Krahn J., and Pufahl D.E. (1981). The Relationship between Limit Equilibrium Slope Stability Methods. In Proceedings of the 10th Conference of the International Society for Soil Mechanics and Foundation Engineering (ISSMFE), Stockholm, Swe-den, 3: 409–416

Girma, F., Raghuvanshi, T.K., Ayenew, T., & Hailemariam, T. (2015). Landslide hazard zonation in Ada Berga District, Central Ethiopia –J. Geomatics, v.90: pp. 25-38

Goodman, R. E. (1989). Introduction to rock mechanics (Vol. 2). New York: Wiley.

Goodman RE. Kieffer DS. (2000). Behavior of rock in slope. Journal of Geotechnical and Geoenvironmental Engineering. V.126, Issue 8 https://doi.org/10.1061/(ASCE)1090-0241(2000)126:8(675)

Griffiths, D.V., Lane, P.A. (1999). Slope stability analysis by finite elements. Geotechnique 49 (3), 387e403.

Hack, R., 2002. An evaluation of slope stability classification. In: C. Dinis da Gama, L. Ribeira e Sousa (eds.), Proc. ISRM EUROCK'2002, Portugal, Madeira, Funchal, 25–28 November 2002, Publ. Sociedade Portuguesa de Geotecnia, Av. do Brasil, 101, 1700–066 Lisboa, Portugal. pp. 3–32.

Hamza, T., & Raghuvanshi, T. (2017). GIS-based landslide hazard evaluation and zonation – A case from Jeldu District, Central Ethiopia. Journal of King Saud University Science, 29(2), 151-165. doi: 10.1016/j.jksus.2016.05.002.

Hocking, G., 1976. A method for distinguishing between single and double-plane sliding of tetrahedral wedges. Int. J. Rock Mech. Min. Sci. Geomech. Abstr. 13, 225–226.

Hoek, E. (2000). A slope stability problem in Hong Kong. Practical Rock Engineering. pp 92- 104.

Hoek, E., 2007. Practical rock engineering. http://www/rocscience.com/hoek/ Practical Engineering. asp. Accessed 4 March 2022.

Hoek, E., Torres, C.C., Corkum, B. (2002). Hoek-Brown failure criterion – 2002 Edition. In: Proc. NARMS-TAC Conference, Toronto, 2002, 1: 267–273.

Hoek E., Marinos P. (2007). A brief history of the development of the Hoek-Brown failure criterion. Soils Rock 30:85–92

Hoek, E. and Bray, J.W. (1981) Rock Slope Engineering. Revised 3rd Edition, the Institute of Mining and Metallurgy, London, 341-351.

Hossain, M. M., 2011. Stability analysis of anchored rock slopes against plane failure subjected to a surcharge and seismic loads. Retrieved from http://ro.ecu.edu.au/ theses/139 on March 18' 2017.

Hudson, J.A., and Harrison, J.P. (1997). Engineering rock mechanics. Pergamon, London.

ISRM, (1978). International Society of Rock Mechanics. Suggested Methods for Determining Tensile Strength of Rock Materials. International Journal of Rock Mechanics and Mining Sciences, Geomechanics Abstract, 15(3), pp. 99-103. 27.

Jampani H, Bhupathi N. (2017). Stability Analysis of Slope with Different Soil Types and Its Stabilization Techniques.

Janbu, N. (1954). Application of Composite Slip Surface for Stability Analysis. European Conference on Stability of Earth Slopes, Stockholm.

Jemal S. (2005). Slope Stability Studies along Gohatsion Dejen Road. Unpublished MSc Thesis, Addis Ababa University, Ethiopia.

Jing, L. (2003). A review of Techniques, Advances, and Outstanding Issues in Numerical Modelling for Rock Mechanics and Rock Engineering. International Journal of Rock Mechanics & Mining Sciences, vol. 40, pp. 283-353.

Johnson, R.B. and Degraff, J.V. (1991). Principles of Engineering Geology, John Wiley and Sons, New York, 497 pp.

Karaman, K., Ercikdi, B., Kesimal, A., 2013. The assessment of slope stability and rock excitability in a limestone quarry. Earth Sci. Res. SJ. 17 (2), 169–181.

Kasahun M. (2014). Slope Stability Assessment for Selected Sections along Mana BegnaLemlem Bereha Road, Northwestern Ethiopia. Unpublished MSc Thesis,

Addis Ababa University, Ethiopia.

Keefer, D. (2000). Statistical analysis of an earthquake-induced landslide distribution — the 1989 Loma Prieta, California event. Engineering Geology, *58*(3-4), 231-249. doi: 10.1016/s0013-7952(00)00037-5.

Krabbenhoft, K., Lyamin, A.V., Sloan, S.W. (2007). Formulation and solution of some plasticity problems as conic problems. Int. J. Solid Struct. 44 (5), 1533e1549.

Krahn, J. (2004). Stability Modelling with SLOPE/W. An Engineering Methodology, Published by GeoSlope International.

Koca TK. (2020). Comparative analyses of finite element and limit equilibrium methods for heavily fractured rock slopes. J Earth Syst Sci 129:65–76

Kulhawy, F.H., Mayne P.W. (1990). *Manual on Estimating Soil Properties for Foundation Design*. Palo Alto, CA: EPRI.

Lamessa, G., & Meten, M. (2021). Stability analysis of rock slope along selected road sections from Gutane Migiru town to Fincha sugar factory, Oromiya, Ethiopia. SN Applied Sciences, *3*(2). doi: 10.1007/s42452-020-04026-w

Li, L.C., Tang, C.A., Zhu, W.C., Liang, Z.Z. (2009). Numerical analysis of slope stability based on the gravity increase method. Comput. Geotech. 36 (7), 1246e1258.

Lisle RJ. (2004). Calculation of the daylight envelope for the plane failure of rock slopes. Geotechnique 54(4):279–280

Liu, S.Y., Shao, L.T., Li, H.J. (2015). Slope stability analysis using the limit equilibrium method and two finite element methods. Comput. Geotech. 63, 291e298.

Markland, J.T. (1972). A useful technique for estimating the stability of rock slopes when the rigid wedge sliding type of failure is expected. Imp. Coll. Rock Mech. Res. Rep. 19, 10.

Mebrahtu TK., Heinze T., Wohnlich S., Alber M. (2022). Slope stability analysis of deep-seated landslides using limit equilibrium and finite element methods in the Debre Sina area. Bullet Eng Geol Environm, Ethiopia. https://doi.org/10.1007/s10064-022-02906-6

Meyer, W., Pilger, A., Rosier, A., Stets, J. (1975). Tectonic evolution of the northern part of the Main Ethiopian Rift in Southern Ethiopia. Schweizerbart, Stuttgart, pp. 352-

362.

Morgenstern, N., & Price, V. (1965). The Analysis of the Stability of General Slip Surfaces. Geotechnique, Vol. 15 (No. 1), pp. 77-93.

Morton, W.H., Rex, D.C., Mitchell, J.G., Mohr, P. (1979). Rift ward younging of volcanic units in the Addis Ababa region, Ethiopian rift valley. Nature, 280: 284-288.

Palmstrom, A. (2005). Measurements of and correlations between block size and rock quality designation (RQD). Tunnelling and Underground Space Technology, 20(4), 362–377.

Pantelidis L. (2009). Rock-slope stability assessment through rock mass classification systems. International Journal of Rock Mechanics and Mining Sciences, 46(2), 315-325.

Park, H., and West, T. (2001). Development of a probabilistic approach for rock wedge failure. Eng Geol 59:233–251.

Pardeshi, S. D., Autade, S. E. and Pardeshi, S. S. (2013). Landslide hazard assessment:491 recent trends and techniques. Springer Plus, 2(1): 523pp

Raghuvanshi, T. K. (2017). Plane failure in rock slopes–A review on stability analysis techniques. Journal of King Saud University-Science.

Raghuvanshi, T.K., Ibrahim, J., Ayalew, D. (2014). Slope stability susceptibility evaluation parameter (SSEP) rating scheme – an approach for landslide hazard zonation. J. Afr. Earth Sci. 99, 595–612.

Rocscience, 2004. Dips 6.0, http://www.rocscience.com/software/dips

Rocscience, 2004. Rocdata 3.0, http://www.rocscience.com/software/rocdata

Rocscience, 2004. RocPlane 2.0, http://www.rocscience.com/software/rocplane

Rocscience, 2004. Phase V 2.0, http://www.rocscience.com/software/phase

Rocscience, 2004. Slide 5.0, http://www.rocscience.com/software/slide

Rocscience, 2004. Swedge 4.0 http://www.rocscience.com/software/swedge

Romana, M. (1985). New adjustment ratings for application of Bieniawski classification to the slope. In: Int. Sym. Role Rock Mech., Zacatecas, pp. 49–53.

Salunkhe, D.P., Ch van, G., Bartakke, R.N., Kothavale, P.R., 2017. An overview on

methods for slope stability analysis. Int. J. Eng. Res. Technol. 6 (3), 528–535.

Samuel M. (2011). Slope Stability Analysis on a Selected Slope Section along the Road Gohatsion-Dejen. Unpublished MSc Thesis, Addis Ababa University, Ethiopia.

Sharma, S., Raghuvanshi, T.K., & Anbalagan, R. (1995). Plane failure analysis of rock slopes. Geotechnical & Geological Engineering, 13(2), 105-111.

Sharma, S., Raghuvanshi, T., & Sahai, A. (1999). An engineering geological appraisal of the Lakhwar dam, Garhwal Himalaya, India. Engineering geology, 53(3-4), 381-398.

Shukla, S.K., Khandelwal, S., Verma, V.N., Sivakugan, N., (2009). Effect of surcharge on the stability of anchored rock slopes with water-filled tension cracks under seismic loading condition. Geotech. Geol. Eng. 7 (4), 529–538.

Singh, B., and Geol, R.K. (1999). Rock mass classification: a practical approach in civil engineering. Amsterdam, Elsevier Science, 282 p.

Singh, B., Goel, R.K., (2002). Software for engineering control of landslides and tunneling hazards. A.A Balkema Publishers, Krips, Mappel, The Netherlands, p. 344.

Sloan, S.W. (2013). 51st Rankine lecture: geotechnical stability analysis. Geotechnique 63 (7), 531e572.

Spencer, E. (1968). A Method of Analysis of the Stability of Embankments Assuming Parallel Inter-Slice Forces. *Géotechnique*, *18*(3), 384-386. doi: 10.1680/geot.1968.18.3.384

Stead, D., Eberhardt, E., Coggan, J.S., (2006). Developments in the characterization of complex rock slope deformation and failure using numerical modeling techniques. Eng. Geo. 83, 217–235.

Sternik, K. (2013). Comparison of slope stability predictions by gravity increase and shear strength reduction methods. Tech. Trans. Environ. Eng. 110, 121e130.

Stianson JR., Chan D., Fredlund DG. (2015). Role of admissibility criteria in limit equilibrium slope stability methods based on finite element stresses. Comput Geotech 66:113–125. https://doi.org/10. 1016/j.compgeo.2015.01.014

Swan CC., Seo YK. (1999). Limit state analysis of earthen slopes using dual continuum/FEM approaches. Int J Numer Anal Methods Geomech 23(12):1359–

1371

Tang H., Yong R., EzEldin M. (2016). Stability analysis of stratified rock slopes with spatially variable strength parameters: the case of Qianjiangping landslide. Bull Eng Geol Environ 76:839–853. https://doi.org/10.1007/s10064-016-0876-4

Temesgen, B., Mohammed, U., & Korme, T. (2001). Natural Hazard Assessment Using GIS and Remote Sensing Methods, with Particular Reference to the Landslides in the Wondogenet Area. Solar Terrestrials & Planetary Science (C) 26(9): 665-615.

Tesfaye, M., Regassa, B. and Garo, T. (2023) 'Rock slope stability modeling using kinematic and limit equilibrium methods along Woliso to Wonchi Lake Road, Central Ethiopia', *Modeling Earth Systems and Environment* [Preprint]. doi:10.1007/s40808-023-01780-9.

Tschuchnigg, F., Schweiger, H.F., Sloan, S.W., Lyamin, A.V., Raissakis, I. (2015b). Comparison of finite finite-element limit analysis and strength reduction techniques. Geotechnique 65 (4), 249e257

Ulusay, R., & Karakul, H. (2015). Assessment of basic friction angles of various rock types from Turkey under dry, wet, and submerged conditions and some considerations on tilt testing. Bulletin Of Engineering Geology And The Environment, *75*(4), 1683-1699. doi: 10.1007/s10064-015-0828-4

Vásárhelyi, B. (2009). A possible method for estimating the Poisson's rate values of the rock masses. Acta Geodaetica Et Geophysica Hungarica, *44*(3), 313-322. doi: 10.1556/ageod.44.2009.3.4

Wang, J., & Ji, H. (2013). Analysis of Rock Slope Stability Based on Limit Equilibrium Method. Advanced Materials Research, *711*, 333-337. doi: 10.4028/www.scientific.net/amr.711.333

Wang, X., Niu, R. (2009). Spatial forecast of landslides in three gorges based on spatial data mining. Sensors 9, 2035–2061

Woldearegay, K. (2013). Review of the occurrences and influencing factors of landslides in the highlands of Ethiopia: With implications for infrastructural development. Momona Ethiopian Journal of Science, 5(1), 3-31.

Wyllie, D. C., & Mah, C. W. (2004). Rock Slope Engineering 4thEd. The Institution of Mining and Metallurgy London.

Wyllie, D. C., & Norrish, N. (1996). Landslides: Investigation And Mitigation (pp. 474-504). Transportation Research Board.

ZainAlabideen, K., Helal, M., 2016. Determination of the safe orientation and dip of a rock slope in an open pit mine in Syria using kinematic analysis. Al-Nahrain Univ. College Eng. J. (NUCEJ) 91 (1), 33–45.

APPENDICES

Appendix 1: The shear strength parameters of structurally controlled slope sections as determined using Rockdata software using Barton & Bandi's (1990) non-linear failure criterion.

Slope section	Input parameters						Output result		
	Joint set	JRC	JCS (Mpa)	γ (MN/m^3)	phir	Sh (m)	Cohesion		Φ (^{0})
							C (Mpa)	t/m2	
RSS1	JS1	9	82.61	0.2474	25.83	30	0.054	5.506	41.73
	JS2	7	71.50	0.2474	26.05	30	0.034	3.467	38.20
	JS3	5	74.22	0.2474	27.88	30	0.022	2.243	36.74
RSS2	JS1	4	66.27	0.2479	21.81	32	0.014	1.427	28.76
	JS2	3	58.08	0.2479	22.50	32	0.010	1.019	27.57
JRC= joint roughness coefficient, JCS= joint compressive strength, phib= basic friction angle, γ= unit weight of the rock, Sh= slope height, c = cohesion. Φ= friction angle									

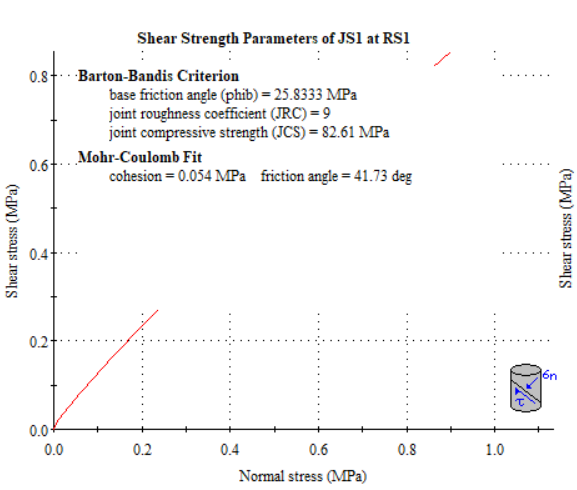

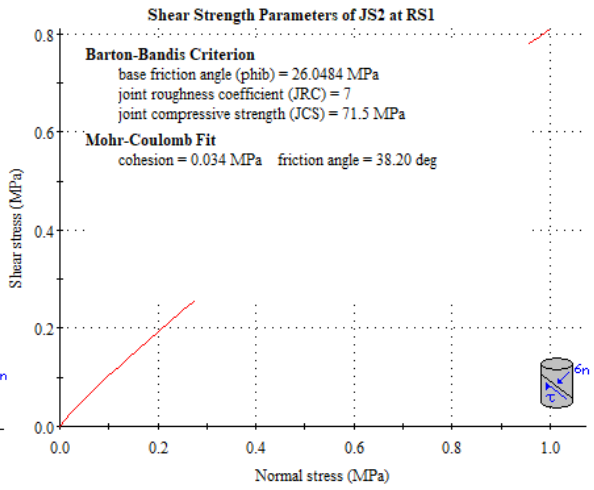

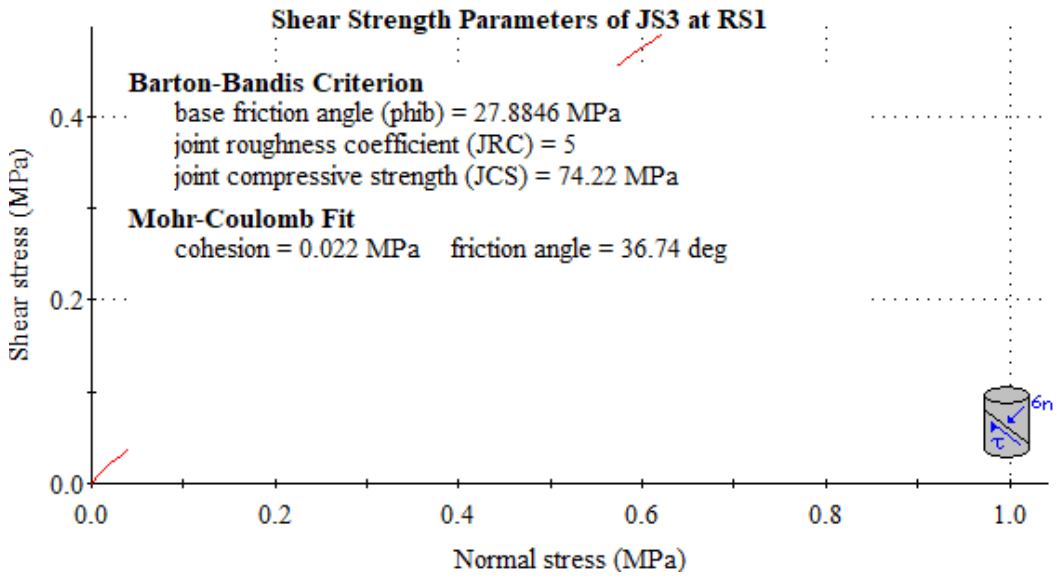

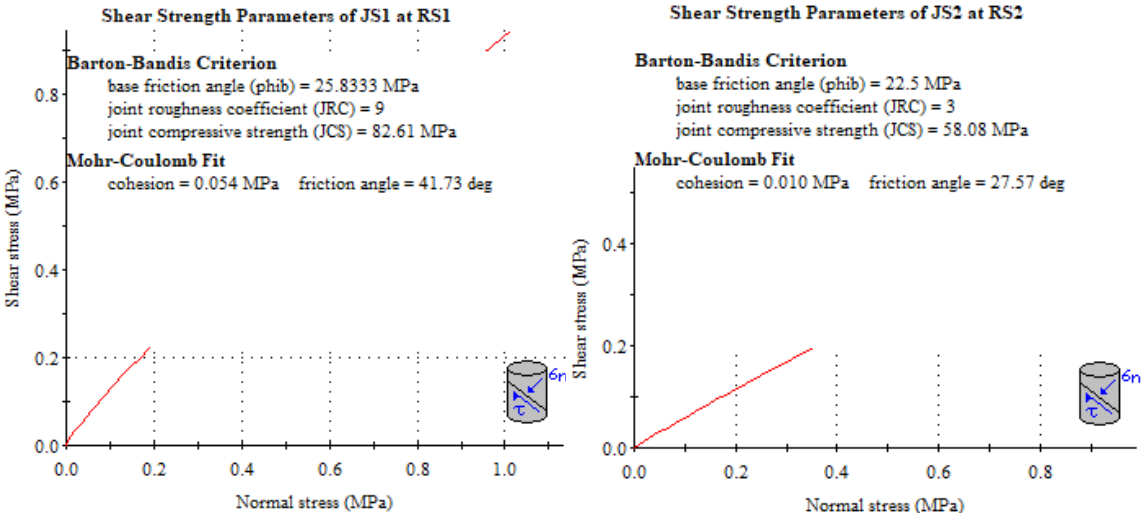

Appendix 2: The shear strength parameter of the non-structural controlled slope section

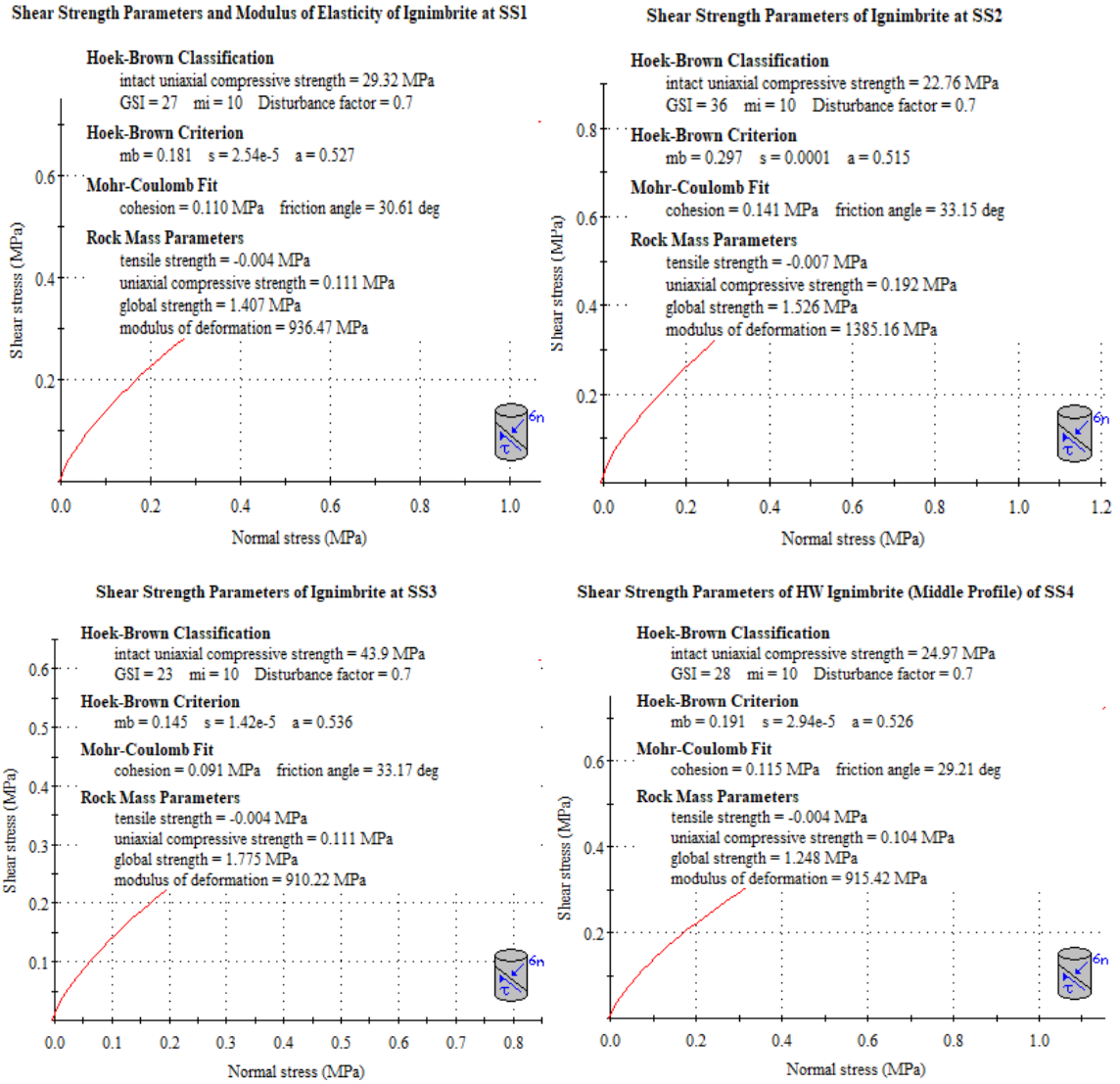

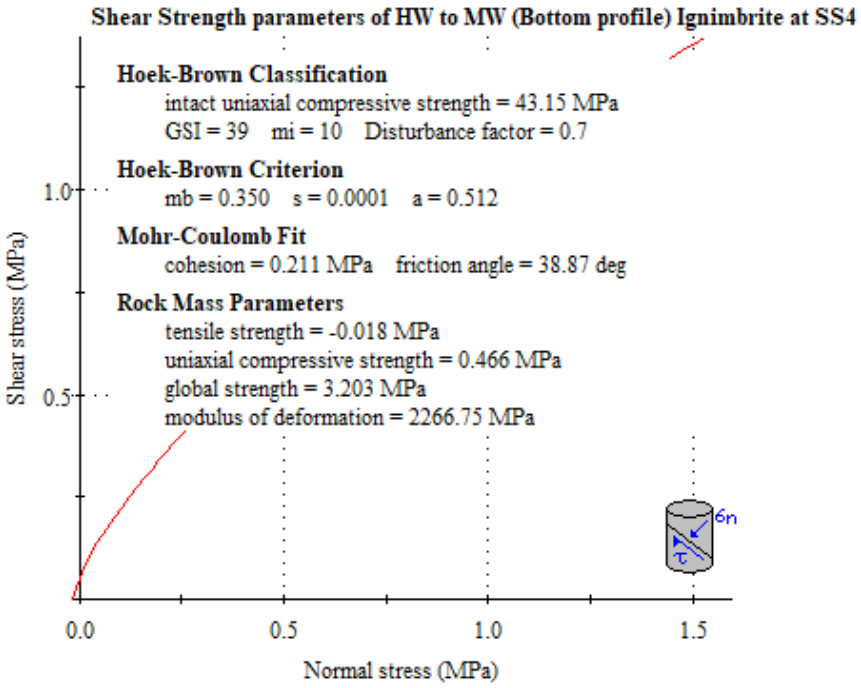

Appendix 3: Standard GSI built-in Rocdata software (Rocscience 3.0 Rocscience, 2004)

Appendix 4: Standard roughness coefficient built-in Rocdata software (Rocscience 3.0 Rocscience, 2004)

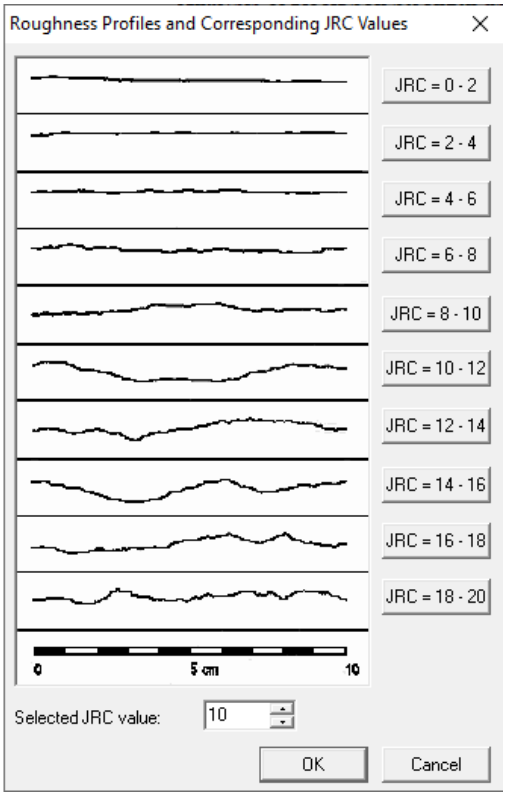

Appendix 5: Disturbance factor built in Rocdata software (Rocscience 3.0 Rocscience, 2004)